Alma Mater Studiorum - Università di Bologna

SCUOLA DI SCIENZE

Dipartimento di Chimica Industriale "Toso Montanari"

Corso di Laurea Magistrale in

Chimica Industriale

Curriculum: Advanced Spectroscopy in Chemistry

Classe LM-71 - Scienze e Tecnologie per la Chimica Industriale

Investigation of gold-based catalysts for liquid phase oxidation of glucose to glucaric acid

CANDIDATE
Carolina Alejandra Garcia Soto

SUPERVISOR
Prof. Nikolaos Dimitratos

CO-SUPERVISOR
Eleonora Monti

Session I

Academic Year 2018/2019

ABSTRACT

Glucaric acid (GA) is one of the building block chemicals derived from sugar biomass with higher added value and better perspective for future exploitation. GA can be synthesized by oxidation of D-Glucose (Glu) through Gluconic acid (GO) as intermediate and it can be employed for many uses; for instance, it is a precursor of adipic acid, a monomer for Nylon-6,6. Nowadays, GA is produced by oxidation of Glu with either stoichiometric oxidants (HNO_3), or by means of electrochemical or biochemical synthesis. However, these processes show drawbacks from either the environmental or the economic viewpoint. Therefore, the study of a more sustainable process to produce GA from Glu is of great scientific and practical interest using supported metal nanoparticles. For this reason, gold nanoparticles (Au NPs) supported on activated carbon (AC) has been studied as catalysts for the oxidation of glucose, using O_2 as oxidant in the presence of a base (sodium hydroxide). Using sol immobilization technique, preformed Au NPs have been supported on AC following different experimental procedures. UV-Vis spectroscopy, XRD, TEM and TG analysis were utilized in the characterization of the catalysts. The operational conditions were optimized obtaining 24% of yield of GA, 37% to GO and 27% to byproducts in 1 h, 1000 rpm, 10 bar of O_2 and Glu:Au:NaOH molar ratio of 1000:1:3000. Under such conditions, all catalysts show relatively high glucose conversion (≥82%) with different GA yields. The effect of PVA:Au weight ratio is of vital relevance given that higher PVA concentrations can lead to smaller nanoparticles but the presence of PVA ligands can affect the initial rate of reaction. After 1 hour, the catalytic activity is very similar amongst all catalysts: glucose conversion is ≥90% while GO+GA yield is around 58-61%. Therefore, the oxidation reaction was performed at 15 min where Au/AC PVA0 reached the highest yield of GA (16%) and Au/AC PVA2.4 gave the lowest (8%). It is evident that the presence of PVA influences to a higher degree the reaction rate than the Au NPs size. Hence, the effect of different heat treatments where applied for the removal of PVA: washing with water at 60°C or heat treatment (120-250°C) with Air/H_2. Washing treatment and heat treatment at 120°C with Air/H_2 may have resulted in the mildest treatments for the removal of PVA while at 200 and 250°C with Air/H_2 the average crystallite size increased giving a lower yield of GA. Finally, two different supports have been used in order to study the effect of metal-support interaction in the immobilization of Au NPs: zirconium oxide and activated carbon. Au/AC catalyst demonstrated a higher conversion of gluconic acid to glucaric acid at short reaction times (15.1% yield GA) compared to gold supported on ZrO_2 (2.4% yield GA).

CONTENT

1. INTRODUCTION

1.1. **Gold nanoparticles and methods of preparation**

Gold nanoparticles have been studied in the past recent years for their ability to form different shapes like spheres, cages, prisms, wires, rods[1] at different sizes with a potential application in imaging, photothermal therapy[2], sensors[3] and catalysis.[4] The reasons behind the success of gold NPs in nanoscience and nanotechnology are due to the high chemical and physical stability, the intrinsic biocompatibility of gold nanostructures, the ease of surface functionalization with organic and biological molecules and the multitude of optical properties related to surface plasmons.

Gold nanoparticles have a particular characteristic, among other types of NPs like Cerium and Iron-based nanoparticles, to work as nanozymes exhibiting an oxidase-like activity[5]. Depending on the functionalization of the surface, gold nanoparticles can work in the oxidation of glucose and detection of Hg ions, DNA or other macromolecules.[6]

Another remarkable property of gold NPs are the multitude of optical and electronic properties related to surface plasmons. Gold NPs display a surface plasmon resonance when the frequency of oscillating electrons present in the conduction band of the gold resonates with the frequency of incoming light radiation resulting in a plasmon band than can be observed in the UV-VIS-NIR. This special feature helps in the characterization in size and shape of nanoparticles.[7] This is due to the large number of easily polarizable conduction electrons, which is a general prerequisite for preferential interaction with electromagnetic fields and the generation of nonlinear optical phenomena. In fact, compared to other organic and inorganic chromophores, Au NPs with size above 2 nm have a larger extinction cross-section, possibility reaching 100% of light-to-heat conversion efficiency, high photostability, and the ability to amplify the electromagnetic field at nanometric distance from the metal surface.[8]

1.1.1. **Reactions catalyzed by gold nanoparticles**

Gold belongs to the group VIII metals along with copper (Cu) and silver (Ag) with a d-band fully occupied. These metals were seen in the past as catalytically inert unless they were activated by losing of electrons to generate vacancies in the d-band. But no one knew that gold (with a higher ionization energy compared to Cu and Ag) would become one of the most important

catalyst in recent times. Supported gold nanoparticles occupy a substantial place in the application of heterogeneous catalysis and it had been proved to be a powerful catalyst in many reactions including selective oxidation of alcohols, alkyne oxidation, hydrogenation, C-C coupling reactions, reduction of NO_2 to -NH_2 and several others.[9,10]

One of the most important and model reactions for gold catalysis is the oxidation of CO to CO_2 in atmospheric air. This reaction has a huge impact in environmental application due to the conversion of toxic compounds in air while avoiding the reduction of the valuable H_2. The oxidation of CO was optimized to operate at ambient conditions, and even at −76°C.[11] The study of this reaction led to the conclusion that the support has a strong involvement in the reaction since Au NPs supported on activated carbon or polymers such as PMMA, are not active at all for CO oxidation even at temperatures above 373 K. On the other hand, when metal oxides are used as support, the activity of the catalyst is very high in the case of TiO_2, α-Fe_2O_3, and Co_3O_4 and mildly active on Al_2O_3 and SiO_2 in the presence of moisture.[12]

Gold-catalyzed hydrogenations of π-π systems (alkenes, dienes, alkynes, and aromatics) have also widely investigated. In the presence of Au NPs supported on metal oxides, alkynes are selectively hydrogenated over alkenes.[13] In a study for the hydrogenation of acetylene to ethylene results that hydrogenation proceeds with 100% selectivity towards C_2H_4, both in the presence and the absence of C_2H_4. The key for such selectivity to C_2H_4 resides in a non-competitive adsorption of C_2H_2 and C_2H_4 on the Au surface when both hydrocarbons are present in the feed. By means of Density Functional Theory (DFT) calculations and experiments over Au/CeO_2 it was demonstrated that C≡C bonds are adsorbed in the edges of Au_{19} whereas C=C bonds are not, showing C_3H_6 selectivities up to 95%. Contrariwise, Pd absorbs both, triple and double bonds. On this basis, gold catalysts can be considered a promising alternative to promoted Pd-based catalysts used industrially in the gas-phase deacetylenization of C_2 and C_3 cuts from steam crackers.[14]

Another reaction of interest is the reduction of nitro compounds into amines. This type of reaction is generally carried out with Pt or Pd but providing either unselective reduction or different chemoselectivities. It has been reported that Au catalysts (Au/TiO_2 or Au/Fe_2O_3) promote the reduction of functionalized nitroarenes into anilines in yields close to 100%.[15] Such observation was that the nitro group is selectively reduced in the presence of other reducible functionalities like carbon double bonds, nitriles or amides.

The reduction of 4-nitrophenol to 4-aminophenol by sodium borohydride in aqueous solution has become a model reaction for Au nanoparticles for structure-activity relationships. No byproducts are formed, and it is easy to follow in UV-Vis spectroscopy due to a strong absorption at 400 nm of 4-nitrophenol.[16] Used for the study of the catalytic activity of gold nanoparticles stabilized by different molecules (dendrimers PAMAM or PPI[17], resins[18] or collagen[19]) or synthesized by biological methods (enzyme crystals[20], bacteria[21] or fungi[22]).

C-C coupling reactions have a special attention for biologically active compounds and pharmaceutical organic compounds. Au nanoparticles (especially the 1 to 20 nm size range) can catalyze carbon-carbon coupling reactions, including Ullmann homocoupling of halides, oxidative homocoupling of organoboronates, Suzuki cross-coupling of phenylboronic acid and halides, Sonogashira cross-coupling of iodobenzene and phenylacetylene, and A3 coupling reaction of phenylacetylene, amines, and aryl or alkyl aldehydes (figure 1).[23]

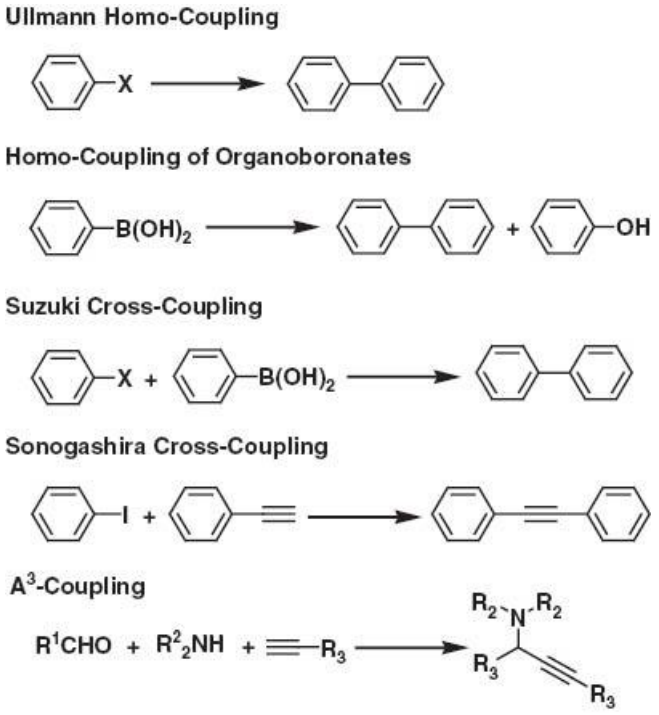

Figure 1. Various carbon-carbon coupling reactions catalyzed by gold nanoparticles (where X = I, Br, and Cl).

These and other reactions can be mentioned to expose the wide range of applications in organic synthesis. It can easily be foreseen that supported Au NPs can promote more rearrangements, C−X couplings, cycloadditions and other reactions and further work is expected. In addition, a need for innovative preparation procedures aimed at reducing the Au particle size to a defined point with uniform clusters and to prepare samples with the optimal nanoparticle morphology.

1.1.2. **Methods of preparation**

The obtention of active catalysts heavily depends on the preparation method since several parameters can be controlled like the average size of the nanoparticles, distribution, oxidation state and coverage of surface metal. Two approaches can be considered in the synthesis of nanoparticles: Top-down methods where the bulk material is mechanical grinded to obtain particles in the nanoscale with the subsequent addition of protecting agents; Bottom-up methods rely on the reduction of metal salts. These methods are the most suitable for the synthesis of catalysts, especially supported nanoparticles can work as heterogeneous catalyst which facilitates the separation of products and catalyst. Several methods are reported for the preparation of gold nanoparticles e.g. impregnation, deposition-precipitation, anionic exchange, colloidal method, even biogenic methods.[24] However, the preparation method used influences the dispersion of the metal particles on the support. Highly dispersed nanoparticles contain a high number of low coordinate metal sites. These active sites are important in the catalytic cycle hence, the dispersion of the metals will have a positive effect on the activity of the catalyst.[25]

Gold nanoparticles supported on metal oxide surfaces or carbon supports are typically prepared upon reduction of Au (III) substances such as $HAuCl_4$ or $NaAuCl_4$. Although it is expected that cationic gold will certainly be completely reduced to metallic gold clusters, recent experiments have shown that Au NPs/M_xO_y may also contain cationic gold species in either the oxidation state of +1 or +3. Such species can be quantified with X-ray photoelectron spectroscopy (XPS) by deconvolution of the characteristic Au $4f_{7/2}$ peak.[26]

- *Impregnation*

The impregnation method is widely used in catalyst synthesis due to its simplicity and low cost. The impregnation consists on the dispersion of the metal precursor in aqueous solution onto a support material followed by drying step and calcination. Different types of metal oxide support can be used and there is no need to adjust the pH.

In the thermal treatment, specifically during the drying, the metal ions and counter ions are deposited in the surface of the support. The disadvantage is that the presence of chlorine ions leads to the sintering of the metal giving large Au nanoparticles. This can be reversed by pretreatment with a reducing gas (H_2, forming gas) resulting in the removal of the chlorine species, thus the formation of smaller nanoparticles and more active catalysts.[27] In addition, this method has a difficulty to produce AuNPs with a specific narrow size distribution unless the support has a well-defined porous structure.

- *Anion adsorption*

For the formation of supported nanoparticles, the interaction between the metal precursor and the support is crucial. It has been demonstrated that among the key factors for the preparation, the isoelectric point (IEP) of the support is essential. When the pH of the solution is lower than the IEP of the oxide, the overall charge of the surface of the oxide is positive (with OH_2^+groups in the surface) and anions from the solutions can be adsorbed. Conversely, when the pH is higher than the IEP, the overall charge of the oxide surface is negative (with O^- groups in the surface) and cations can be adsorbed.

With the most commonly used gold precursor, $HAuCl_4$, the interaction with the support proceeds by an anionic adsorption (**anion adsorption**), whereas with a second precursor such as $Au(CH_3)(NH_2)_2$ the formation of a surface complex is due to a cationic adsorption (**cation adsorption**).[28] As a result, oxides with IEP ≈ 7 such as TiO_2, CeO_2, ZrO_2, Fe_3O_3 produce highly active catalysts while an acidic support such as SiO2 (IEP = 1-2) will usually be inactive.

Pitchon and co-workers designed a method called *direct anionic exchange* and they tested alumina (IEP=8-9) as added support into a solution of $HAuCl_4$ and a continuous increase in the pH of the solution over time is observed. [29] The pH of the solution of concentration 2.23×10^{-4} M

is 3.4 at room temperature, though it increases during the course of the preparation to ca. 4.1. In the same manner, for a greater concentration of $HAuCl_4$, 1.44×10^{-3} M, an increase in pH from 2.9 to 3.7, is observed when the solution is in contact with the support. At this pH, the gold species present in the solution are $[AuCl_3OH]^-$ and $[AuCl_2(OH)_2]^-$, this latter being the main species making possible a reaction between the support and the complexes. Therefore, the increase of pH is due to a loss of H^+ in the solution which protonates the OH groups of Al_2O_3 to form OH_2 on the support surface. After washing with water and calcination at 300°C, the gold loading was close to the nominal one (~2 wt%), but the gold particles were large, 10–20 nm.

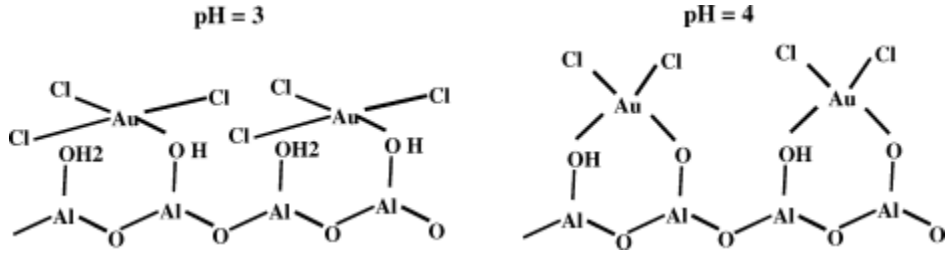

Figure 2. Mechanism of interaction of the gold complex with the alumina surface according to the pH

- *Deposition-precipitation*

Deposition-Precipitation (DP) consists on the deposition of a hydroxide or hydrated oxide of the metal precursor into the surface of the support. The soluble metal precursor becomes insoluble at increasing of pH and precipitates onto the support. The powder support is stirred into a solution containing the soluble metal precursor to which the precipitating agent, usually a base, is gradually added. Then, the solid sample is recovered, washed, dried, and activated.

Catalysts supported on TiO_2 are active, but a general trend is that the catalysts prepared by DP Urea are more active than those prepared by impregnation, whatever the gold content. The performances in CO oxidation of the impregnated catalysts approach those of DP Urea catalysts, with a TOF (Turnover frequency) ratio close to 2. Not only the activity of gold catalysts but also TOF in CO oxidation increases when Au NPs reaches a size smaller than 2-3 nm. The lower activity of the impregnated catalysts can be related to the fact that their average particle size is slightly larger and their particle size distribution is broader than those of the DP Urea samples. This method gave nanoparticles of 3- 5 nm size. [30]

The main difference with the procedure used for anion adsorption is that the pH of the solution containing both $HAuCl_4$ and the oxide support is adjusted to a fixed pH higher than the support IEP by the addition of a base, most often NaOH (as well Na_2CO_3 or urea); the mixture is usually heated at 70–80°C and stirred for approximately 1 h. A flow of H_2 can be applied in order to convert the Au^{3+} ions to AuNPs. As for anion adsorption, the catalyst is washed with water to remove as much of sodium and chlorine as possible, dried between room temperature and 100°C, and usually calcined in air.

This method was found suitable for the deposition of gold on oxide supports of IEP higher than 5, such as magnesia, titania, alumina, zirconia, and ceria. It is not suitable for silica (IEP ≈ 2), silica-alumina (IEP ≈ 1), and tungsta (IEP ≈ 1), activated carbon or zeolites due to their high acidity. However, deposition-precipitation with ammonia has been successfully applied to these supports.

- *Sol immobilization*

In sol immobilization technique, the metal precursor is reduced and the nanoparticles formed are stabilized by the presence of a surfactant or stabilizing agent leading to a colloidal solution, afterwards the support is added.

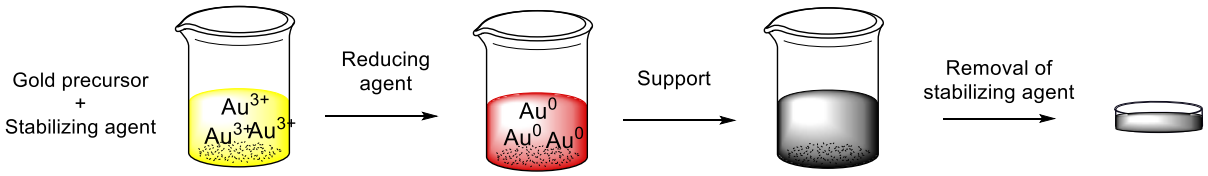

Figure 3. Schematic procedure of sol immobilization for supported gold nanoparticles

One of the most widely reducing agents used is sodium borohydride ($NaBH_4$), but sodium citrate, ascorbic acid[31] and alcohols are used as well.[32] The nature of the reducing agent is very important: stronger the reductive potential of the agent, lower the time of nucleation.[33] Polte et al. studied the formation mechanism using a static mixer in continuous flow analyzing with small angle X-ray scattering (SXAS). The first step is the initial and rapid reduction of the gold precursor within less than 200 ms accompanied by the formation of primary particles (nuclei). In a second step, the primary particles grow due to coalescence along with a corresponding decrease in the

number of particles. If the solution lacks any stabilizing agent, the growth can continue even 24 h after the starting point.[34]

The role of the stabilizing agent is to prevent the agglomeration of the nanoparticles into larger particles. The most common stabilizing agents for catalyst preparation are polyvinyl alcohol (PVA), Polyvinyl Pyrrolidone (PVP) and tetrakis (hydroxymethyl) phosphonium chloride (THPC). A recent study compares three surfactants (PVA, PVP and THPC) and they conclude that the colloidal method using PVA provides the best catalyst in their experiment compared to the one obtained by deposition-precipitation.[35] In another study, it was concluded that the use of high ratios of PVA/Au must be avoided (≤3) in order to assure total immobilization of Au NPs.[36]

Sol immobilization has proved significant advantages given the obtention of a more uniform and narrow distribution of nanoparticles in the surface of the support. For example, in the synthesis of Au-Pd NPs supported in carbon, the surface area of Au-Pd/CSI (Colloidal Sol Immobilization) was higher (961.7 m^2/g) than the surface area (849.1 m^2/g) of the catalyst prepared by impregnation. Similar results are obtained in bimetallic Au-Pd NPs supported in TiO_2.[37,38]

1.2. **Oxidation of glucose to glucaric acid**

Biomass is naturally occurring organic material that can be used as a renewable feedstock for a sustainable production of chemicals and fuels. Large part of biomass comes from vegetal sources which is rich in carbohydrates in the form of polysaccharides (starch, cellulose and hemicellulose) and lignin (polymer based on phenyl propane units). The hydrolysis of cellulose and starch gives access to Glucose monomers. Glucose is the monosaccharide mostly used as platform chemical for the synthesis of other compounds like plastics and fuels (figure 4). Nowadays, numerous chemical products are obtained by fermentation/enzymatic processes starting from glucose such as alcohols (ethanol, butanol), organic acids (citric acid, itaconic acid, gluconic acid) and others.[39] Gluconic acid is an oxidized product of glucose and is used as a chelating agent and a raw material of pharmaceuticals and foods. Current commercial production of sodium gluconate uses submerged fermentation with *Aspergillus niger* (6×10^4 tons per year)[40] but electrolytic and catalytic methods are being developed. Gluconic acid is precursor of its lactone form (Glucono-δ-lactone) and its salt (sodium/calcium gluconate) and other acids like Glucaric acid.

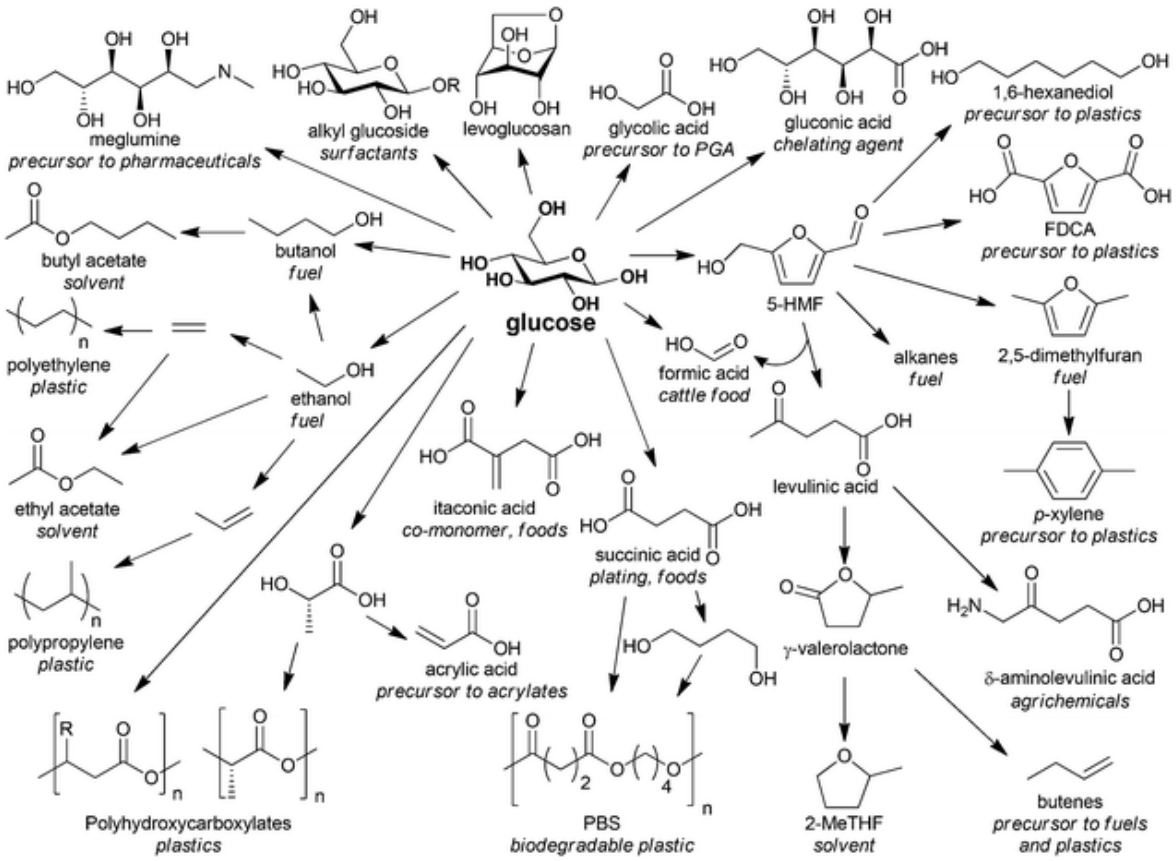

Figure 4. Derivatives of glucose and their applications

Glucaric acid, also known as saccharic acid, is a dicarboxylic acid with the formula $C_6H_{10}O_8$ and with four chiral centers. It belongs to the group of aldaric acids. Glucaric acid is found in fruits, vegetables and mammals and has been investigated for therapeutic applications in cholesterol and cancer-related diseases.[41] Potential commercial applications include use as a metal sequestering agent, retarding agent for metallic mordants in the dyeing of textiles, and corrosion inhibitor for metals.[42]

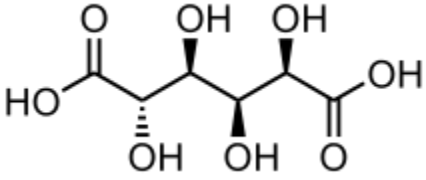

Figure 5. Glucaric acid structure

Glucaric acid was identified as a "top value-added chemical from biomass" in a report of the National Renewable Energy Laboratory, which also described its potential use as a building block for a number of polymers, including new nylons and hyperbranched polyesters.[43] Adipic acid (1,6-hexanedioic acid) and its derivative, ε-caprolactam, are mainly used as building blocks for polyamides (e.g., Nylon-6,6 and Nylon-6, respectively). The global annual productions of adipic acid and ε-caprolactam are 2.2 and 4 million metric tons, respectively.[44] In 2012, more than 90% of the global adipic acid production relied on the nitric acid oxidation of cyclohexanol or a mixture of cyclohexanol–cyclohexanone (KA-oil), all derived from fossil-based benzene.[45] The bio-based production of adipic acid, particularly from renewable resources, would be an attractive alternative that would address environmental concerns regarding the harsh chemicals used in the chemical production route. And here is where glucaric acid would play an important role in the future.

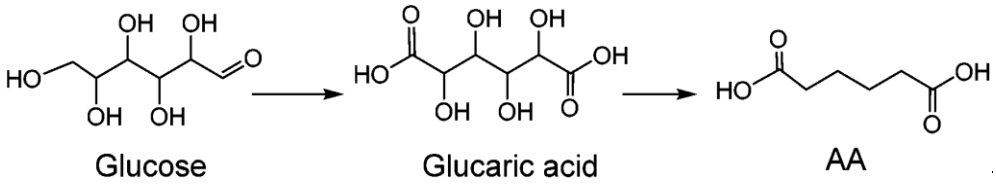

Figure 6. Schematic illustration of a two-step process for the production of adipic acid from glucose

Nowadays, glucaric acid is readily prepared by oxidation of glucose or starch with nitric acid.[46] The synthetic preparation of glucaric acid dates back to the 1888 report of Sohst and Tollens who carried out the nitric acid oxidation of glucose to glucaric acid, isolated as monopotassium glucarate.[47]

Figure 7. Nitric acid oxidation of glucose to glucaric acid

Although modest yields (40–45%) of glucaric acid are realized by nitric acid oxidation of glucose, the method remains attractive for commercialization because of its relative simplicity

with nitric acid serving as both solvent and source of the oxidizing agent. The generation of significant amounts of inorganic salts and toxic by-products (due to the partial decomposition of nitric acid to NO_x and N_2O) are the major issues confronting the sustainability of this current route.

For that reason, alternative processes have been developed. Microbial production of glucaric acid has been addressed by fermentation strategies and metabolic engineering in several studies. By modification of *Escherichia coli*, coexpression of 3 genes obtained from *Saccharomyces cerevisiae*, *Pseudomonas syringae* and mice led to production of glucuronic acid through the intermediate *myo*-inositol. Inclusion of uronate dehydrogenase (Udh) from the bacteria, facilitated the conversion of glucuronic acid to glucaric acid. The increased overall flux such that glucaric acid concentrations in excess of 1 g/L were observed.[48]

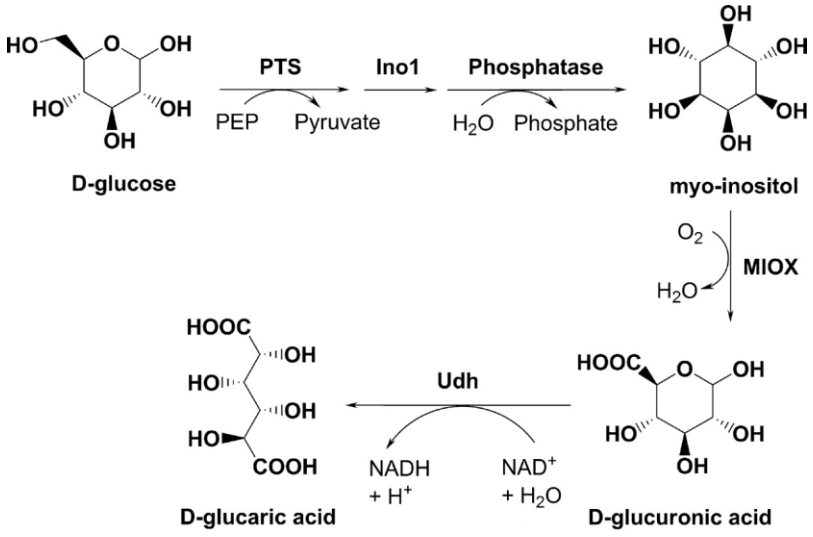

Figure 8. Enzymatic synthesis of glucaric acid using recombinant *E.coli*

Another approach is the use of 4-acetamido-TEMPO (2,2,6,6-tetramethyl pyperidine-1-oxyl) as a catalyst in the presence of an oxidant (sodium hypochlorite or potassium hypochlorite) and sodium or potassium bromide as co-catalyst. The oxidation process allowed the convenient conversion of glucose to glucaric acid in high yield (>90%), under strongly basic conditions.[49]

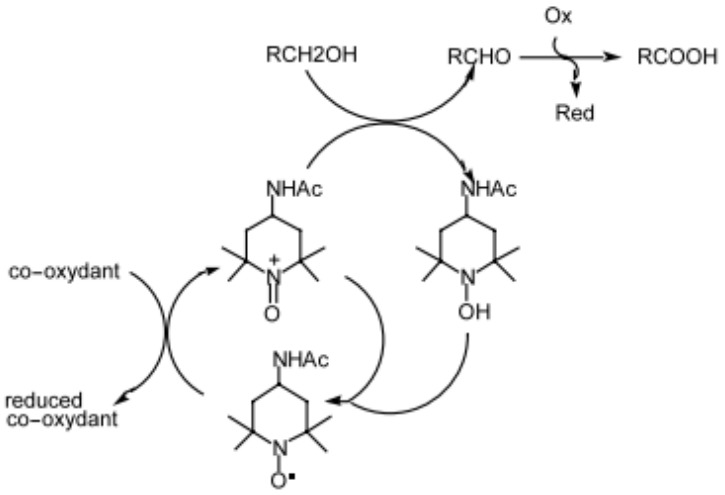

Figure 9. Redox system for TEMPO-like nitroxide mediated oxidations

The primary products are the dipotassium or disodium salts of glucaric acid. At pH values between 11.4 and 11.6, and at temperatures below 5°C, the nitroxide mediated oxidation of D-glucose yields glucaric acid salts with high selectivity and good yields (more than 85%, isolated as the monopotassium salt). Nonetheless, the drawbacks of this reaction are several such as: i) the salts obtained require further purification to glucaric acid generating large quantities of waste and ii) the oxidants used are expensive making this process less sustainable and environmentally benign.

The oxidation of glucose could also be achieved by electrocatalytic reaction to obtain gluconic acid and glucaric acid as main products. The reaction is performed in an electrocatalytic reactor using MnO_2 nanoparticles supported on porous of titanium oxide as anode and stainless-steel mesh as the cathode. A 99% of conversion of glucose with 15% selectivity to gluconic acid and 84% to glucaric acid are obtained at conditions of 30°C, neutral pH and a current 6 mA cm^{-2}.[50] The cost of scaling this technology must be justified despite the absence of oxidants or acid/base strong solutions.

1.3. **Use of gold nanoparticles for oxidation of glucose**

Platinum and palladium nanoparticles have been used and evaluated for the oxidation of glucose giving high yields to gluconic acid (80 – 99%). Pt generally deactivates and have relatively

low gluconic acid yield. Under weakly basic conditions, catalyst deactivation occurs due to the formation of platinum oxide (PtO_2). If the reaction is performed without base, higher temperatures are required for higher glucose conversion but the selectivity to gluconic acid decreases.[51] Deactivation and metal leaching of the metal have driven to explore other alternatives.

Rossi and co-workers were the first to investigate the use of gold nanoparticles in the oxidation of glucose to gluconic acid. The maximum selectivity (higher than 99%) towards gluconic acid was obtained in basic conditions of pH at 7-9.5 at 50°C. It was also demonstrated that Au have good resistance to leaching in pH higher than 9.5 since gold was not found on the reaction medium even after several runs.[52] Two years later, Claus and co-workers studied the influence of gold nanoparticles size using activated carbon as support. They obtained nanoparticles of 3-6 nm using sol immobilization method. It was demonstrated that enlarging the specific surface area, caused by a decrease in particle size, the catalytic activity was increased. In addition, by increasing the pH value of the reaction mixture from 7.0 to 9.5 (50°C), the initial reaction rate of gluconic acid formation could be accelerated by a factor of 3.2 (3.15 mmol $L^{-1}min^{-1}$ at pH 9.5 vs 1.00 mmol L^{-1} min^{-1} at pH 7.0) indicating that higher pH values obviously favor the adsorption of glucose on the catalyst surface.[53]

Since the formation of gluconic acid is of vital relevance as an intermediate for the oxidation to glucaric acid, a variety of gold-based heterogeneous catalysts have been explored for this purpose. Miedziak et al. used Au supported in MgO with a metal loading of 0.5% in base-free conditions since MgO acts as a base obtaining 100% selectivity to gluconic acid at 60°C for 24 h at atmospheric pressure.[54] Nevertheless, leaching of the support into the reaction medium makes it unsuitable for this application. On a subsequent study, Au/TiO_2 was investigated and they concluded that the catalyst prepared by immobilization method gave the highest conversion of glucose (88%) and gluconic yield (84%) with PVA:Au weight ratio of 0.1 (1 h reaction, 160°C, 3 bar O_2, 1000 rpm).

Very few studies have been reported dealing with the direct oxidation of glucose to glucaric acid because the subsequent oxidation of gluconic acid to glucaric acid is slow and difficult. The direct oxidation of glucose to glucaric acid has been reported by Rennovia Inc's patent with yields up to 70% for 5 h using supported mono and bimetallic Pt and Au catalysts on TiO_2, ZrO_2 and SiO_2 in the temperature range of 90-112°C under 27 bar O_2 pressure and neutral pH conditions.[55] Pt catalysts have been reported to achieve a maximum of 74% glucaric acid yield at initial pH of

7.2, 80°C, 13.2 bar O_2 but with a very high glucose:Pt molar ratio of 54:1.[56] Derrien et al. studied the effect of base-free conditions and demonstrated that Au-Pt alloy bimetallic nanoparticles supported on ZrO_2 with a crystallite size of 6 nm resulted in the most active catalyst, yielding 50% of glucaric acid but at very high pressure (under 40 bar of air, 100°C, Glucose:metal molar ratio of 80:1).[57] On the other side, Solmi et al. studied this reaction in more detail the reaction conditions (O_2 pressure, base concentration, quantity of catalyst and alloying Au with Bi in NPs) and concluding the need of basic environment (Glucose:NaOH molar ratio of 1:3) to take the parameters to milder conditions, lower reaction times and the possibility to carry out the reaction at higher metal molar ratios (Glucose:Me molar ratio of 500:1) compared to other studies or to Pt based catalysts.[58]

Studies have been performed to have a better insight into the reaction mechanism. In 2005, Rossi's team continued with the investigation and confirmed the formation of gluconate and hydrogen peroxide through a two-electrons mechanism (figure 10).The key point is represented by the electron rich gold species, formed by the hydrated glucose anion with gold surface atoms, which is supposed to activate molecular oxygen by nucleophilic attack. Supposing an efficient nucleophilic behavior determined by the electronic properties of nanometric gold particles (<10 nm). In the dioxogold intermediate either Au^{+}-O_2^{-} or Au^{2+}-O_2^{2-} couples can be formally considered as a bridge for the two electron transfer from glucose to dioxygen.[59] Saliger et al. proposed recently the use of H_2O_2 as oxidizing agent in glucose oxidation under alkaline conditions. They found that oxygen and hydrogen peroxide comprise the same rate-determining step leading to similar activation energies (48 kJ/mol for H_2O_2 and 47 kJ/mol for O_2 at 30-60°C range). It was assumed that O_2 formed by decomposition of H_2O_2 is the effective oxidizing agent.[60]

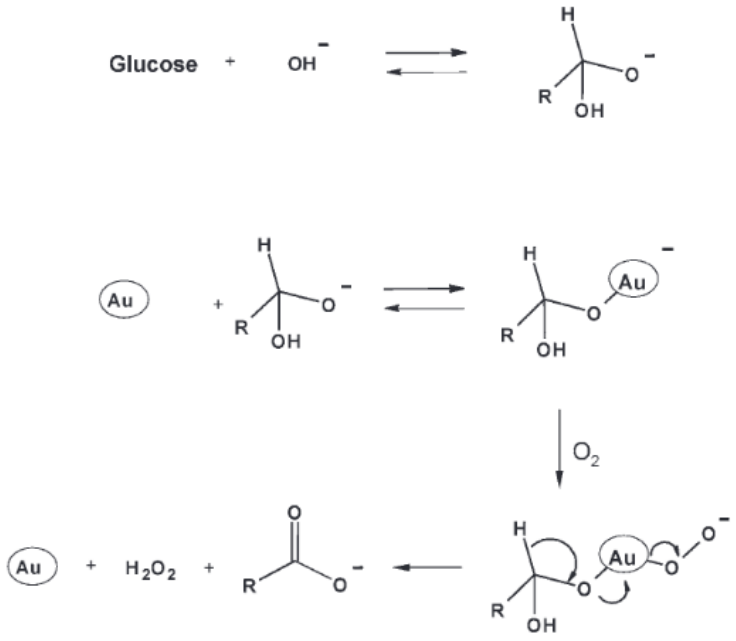

Figure 10. Proposed mechanism for alkali promoting effect in glucose oxidation and H_2O_2 formation as a reaction product

In addition, alkaline pH results in an increase of heterogeneous catalyst activity due to the stabilization of the particle size and preventing metal leaching in the reaction medium. Acidic conditions increase the selectivity to gluconic acid but suppresses enormously the oxidation reaction.[61] Efforts have been made to avoid the use of basic conditions in the oxidative reaction because of the promoting effect of hydroxyl groups in the isomerization of glucose to fructose and mannose. Despite this effect, it has been proved that OH groups on the surface of Au sites are required for a high yield of gluconic acid. Similar results were reported in base-free conditions but at much longer times (18 h).[36]

2. SCOPE

Gold catalysts have been proved to be stable and highly active capable to perform a wide range of reactions. As heterogeneous catalysts in liquid phase reactions, separation of products and catalyst result very convenient. Therefore, in this work preformed colloidal gold nanoparticles supported on activated carbon have been prepared following different experimental procedures of sol immobilization technique. The influence of the weight ratio of PVA to metal used in the colloidal formation and the heat treatment followed the deposition of the gold nanoparticles onto the support for stabilizing agent removal will be discussed. The catalysts have been characterized during the preparation by several spectroscopic techniques such as UV-VIS spectroscopy, X-Ray diffraction, TEM and TGA.

The catalytic activity of the catalysts has been evaluated through the liquid phase oxidation of glucose to glucaric acid using oxygen as oxidant, a high added value bio-based chemical. In addition, optimization of the reaction parameters conditions is investigated to obtain the maximum yield and selectivity toward glucaric acid at mild conditions. Assessment between characteristics of the catalyst and the catalytic activity have been discussed. Finally, zirconia oxide has been used as support for the preparation of gold-based catalyst and the catalytic activity has been compared against carbon-supported Au nanoparticles for investigating the role of weak and strong metal interactions and influence of support (oxide versus carbon).

3. EXPERIMENTAL PART

The experimental work is divided into four main sections:

- *Synthesis of catalysts:* Using different experimental procedures of sol immobilization technique, varying PVA:Au weight ratio in gold colloidal formation and two methodologies for the removal of stabilizing agent, gold nanoparticles supported on activated carbon and zirconium oxide are prepared and analyzed by UV-VIS spectroscopy, XRD, TEM and TGA.

- *Optimization of reaction conditions:* Different parameters such as stirring rate, Glu:Au molar ratio and reaction time are evaluated to identify key conditions to increase the yield and selectivity to glucaric acid.

- *Screening of catalysts:* The catalysts are tested in the oxidation of glucose utilizing the optimized conditions obtained in this work to correlate the structure – activity relationship.

- *Effect of the support:* activated carbon and zirconium oxide are used as support and the catalytic activity of both catalysts is compared to evaluate a possible effect in the oxidation reaction.

3.1. **Reagents**

In the table 1 are shown the chemical reagents used in the preparation of catalysts, oxidation reaction experiments and calibration curve solutions for HPLC.

Compound	**Formula**	**Molecular weight (g/mol)**	**Purity**
Glucose	$C_6H_{12}O_6$	180.16	>99%
Gluconic acid	$C_6H_{12}O_7$	196.16	97%
Glucaric acid	$C_6H_{10}O_8$	210.14	98%
Oxalic acid	$C_2H_2O_4$	90.03	>99%
Tartaric acid	$C_4H_6O_6$	150.09	>99%
Tartronic acid	$C_3H_4O_5$	120.06	>97%
Lactic acid	$C_3H_6O_3$	90.08	85%
Formic acid	CH_2O_2	46.02	>95%
Glyceric acid	$C_3H_6O_4$	106.08	>97%
Glycolic acid	$C_2H_4O_3$	76.05	99%
Arabinose	$C_5H_{10}O_5$	150.13	>98%
Fructose	$C_6H_{12}O_6$	180.16	≥99%
Mannose	$C_6H_{12}O_6$	180.16	99%
2-keto-D-gluconic acid (2KDG)	$C_6H_{10}O_7$	194.139	99%
5-keto-D-gluconic acid (5KDG)	$C_6H_{10}O_7$	194.139	98%
Mesoxalic acid	$C_3H_2O_5$	118.045	98%
Tetrachloroauric acid trihydrate	$HAuCl_4*3H_2O$	393.83	>99%
Polyvinyl alcohol	$(C_2H_4O)_n$	13.000-23.000	87-89% hydrolyzed
Sodium borohydride	$NaBH_4$	37.83	98%
Sodium hydroxide	NaOH	39.99	>98%
Activated carbon NORIT SX1G	Carbon	/	Information not provided
ZrO_2	ZrO_2	123.21	Information not provided

Table 1. Reagents used for catalyst preparation, oxidation reaction of glucose and calibration curves for HPLC

3.2. **Preparation of catalysts**

Supported gold catalysts were prepared following four different procedures by sol immobilization technique to produce a catalyst with nominal metal loading of 1% wt.

Method A

For the preparation of 1 g of catalyst, 0.02 g of $HAuCl_4*3H_2O$ were dissolved in 100 ml of distilled water (200.85 mg/l of gold precursor – 0.51 M Au). Then, 0.643 ml of PVA solution (0.1010 g/ml) were added as a stabilizing agent (PVA:Au = 0.5:1 weight ratio). After 3 min, 0.0077 g of sodium borohydride were added to the solution under stirring ($NaBH_4$:Au = 4:1 molar ratio) to obtain a dark red colloidal solution. The pH of the solution was adjusted to 2 by the addition of concentrated sulfuric acid. Three minutes later, 0.9947 g of support (activated carbon or ZrO_2) was added to the solution to immobilize the gold nanoparticles. The reaction was set under stirring at room temperature for 4 h. The catalyst was filtered using a Buchner funnel with two filter papers. The slurry was washed with distilled water until the washing water reached pH 6-7. The solid was dried overnight in a watch glass at room conditions. Then, a suspension was done with the catalyst in 20 ml of distilled water and kept at 60°C for 4 h under stirring. The catalyst was again filtered as previously and let dry overnight. Finally, the solid was dried in an oven at 80°C for 4 h.

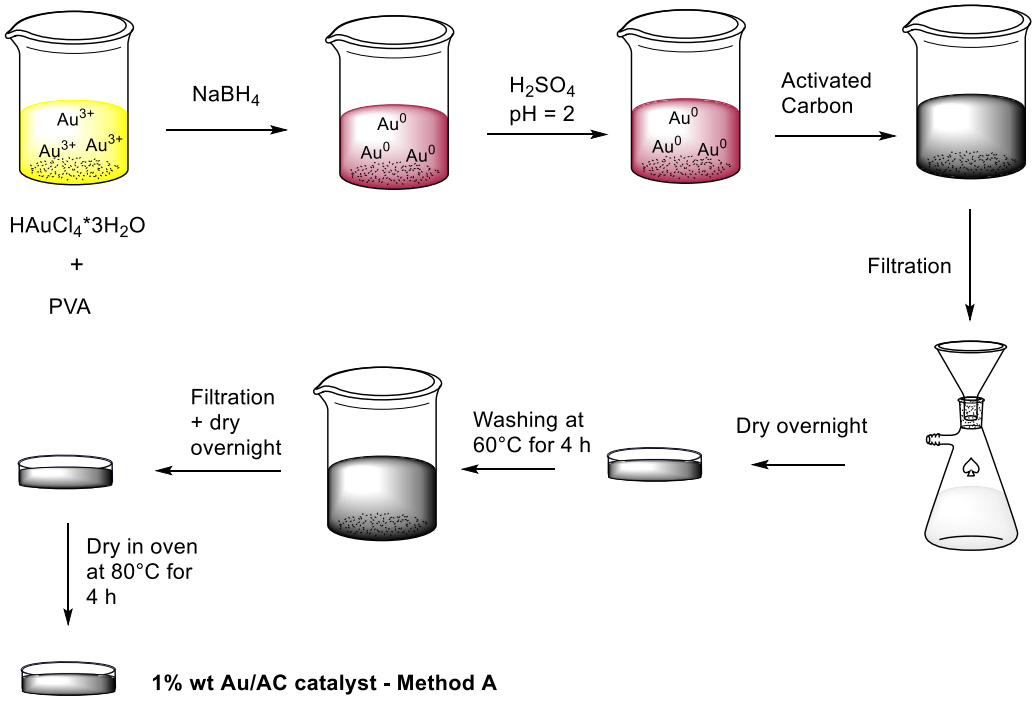

Figure 11. Scheme of Method A for preparation of gold-based catalyst (reference catalyst). Same procedure applies to Au supported in ZrO_2.

Method B

For the preparation of 1 g of catalyst, 0.0209 g of $HAuCl_4*3H_2O$ were dissolved in 390 ml of distilled water (53.58 mg/l of gold precursor – $1.30 * 10^{-4}$ M Au). Then, 0.497 ml of polyvinyl alcohol (PVA) solution (0.1010 g/ml) were added as a stabilizing agent (PVA:Au = 0.65:1 weight ratio). After 3 min, 0.0096 g of sodium borohydride dissolved in 2.5 ml of water were added to the solution under stirring ($NaBH_4$:Au = 5:1 molar ratio) to obtain a red colloidal dispersion. 30 minutes later, 0.99 g of activated carbon was added to the solution to immobilize the gold nanoparticles. The pH of the solution was adjusted to 2 by the addition of sulfuric acid concentrated. The reaction was set under stirring at room temperature for 1 h. The catalyst was filtered using a Buchner funnel with two filter papers. The slurry was washed with distilled water until the washing water reached pH 6-7. The solid was let dry overnight in a watch glass at room conditions. The catalyst was treated with heat in a flow reactor increasing 5°C per minute until reached 120 - 250°C with air for 2 h, then N_2 for 30 min and finally, 1 h in H_2 atmosphere with a flow of 20 ml/min.

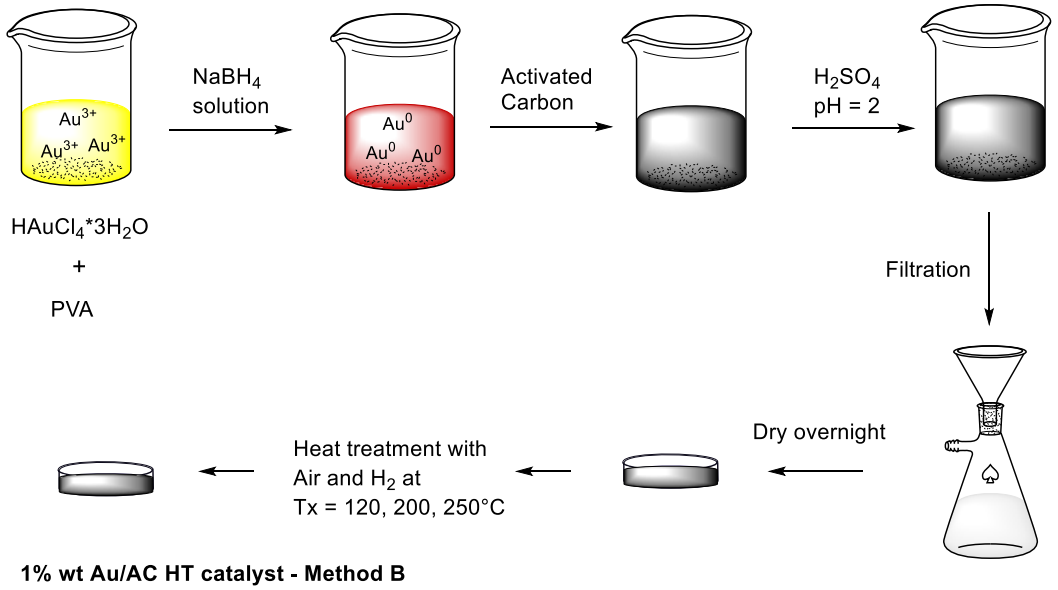

Figure 12. Scheme of Method B for preparation of gold-based catalyst with heat treatment (120-250°C) with air/H_2

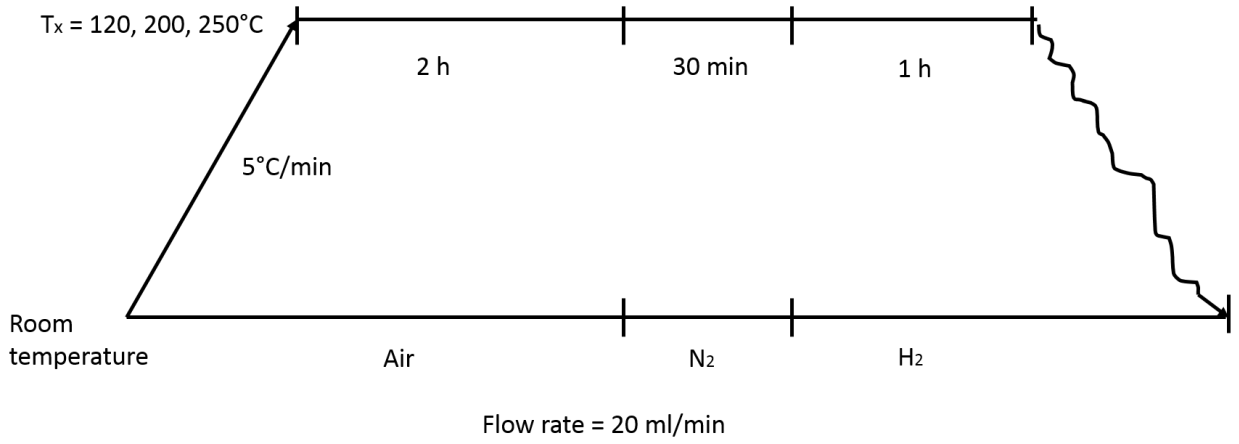

Figure 13. Schematic process of heat treatment of catalysts

Method C

For the preparation of 1 g of catalyst, 0.0209 g of $HAuCl_4*3H_2O$ were dissolved in 390 ml of distilled water (53.58 mg/l of gold precursor – $1.30 * 10^{-4}$ M Au). Then, 0.497 ml of polyvinyl alcohol (PVA) solution (0.1010 g/ml) were added as a stabilizing agent (PVA:Au = 0.65:1 weight ratio). After 3 min, 0.0096 g of sodium borohydride dissolved in 2.5 ml of water were added to the solution under stirring ($NaBH_4$:Au = 5:1 molar ratio) to obtain a red colloidal dispersion. 30 minutes later, 0.99 g of activated carbon was added to the solution to immobilize the gold nanoparticles. The pH of the solution was adjusted to 2 by the addition of sulfuric acid concentrated. The reaction was set under stirring at room temperature for 1 h. The catalyst was filtered using a Buchner funnel with two filter papers. The slurry was washed with distilled water until the washing water reached pH 6-7. The solid was let dry overnight in a watch glass at room conditions. Then, a suspension was done with the catalyst in 20 ml of distilled water and kept at 60°C for 4 h under stirring. The catalyst was again filtered as previously and let dry overnight. Finally, the solid was dried in the oven at 80°C for 4 h.

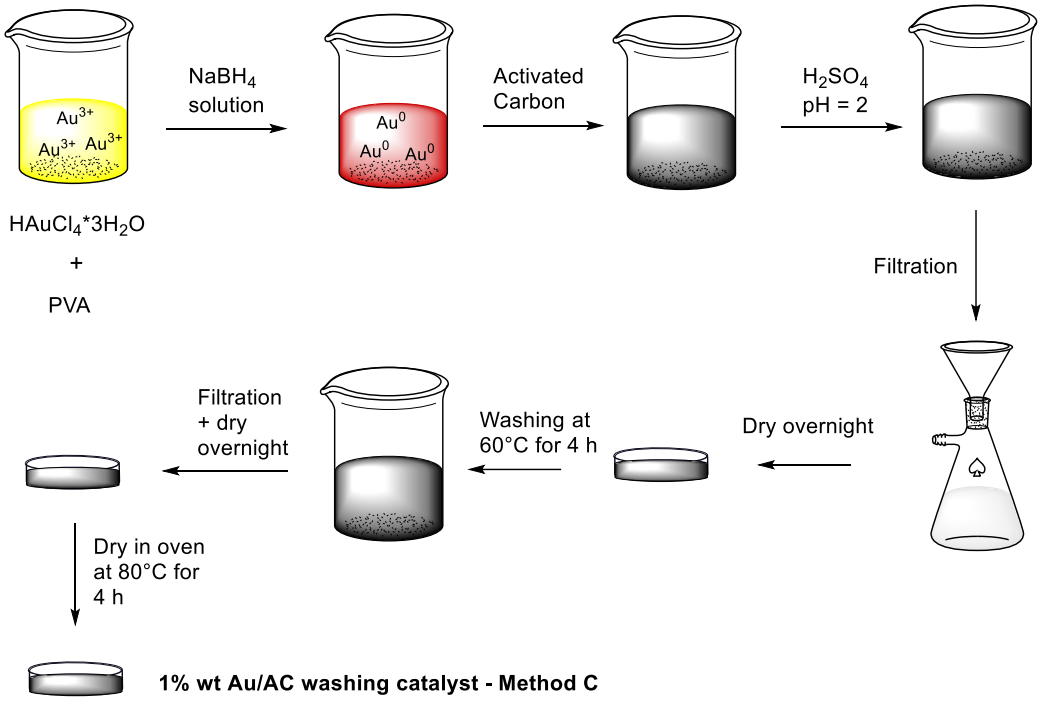

Figure 14. Scheme of Method C for preparation of gold-based catalyst with water washing at 60°C

Method D

For the preparation of 1 g of catalyst, 0.0209 g of $HAuCl_4*3H_2O$ were dissolved in 390 ml of distilled water (53.58 mg/l of gold precursor – $1.30 * 10^{-4}$ M Au). Then, polyvinyl alcohol (PVA) solution (0.1010 g/ml) was added (PVA:Au = 0:1, 0.3:1, 0.6:1, 1.2:1 and 2.4:1 weight ratio). After 3 min, 0.0096 g of sodium borohydride dissolved in 2.5 ml of water were added to the solution under stirring ($NaBH_4$:Au = 5:1 molar ratio) to obtain a red colloidal dispersion. 30 minutes later, 0.99 g of activated carbon was added to the solution to immobilize the gold nanoparticles. The pH of the solution was adjusted to 2 by the addition of sulfuric acid concentrated. The reaction was set under stirring at room temperature for 1 h. The catalyst was filtered using a Buchner funnel with two filter papers. The slurry was washed with distilled water until the washing water reached pH 6-7. The solid was let dry overnight in a watch glass at room conditions. Then, the solid was dried in an oven at 80°C for 4 h.

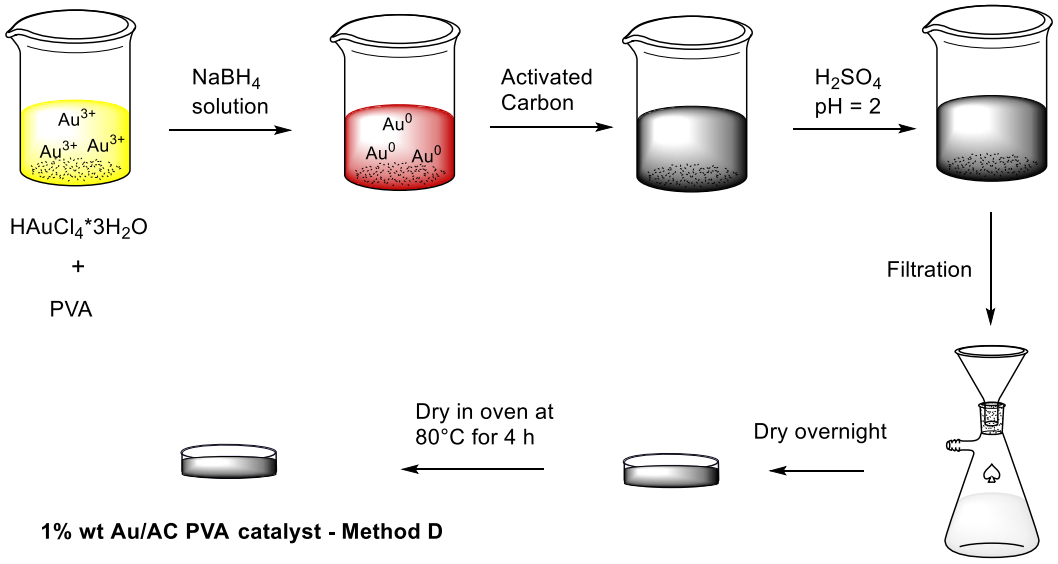

Figure 15. Scheme of Method D for preparation of gold-based catalyst Au/AC PVA

In the table below are summarized all the synthesized catalysts with their characteristics:

Catalyst	**Method preparation**	**PVA:Au weight ratio**	**$NaBH_4$:Au molar ratio**	**Treatment**
Au/AC	Method A	0.5:1	4:1	Washing with water at 60°C
Au/AC HT120°C	Method B	0.65:1	5:1	Heat treatment at 120°C with Air and H_2
Au/AC HT200°C	Method B	0.65:1	5:1	Heat treatment at 200°C with Air and H_2
Au/AC HT250°C	Method B	0.65:1	5:1	Heat treatment at 250°C with Air and H_2
Au/AC washing	Method C	0.65:1	5:1	Washing with water at 60°C
Au/AC PVA0	Method D	0:1	5:1	Drying at 80°C for 4 h
Au/AC PVA0.3	Method D	0.3:1	5:1	Drying at 80°C for 4 h
Au/AC PVA0.6	Method D	0.6:1	5:1	Drying at 80°C for 4 h
Au/AC PVA1.2	Method D	1.2:1	5:1	Drying at 80°C for 4 h
Au/AC PVA2.4	Method D	2.4:1	5:1	Drying at 80°C for 4 h
Au/ZrO_2	Method A	0.5:1	4:1	Washing with water at 60°C

Table 2. List of catalysts prepared by four different procedures of sol immobilization

3.3. **Characterization of catalysts**

The catalysts were characterized during the preparation steps using UV-Vis spectroscopy to observe the formation of colloidal gold through the plasmonic resonance effect. Once the catalyst is fully prepared, X-ray diffraction was performed to observe the crystallographic phases of the gold nanoparticles and estimate the crystallite size. TGA and TEM was done in selected catalysts.

3.3.1. ***UV-VIS spectroscopy***

UV-Vis spectroscopy is a very common technique for the electronic transitions of atoms or molecules. Routinely used in analytical chemistry for the quantitative determination of transition metals, highly conjugated organic molecules and biological macromolecules in liquid samples but also in gaseous or solids samples can be studied.

Transition metal ions can be easily followed through UV-Vis spectroscopy. Metal ions in polar solvents form coordination complexes. From these interactions, electronic transitions can occur known as metal-to-ligand transfer. When zero valent metals interact with photons, the electrons oscillate and a change to longer wavelengths of absorption takes place.

The spectrometer measures the intensity of light passing through the sample (I) and compares the intensity of the light before passing through the sample (I_0). The ratio of these two intensities is transmittance. The absorbance is related to transmittance by the following equation:

$$A = -log\frac{T}{100}$$

A = absorbance

T = transmittance

Usually, the source of irradiation comes from a Tungsten filament for the visible range (350 – 2500 nm) and a deuterium lamp for the ultraviolet range (190 – 400 nm). Then, a monochromator is placed to split the light in different wavelengths. The radiation can reach the sample in two different set up: single beam or double beam. In a double beam instrument, the light

is split into two beams. One beam is used as the reference and the other passes through the sample. The reference beam intensity is taken as 0 absorbance and the ratio of the two beam intensities is displayed.

The spectrometer used to observe the plasmon resonance peak related to the metallic gold nanoparticles was a Perkin Elmer UV-VIS-NIR Lambda 19 from 750 nm to 190 nm wavelength.

3.3.2. ***XRD (X-ray Diffraction)***

X-ray diffraction is a largely used technique that allows to obtain information regarding the crystalline phase, crystallite size, etc. Electrons vibrate under the electric field generated by the x-ray beam, they backscatter a beam with the same wavelength as the incident beam. X rays waves have to be in phase with each other to have constructive interference. If these conditions are not met, the destructive interference reduces the reflected intensity to zero. Bragg's law gives the conditions needed for diffraction making possible to calculate the planes in crystal lattice and therefore, obtain the crystallographic structure, lattice distance, etc.

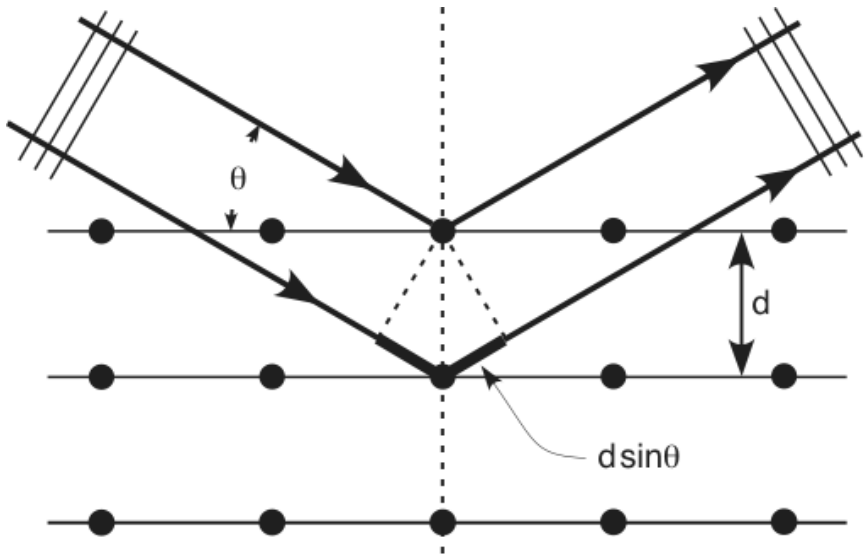

Figure 16. X-ray diffraction on a crystal lattice

$$n\,\lambda = 2\,d\,sin\theta$$

n = integer (diffraction order)

λ = wavelength of the x-rays

d = distance between adjacent planes in the lattice

θ = incident angle of the x-ray beam

The width of the peaks can help us in the determination of the size strain. If the peaks are wide, the crystallite size is small in comparison to a crystallite estimated from a narrow peak. Simplifying, the crystallite size is inversely proportional to the width peak. The Scherrer Equation estimate the size of the crystallite:

$$FWHM(2\theta) = \frac{K\,\lambda}{L\,cos\theta}$$

FWHM = Full Width Half Maximum

λ = wavelength

L = crystallite size

K = the Scherrer constant

This means that peak width (FWHM) varies inversely with crystallite size. As the crystallite size gets smaller, the peak gets broader. The crystallite size broadening is most pronounced at large angles 2Theta. The constant of proportionality, K (the Scherrer constant) depends on how the width is determined, the shape of the crystal, and the size distribution.

Through this analytical technique it was possible to estimate the average dimensions of the gold NPs deposited on the support. XRD analysis were performed with a Bragg-Brentano X'pertPro Panalytical diffractometer using a copper anode (K_α radiation at λ = 1.5418 Å) as source of X-radiation with 0.08° step size and acquisition time of 1300 s per step in 36 - 41° 2θ range. The average gold crystallite size of Au/AC catalysts was calculated from the broadening of the (111) Au plane at 38.2° applying Scherrer's equation.

3.3.3. ***TEM (Transmission electron microscopy)***

Transmission electron microscopy is an analytical technique used for the characterization of surfaces with very high resolution obtained by the transmission of electrons through the sample to form the image. The technique involves sending an electron beam on a sample under vacuum conditions (10^{-4} Pa), in the absence of vibrations and external magnetic fields. The sample consists of a section of a few nanometers of the starting material. Standard TEM grid sizes are 3.05 mm diameter, with a thickness and mesh size ranging from a few to 100 μm. The sample holder is made of copper, molybdenum, gold or platinum with approximately 2.5 mm diameter. The electron source is a tungsten filament that generates electrons through thermionic emission. These are accelerated by an electric potential (100-300 keV), collimated and finally focused on the sample thanks to the use of special lenses. The generated electrons interact with the surface of the sample and a part of them is transmitted without undergoing interaction with the sample. This fraction of electrons is captured by a fluorescent screen on which is obtained a real and enlarged image of the sample.

The TEM images will serve for the calculation of average particle diameter (size), standard deviation and particle size distribution by frequency (%). For every distribution over 300 particles where used from the total number of measured particles (>400 particles) per sample. TEM analysis were performed with TEM/STEM FEI TECNAI F20 microscope at 200 keV. Samples were suspended in ethanol and treated by ultrasound for 15 min. A drop of the suspension was deposited on "quantifoil-carbon film" supported by a grid of Cu. The preparation was dried at 120°C.

3.3.4. ***TGA (Thermogravimetric analysis)***

Thermogravimetric analysis is a technique in which the mass of a sample is monitored against time or temperature. Thermogravimetry was developed around 1900 and basically involves the mass determination of a sample under controlled isothermal or linearly varying temperature in a given atmosphere. A plot of mass as a function of time or temperature is the result of a thermogravimetric experiment. The first derivative of the TGA curve (the DTG curve) may plotted to determine inflection points useful for in-depth interpretations as well as differential thermal

analysis. A block diagram of a typical thermogravimetric apparatus is shown in Figure 17. Sensitivities are usually several micrograms. Total sample masses may range from milligrams to grams. Temperature ranges are usually from room temperature to as high as 2700 K. Major applications of thermogravimetry involve stability analysis of materials in different atmospheres or vacuum.

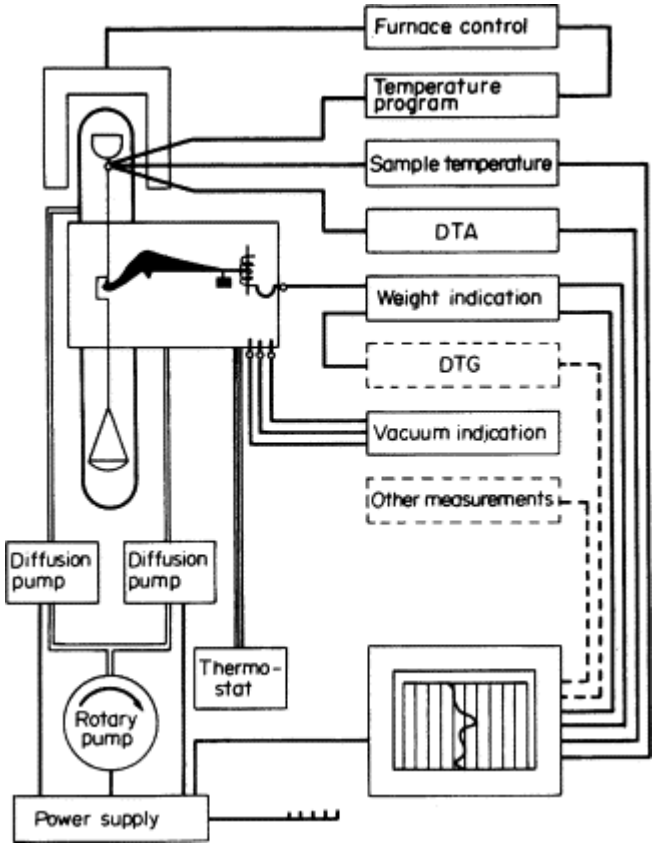

Figure 17. Schematic diagram of a thermogravimetry apparatus with differential thermogravimetry (DTG) facility

To observe the PVA presence on the surface of the catalyst, TG analysis were performed with a RA STD 600 analyzer heating from 20 to 400°C for 1 hour with a heating rate 10°C/min with air (flow 100 ml/min).

3.4. **Oxidation reaction**

3.4.1. Reactor

The oxidation reaction experiments were performed in an autoclave batch reactor of 50 ml capacity. The reactor consists of a stainless-steel vessel connected to the top cover via flanged junction. The reactor has coupled a pressure gauge, a hollow steel capillary for the introduction of a thermocouple (the thermocouple is not in direct contact with the solution inside the reactor), a load line and a discharge line, both controlled by an interception valve.

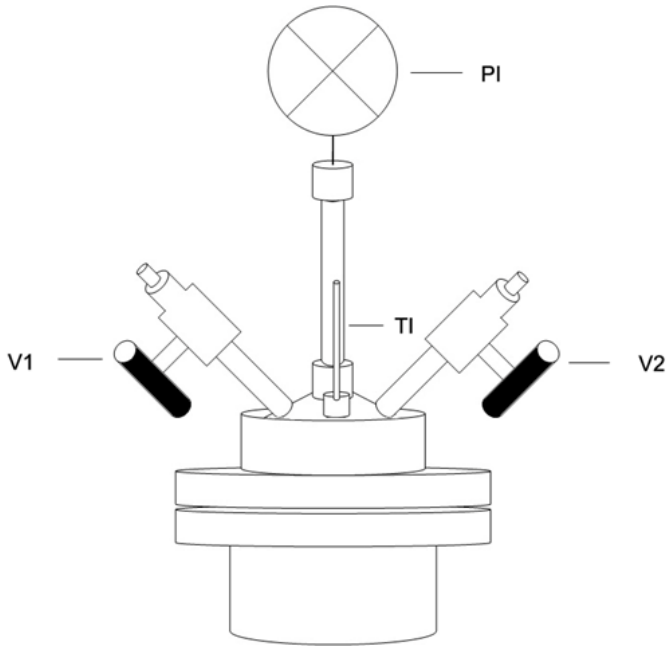

Figure 18. Drawing of the batch reactor used in the oxidation of glucose

PI: Pressure gauge WIKA 315SS (0-25 bar)

V1: Valve for the load line

V2: Valve of discharge line

TI: Capillar tube for insertion of thermocouple

3.4.2. Solution preparation and conditions

The reaction solution consists of 0.7895 g of glucose dissolved in 15 ml of water to obtain a solution of 5% wt of glucose (0.29 M Glucose). Then, 0.5263 g of sodium hydroxide were added to obtain a proportion Glu:NaOH of 1:3; and the catalyst was added. After adding the reagents and catalyst to the vessel, a magnetic agitator was introduced to maintain the solution under stirring. The vessel was tightly closed and 10 bar of gaseous oxygen (as oxidant agent) was loaded. The reactor was placed in contact with a heating mantle that allows to reach the set-point temperature (60°C) by means of feedback heating control with the thermocouple. The magnetic stirring was activated in order to guarantee diffusion and homogeneity of the reagents. Once the solution had reached 60°C, the solution reaction was kept under these conditions. To finalize the reaction, the reactor was cooled down by placing it on ice bath.

3.4.3. Sample treatment

The reaction mixture was collected and centrifuged at 4500 rpm for 15 min to separate the liquid from the catalyst. The final volume was measured and a sample was taken for subsequent analysis and storage. The catalyst was left dry at ambient conditions overnight.

3.4.4. Analysis of products

The quantitative analysis of the samples taken from the reaction mixture were performed using HPLC instrument.

3.4.4.1. ***HPLC (High-performance liquid chromatography)***

HPLC is a specific form of column chromatography generally used in chemistry and analysis to separate, identify, and quantify organic compounds. HPLC mainly utilizes a column that holds packing material (stationary phase), a pump that moves the mobile phase(s) through the column, and a detector that shows the retention times of the molecules. Retention time varies

depending on the interactions between the stationary phase, the molecules being analyzed, and the solvent(s) used.

The sample to be analyzed is introduced in small volume to the stream of mobile phase and is retarded by specific chemical or physical interactions with the stationary phase. The amount of retardation depends on the nature of the analyte and composition of both stationary and mobile phase. The time at which a specific analyte elutes (comes out of the end of the column) is called the retention time. Common solvents used include any miscible combinations of water or organic liquids. Columns are packed with small diameter porous particles. Usually the size of the porous materials used are 1,6 – 5 μm. The column packings used in chromatography are silica gel, charcoal and alumina. This kind of columns have an efficiency about 10,000 plates per column. Typically, the column is 10 - 25 cm long and 4.6 mm in internal diameter. The porous particles in the column usually have a chemically bonded phase on their surface which interacts with the sample components to separate them from one another. The process of retention of the sample components is determined by the choice of column packing and the selection of the mobile phase to push the analytes through the packed column. Although columns are expensive, they are reusable, so the cost can be spread over a large number of samples. The column and all the associated plumbing are able to withstand the pressures used, and also chemically resistant to the mobile phase solvents. Columns are usually made of stainless steel, although glass or plastic are used by some manufacturers.

Generally, UV spectroscopy is attached to detect specific compounds. Many organic compounds absorb UV light of various wavelengths. Such solutes include alkenes, aromatics and compounds having multiple bonds between C and O, N or S. The amount of light absorbed will depend on the amount of a particular compound that is passing through the beam at the time. Another type of detector uses the difference in Refractive Index (RI) between the column eluent and a reference stream of pure mobile phase. They are the closest to an universal detector, as any solute can be detected as long as there is a difference in RI between the compound of interest and the mobile phase.

Figure 19. HPLC instrument used in the analysis of reaction mixture solutions

The reaction mixture quantitative analyses were carried out using an Agilent 1260 Infinity Quaternary HPLC system. Analyses were performed using 0.0025 M sulfuric acid in ultra-pure water as eluent with a flow of 0.5 ml/min. The injection system consisted of a six-way valve with an injection volume of 20 μl. Two Rezex ROA-H+ (8%) 300x7.8 mm ion exclusion columns connected in serie were used for the separation of products. A diode array detector (DAD) set to 202 nm was used to detect organic acids and a refractive index detector (RID) was used to detect monosaccharides. The column compartment was thermostated at 80°C while the RID was kept at a constant temperature of 40°C.

3.4.5. Calculation of reaction products concentration

Calibration curves were done by the analysis of concentrate and diluted solutions (1:2, 1:10 and 1:20) of glucose and main reaction products (glucaric acid, gluconic acid, glycolic acid, tartronic acid, tartaric acid, oxalic acid, lactic acid, 2-keto-D-gluconic acid, 5-keto-D-gluconic acid, fructose, mannose, arabinose, formic acid, glyceric acid and mesoxalic acid) in HPLC instrument under the conditions presented previously.

For the estimation of moles of reaction products, the area's peak of the chromatogram was divided by the response factor (slope of the calibration curve obtained):

$$n_i = \frac{A_i}{m_i} * \frac{v}{1000}$$

n_i = number of moles of compound (i)
A_i = area of the peak corresponding to the compound (i)
m_i = response factor of the compound (i)

Gluconic acid (GO) and glucose peak overlapped in HPLC chromatograms and considering that glucose quantification in DAD is not relevant, the quantification of glucose was calculated by subtracting the GO concentration obtained with DAD from the total GO and glucose concentrations obtained with RID. The final glucose moles can be calculated with the following equation:

$$n_{glucose} = \frac{A_{RID\ GO+GLU} - \frac{A_{DAD\ GO}}{m_{DAD\ GO}} * m_{RID\ GO}}{m_{RID\ GLU}} * \frac{v}{1000}$$

$n_{glucose}$ = moles of glucose
$A_{RID\ GO+GLU}$ = Area of the peak in RID chromatogram related to gluconic acid and glucose
$A_{DAD\ GO}$ = Area of the peak in DAD chromatogram related to gluconic acid
$m_{DAD\ GO}$ = response factor of gluconic acid in DAD
$m_{RID\ GO}$ = response factor of gluconic acid in RID
$m_{RID\ GLU}$ = response factor of glucose in RID

Glyceric acid and arabinose peaks also overlapped but in this case it was not possible to perform a similar estimation as in the case of Glucose-GO mixtures, because there was no proportion between the theoretical sum of single areas and the area of GC peaks. Since these two compounds had a response factor similar to that of the RID detector, both were quantified by using an average response factor applying the formula:

$$C_{glyceric\ acid+arabinose} = \frac{A_{\ RID\ glyceric\ acid+arabinose}}{\frac{m_{\ arabinose} + m_{glyceric\ acid}}{2}} * \frac{v}{1000}$$

$C_{glyceric\ acid+arabinose}$ = Concentration of glyceric acid and arabinose in the solution

m = response factor

v = volume of the reaction mixture

$A_{RID\ glyceric\ acid+arabinose}$ = the peak's area corresponding to glyceric acid and arabinose

Glucose conversion is defined as the moles of glucose converted to the moles of glucose initially charged into the reactor, so the conversion was calculated with the following equation:

$$X = \frac{n_{glucose\ (t=0)} - n_{glucose(t=f)}}{n_{glucose(t=0)}} * 100$$

X = glucose conversion

$n_{glucose(t=0)}$ = initial number of moles of glucose

$n_{glucose(t=f)}$ = final number of moles of glucose

The yield is defined as the amount of product formed (e.g., glucaric acid) to the initial amount of glucose. The yield for a specific product was calculated by dividing the number of moles generated of that compound by the initial number of glucose moles, normalized with respect to the number of C atoms (carbons of the product molecule over carbons of glucose).

$$Y_i = \frac{n_i * C_f}{n_{\ glucose\ (t=0)}} * \frac{v}{1000} * 100$$

$$C_f = \frac{atoms\ of\ Carbon\ in\ the\ molecule\ of\ the\ product}{atoms\ of\ Carbon\ in\ glucose}$$

Y = yield of the product (i)

n_i = number of moles of the product (i)

$n_{glucose(t=0)}$ = initial number of moles of glucose

v = volume of the reaction mixture

C_f = normalization factor for carbon atoms based on the substrate

The selectivity to a specific compound was calculated by dividing the yield to that compound by glucose conversion.

$$S_i = \frac{Y_i}{X_i} * 100$$

S = selectivity of the product (i)

v = volume of the reaction mixture

C balance was calculated by summing the selectivity to all quantified products.

$$C_{balance} = \sum S_i$$

4. RESULTS AND DISCUSSION

4.1. Synthesis and characterization of catalysts

The catalysts were synthesized as described in section 3. Figure 20 shows a picture of gold precursor (cationic gold) in solution and the characteristic red color of gold nanoparticles present in all samples.

Figure 20. Gold precursor in solution (left) and colloidal solution of gold nanoparticles (right)

The spectrum of gold precursor shows a characteristic peak at 300 nm corresponding to gold hydrolyzed complexes (figure 21). Aut0 and Aut1 correspond to the spectra after 3 and 25 minutes of $NaBH_4$ addition, respectively. The spectra display a plasmon peak at approximately 502 nm being characteristic of the surface plasmon resonance of Au metal fine particles. It can be deduced that the size of the gold nanoparticles remains constant while the precursor reduces in the colloidal solution.

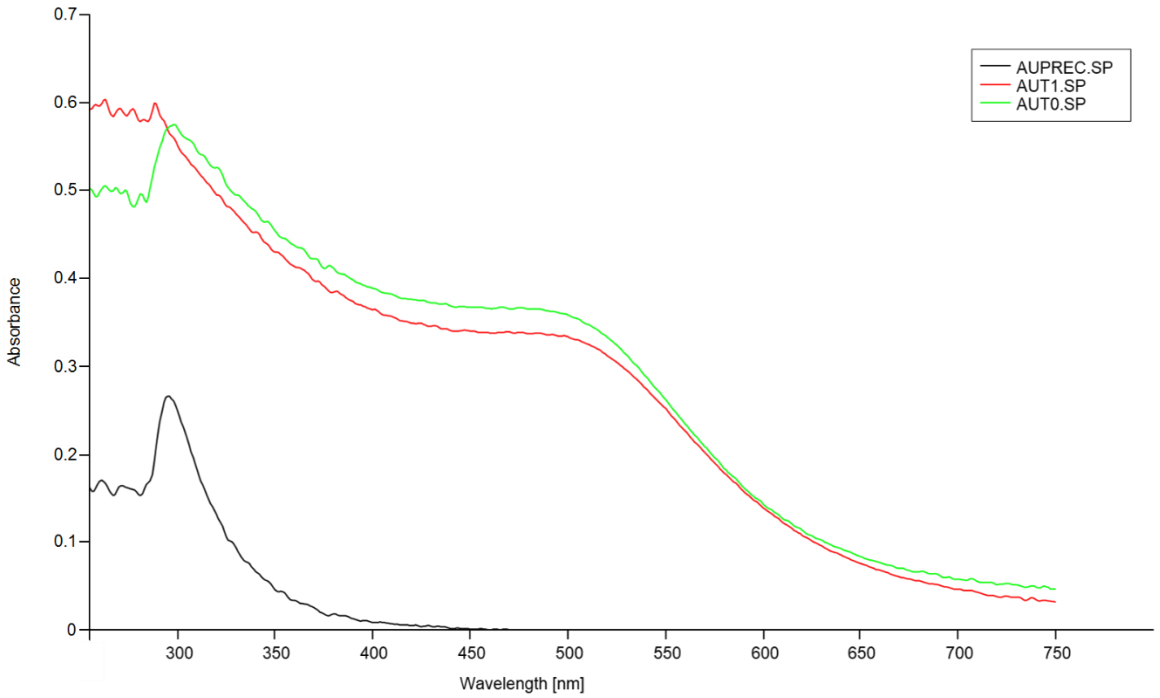

Figure 21. UV-VIS spectra of gold precursor and gold nanoparticles

Figure 22 presents the UV–vis absorption spectra of all synthesized Au colloids. An intense absorption in the 503 – 515 nm region is present in all samples. The position, intensity and width are strongly dependent on the size and shape of the Au particles, as well as of the dielectric properties of the surrounding environment. The spectra corresponding to samples PVA0 and PVA0.3 show a defined peak around 515 nm while the rest of the samples (PVA0.6, PVA0.65, PVA1.2 and PVA2.4) show a less pronounced plasmon resonance peak and a blue shift of approximately 12 nm which can be related to the formation of smaller nanoparticles.[36] Colloidal gold is red when the corresponding nanoparticles are smaller than 20 nm. Independently of the procedure for colloidal formation, we can deduce that gold particles are present in dimensions below or around 20 nm.

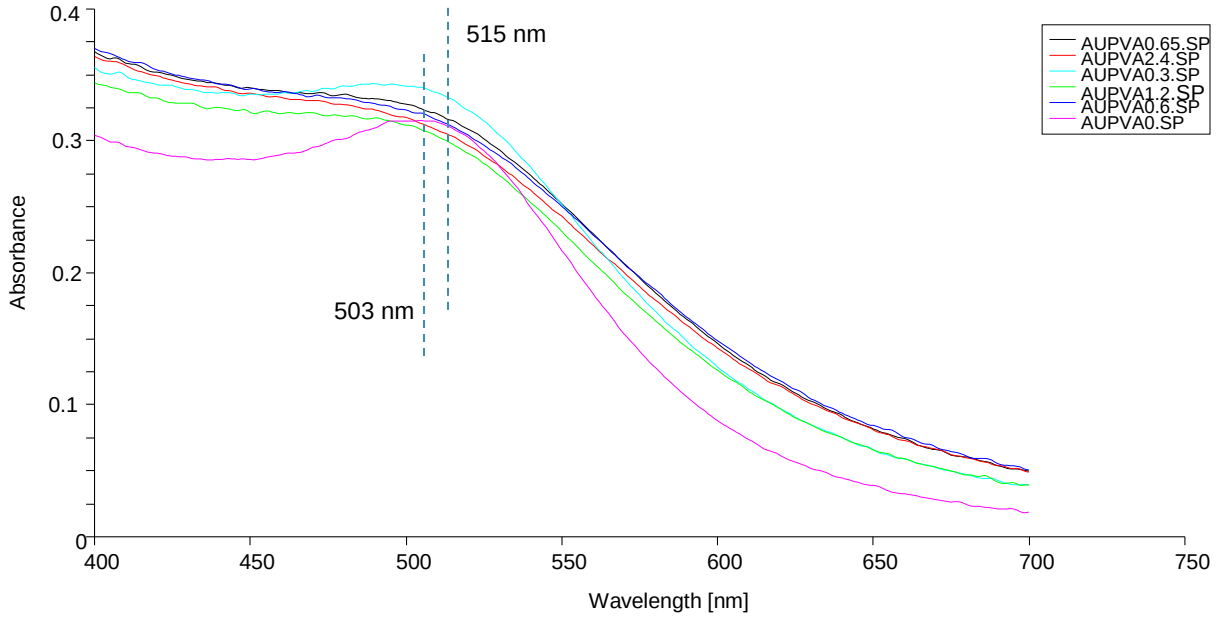

Figure 22. UV-VIS spectra of gold colloids formed by different PVA:Au weight ratio

After the immobilization step (addition of support) and post treatment, the catalysts were submitted to a series of analysis. XRD patterns are shown in figures 23, 24 and 25. The diffraction peak taken for further discussion and analysis is the peak with highest intensity at 38.2° 2θ. Besides the intensity at this 2θ angle was not overlapping with the XRD pattern of AC present in all the figures for comparison. XRD pattern (figure 24) clearly show a broadening of the diffraction peak at 38.2° 2θ as PVA concentration increases. Similar behavior is observed in figure 25 where the broadening of the diffraction peak increases as the temperature in the thermal treatment decreases. Using the Scherrer equation the average crystallite size was estimated using the plane Au (111) at 38.2° 2θ (table 3). It is evident that as PVA concentration increases, the average crystallite size decreases. On the other hand, the use of elevated temperatures (250°C) can increase the average crystallite size by the aggregation of small nanoparticles leading to form bigger ones.

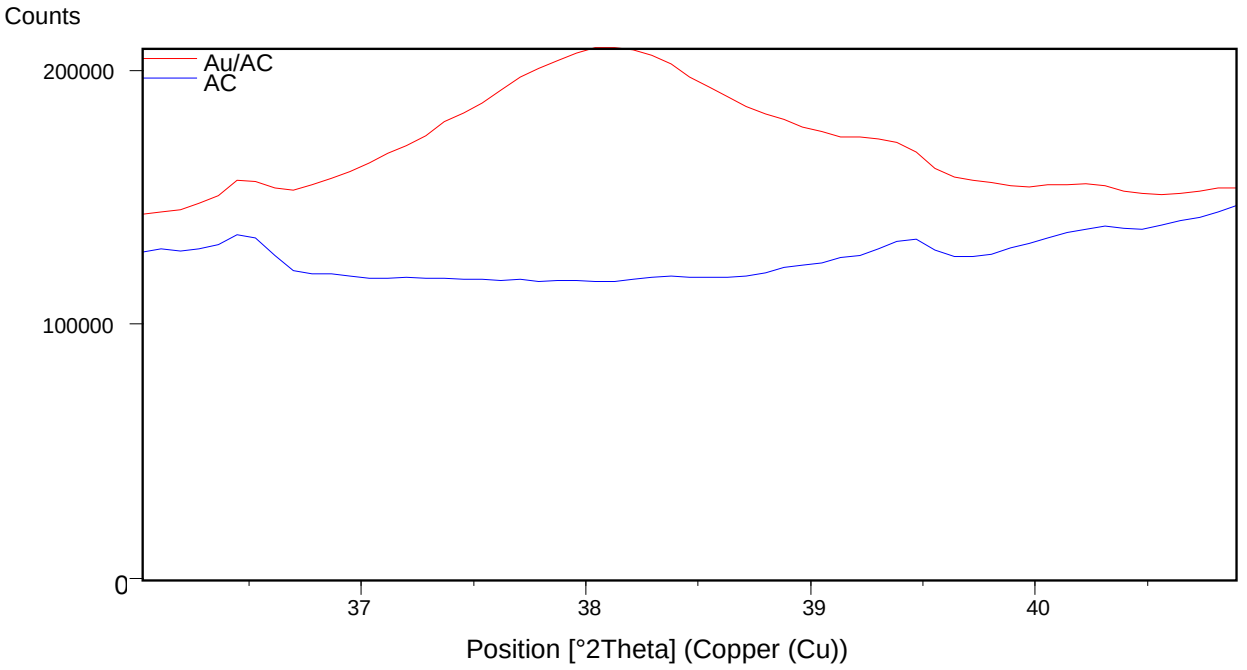

Figure 23. Diffractogram of Au/AC (reference catalyst)

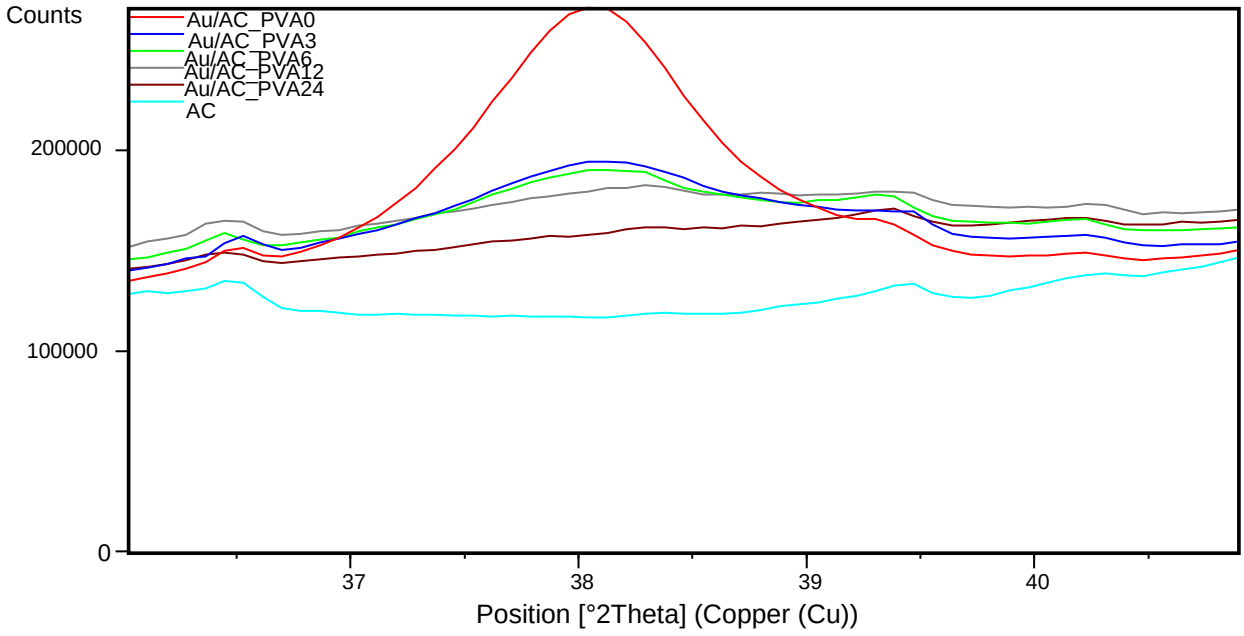

Figure 24. Diffractograms of Au/AC Catalysts with different PVA:Au weight ratios

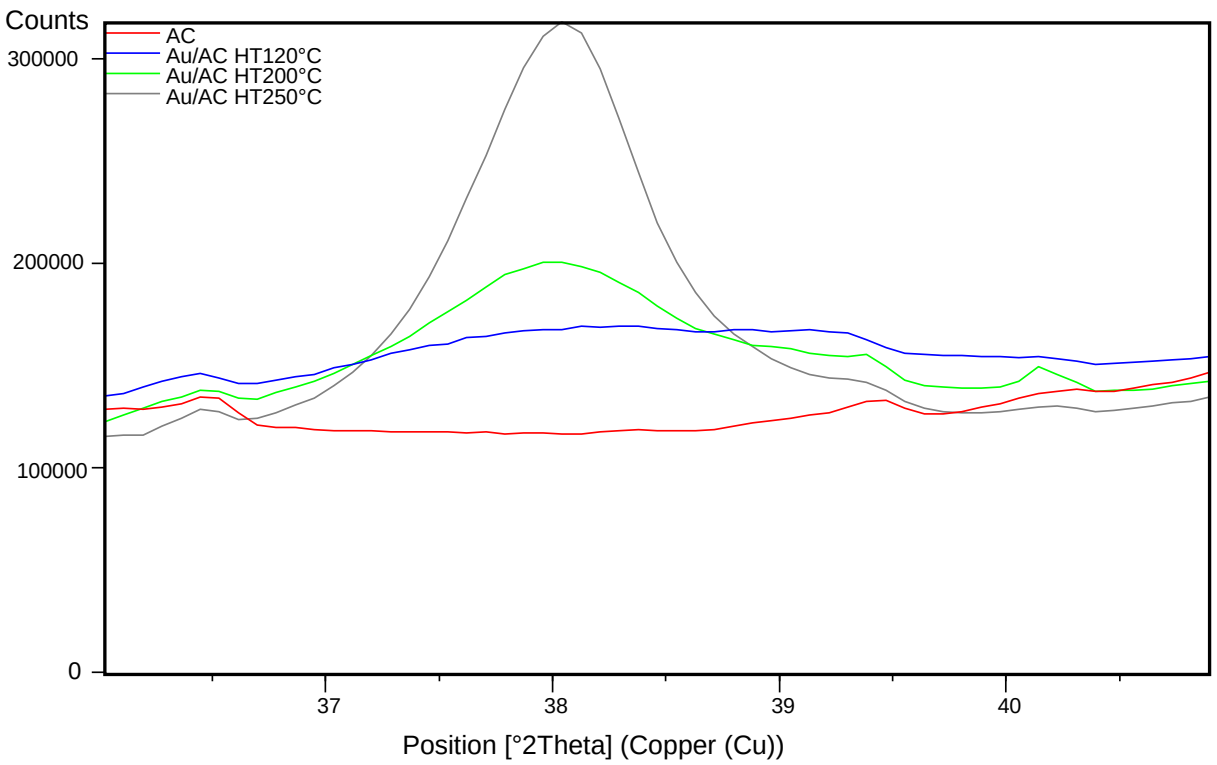

Figure 25. Diffractograms of Au/AC Catalysts heat treated with Air and H_2

Catalyst	Average crystallite size (nm)
Au/AC	5.5
Au/AC PVA0	6.4
Au/AC PVA0.3	3.6
Au/AC PVA0.6	3.1
Au/AC PVA1.2	2.6
Au/AC PVA2.4	2.2
Au/AC HT120°C	2.9
Au/AC HT200°C	4.1
Au/AC HT250°C	7.5

Table 3. Average crystallite size calculated with Scherrer equation

The nanoparticle dimensions were corroborated by TEM observations performed on selected catalysts: Au/AC, Au/AC PVA0 and Au/AC HT250°C (figure 26). For the analysis of nanoparticle size over 400 nanoparticles for each catalyst was performed and the particle diameter (particle size) distributions are shown in figure 27. We can notice in sample Au/AC PVA0 the presence of large particles and agglomerates along with small nanoparticles (figure S4). While for Au/AC HT250°C, well dispersed small nanoparticles are observed (bottom of figure 26). Samples Au/AC and Au/AC HT250°C are not exempt of agglomeration or formation of larger nanoparticles (figures S1 and S7) but it is clearly that these two effects are less visible compared to Au/AC PVA0. The average particle size presented in table 4 indicates the particle size estimated by TEM observations which comply in good agreement with the estimations done by XRD (crystallite size). While TEM estimations were based on a sample taken from the population, XRD measures an average of crystallite size given by all nanoparticles in conjunction. Both values are valid and they can provide a very good idea of the size of NPs on the support. STEM-HAADF images were obtained in TEM analysis and they are shown in figure 28. Scanning Transmission Electron Microscopy (STEM) is a special feature of transmission electron microscope where focusing an electron beam into a very small spot which is scanned over the TEM sample. The scattered electrons are collected in HAADF detector which is very sensitive to differences of the element irradiated based on the atomic number (Z-contrast) giving the images shown in figure 28. This technique allows to distinctly observe the dispersion and agglomeration of gold nanoparticles. It can be observed a very good dispersion of gold nanoparticles over Au/AC HT-250°C and the presence of few ~20 nm NPs (figure S8). Whereas sample Au/AC PVA0 shows again the presence of large particles and agglomerations possibly due to poor dispersion onto the support. Au/AC catalyst seems to have not well dispersed nanoparticles along with some aggregates and small nanoparticles. But overall, Au/AC catalysts seems to have in average smaller nanoparticles compared to the other two catalysts.

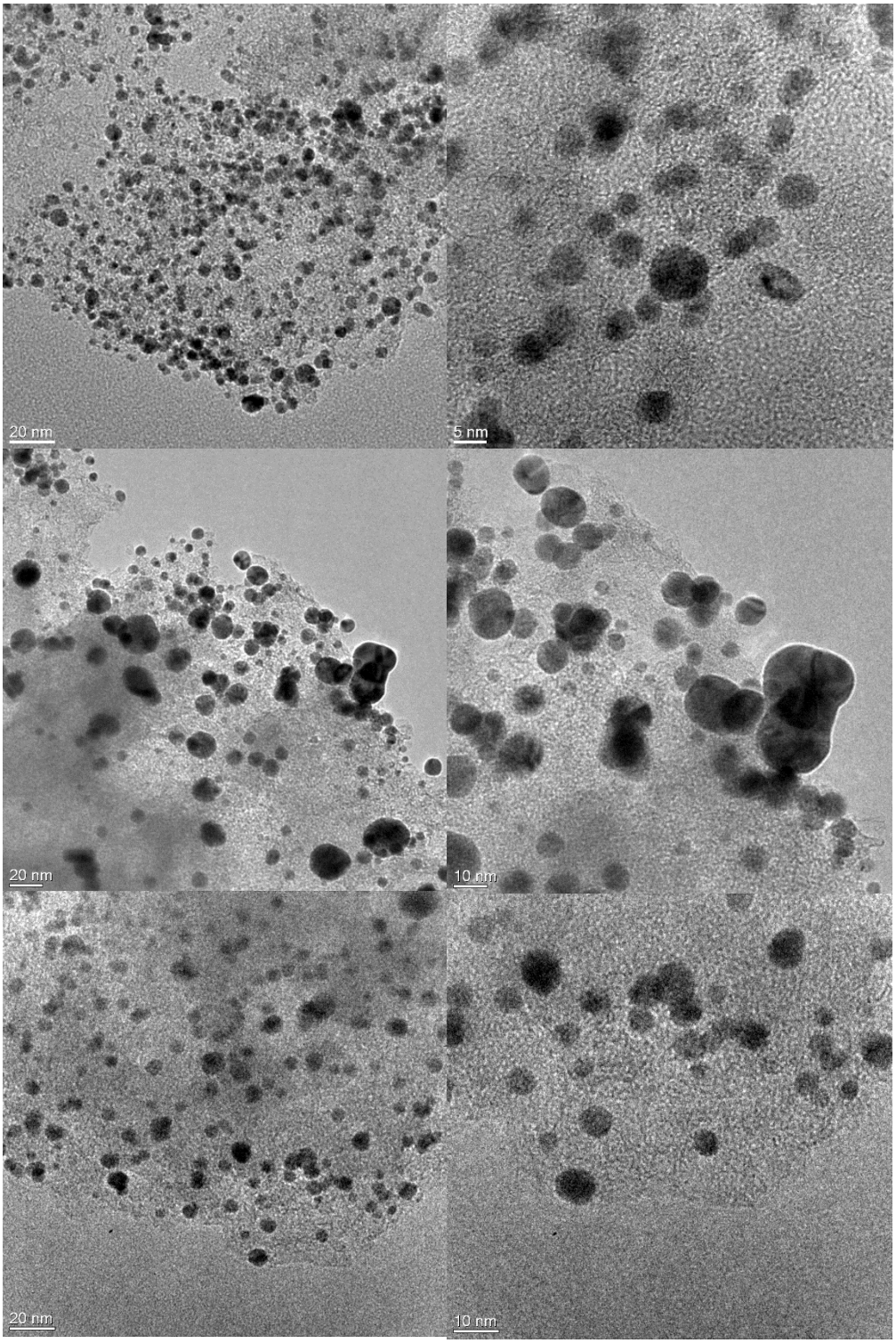

Figure 26. TEM images of catalysts Au/AC (top), Au/AC PVA0 (middle) and Au/AC HT250°C (bottom)

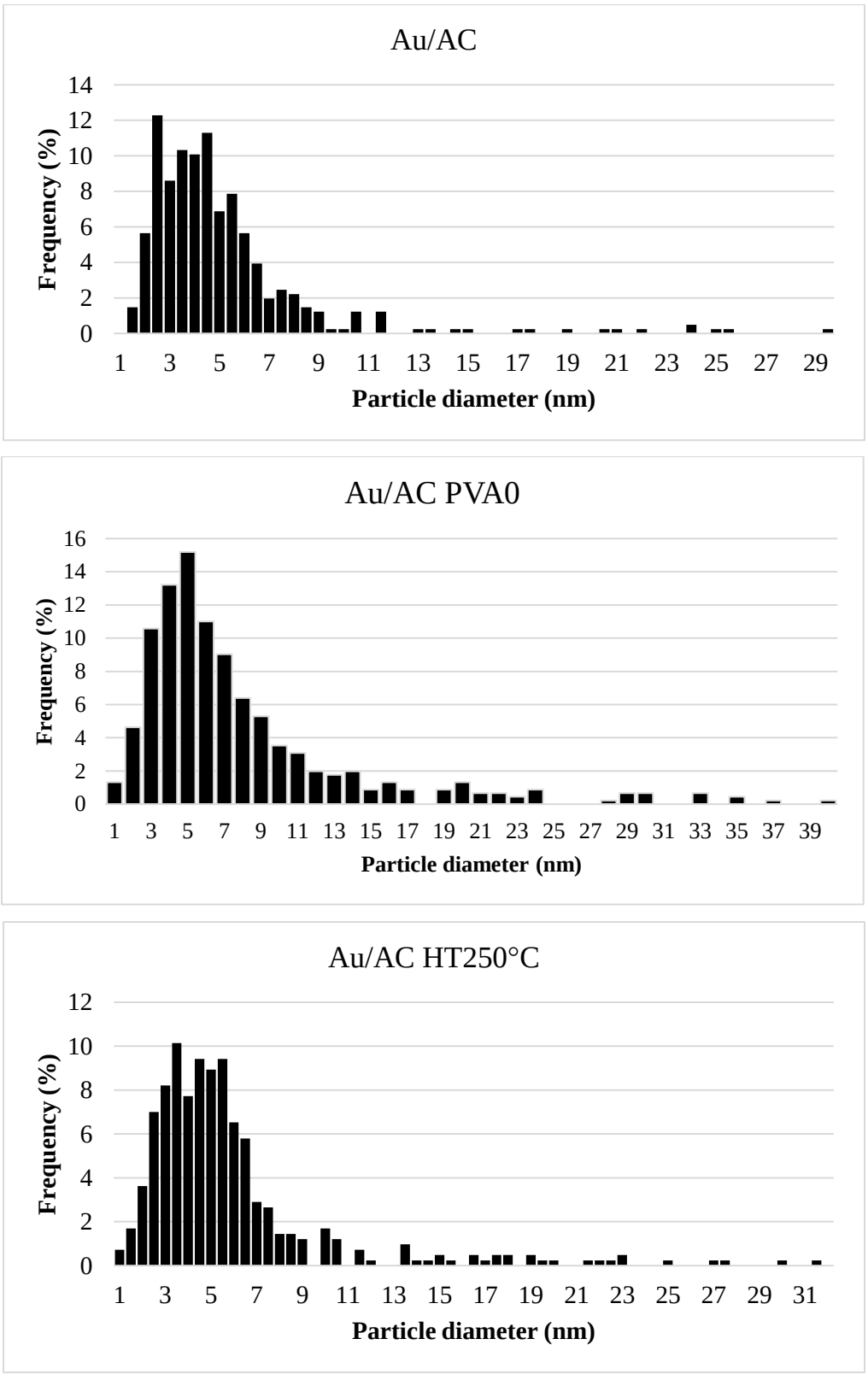

Figure 27. Particle size distribution Au/AC (top), Au/AC PVA0 (middle) and Au/AC HT250°C (bottom)

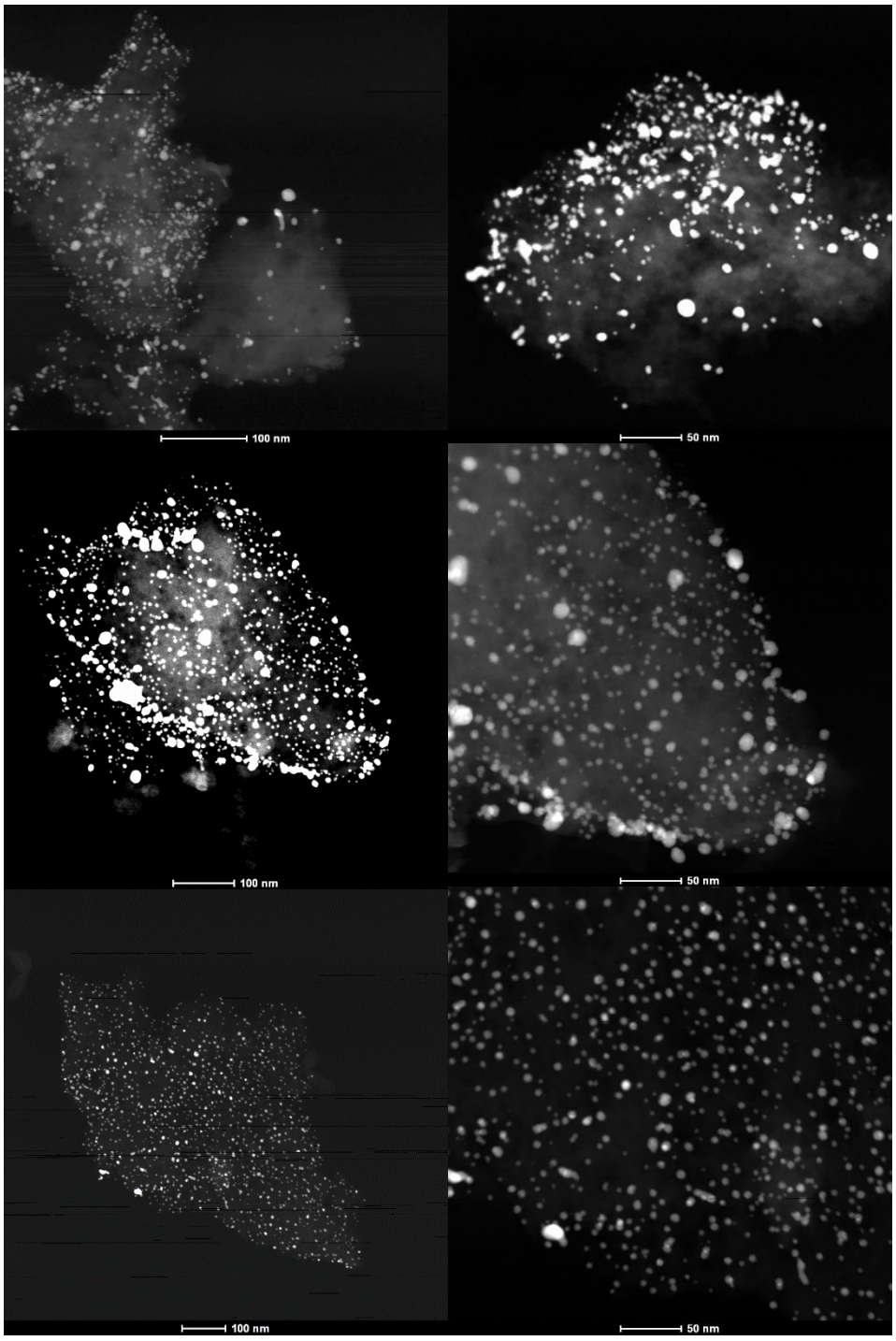

Figure 28. STEM-HAADF images of catalysts Au/AC (top), Au/AC PVA0 (middle) and Au/AC HT250°C (bottom)

Catalyst	Average particle diameter (nm)	Standard deviation (nm)
Au/AC	4.6 (particles <12 nm)	2.0
Au/AC PVA0	6.6 (particles <20 nm)	3.8
Au/AC HT250°C	5.0 (particles <15 nm)	2.4

Table 4. Average particle diameter of Au NPs obtained the TEM analysis

TG analysis was performed in selected catalysts in an attempt to observe the presence of PVA after the heat treatment and the degree of removal. First, the initial weight loss is attributed to water loss since all the catalysts were prepared in water. The weight loss is around 15-17% for Au/AC PVA0 (figure 32) and Au/AC PVA2.4 (figure 31) since these catalysts were not subjected to post treatment for PVA removal. On the other hand, Au/AC HT120°C and Au/AC HT250°C (figure 29 and 30) present an initial weight loss of 7-11%. Further weight loss around 150°C (20 - 40 minutes of the analysis) in Au/AC HT120°C and Au/AC HT250°C is of 2.6% and 1.5%, respectively. This weight loss could indicate the possible calcination of PVA residuals. To confirm this assumption, TGA was performed in catalysts with and without PVA during the preparation (Au/AC PVA2.4 and Au/AC PVA0). In Au/AC PVA2.4 a weight loss of 3.4% is observed while on Au/AC PVA0 it is 2.1%. Comparing the TGA of activated carbon (figure 33) with a weight loss of 1.5% around 125°C and the TGA of the catalysts it is possible to confirm that the difference between the catalyst and the support could indicate the presence of PVA. Although this technique is useful to roughly indicate the relative amount of PVA, other more accurate techniques are needed to study the loss or remotion of PVA residuals in the catalyst.

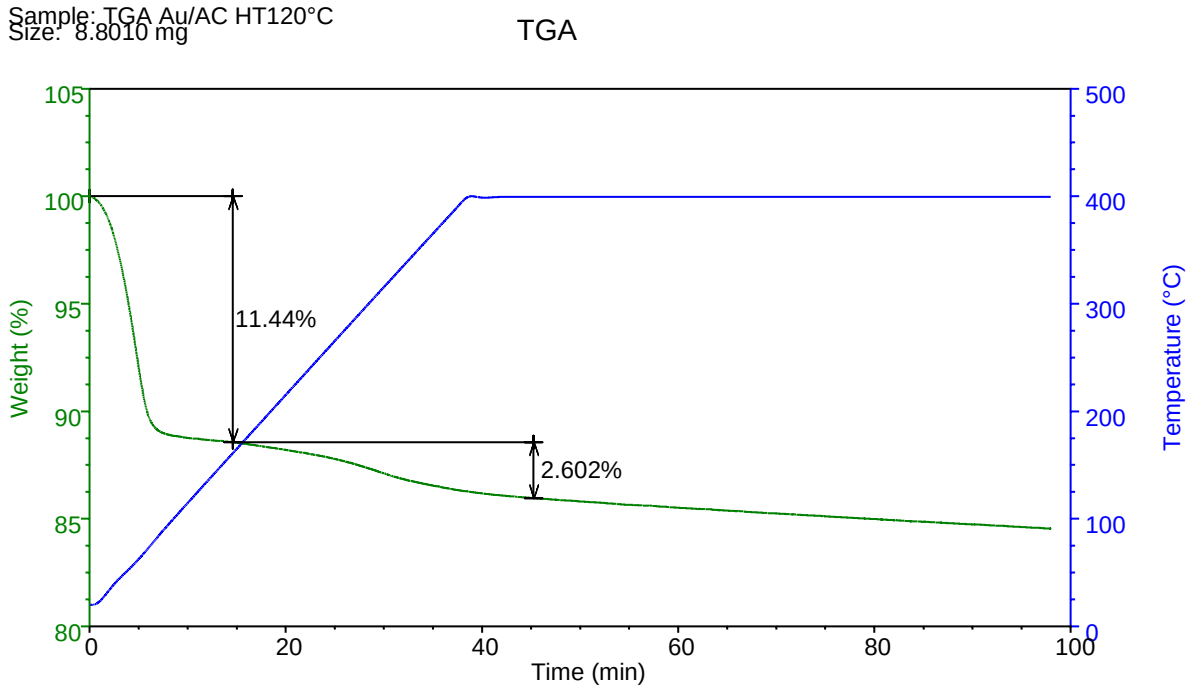

Figure 29. TGA of Au/AC HT120°C at 400°C for 60 min in Air

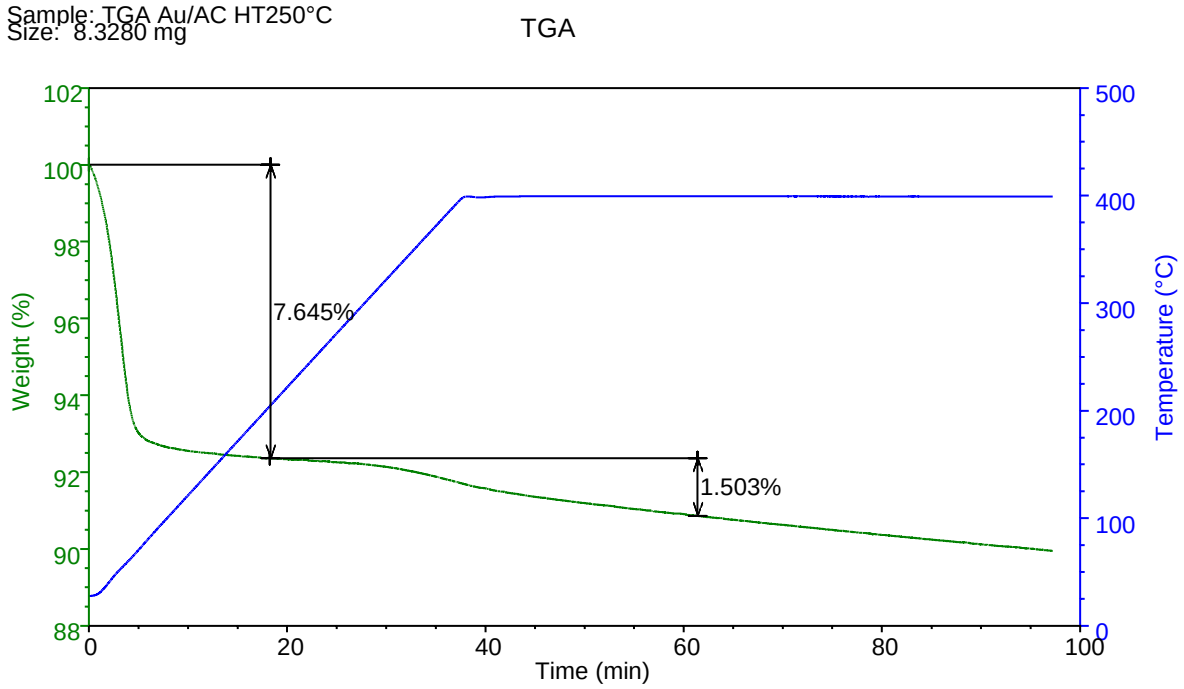

Figure 30. TGA of Au/AC HT250°C at 400°C for 60 min in Air

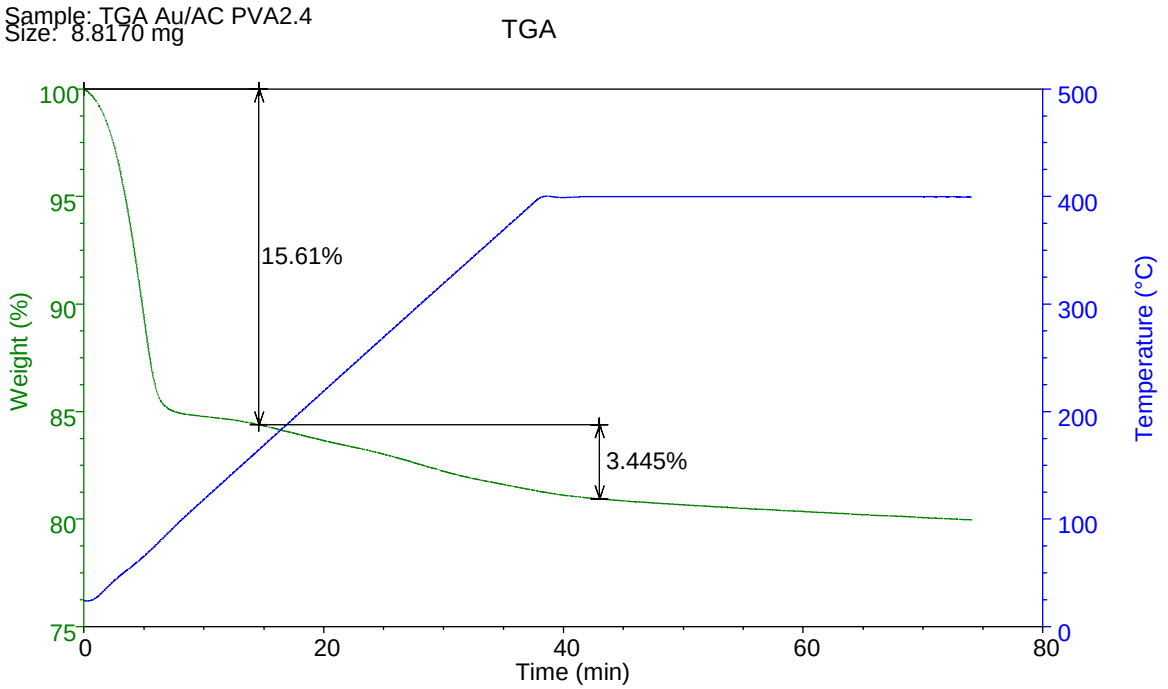

Figure 31. TGA of Au/AC PVA2.4 at 400°C for 40 min in Ai

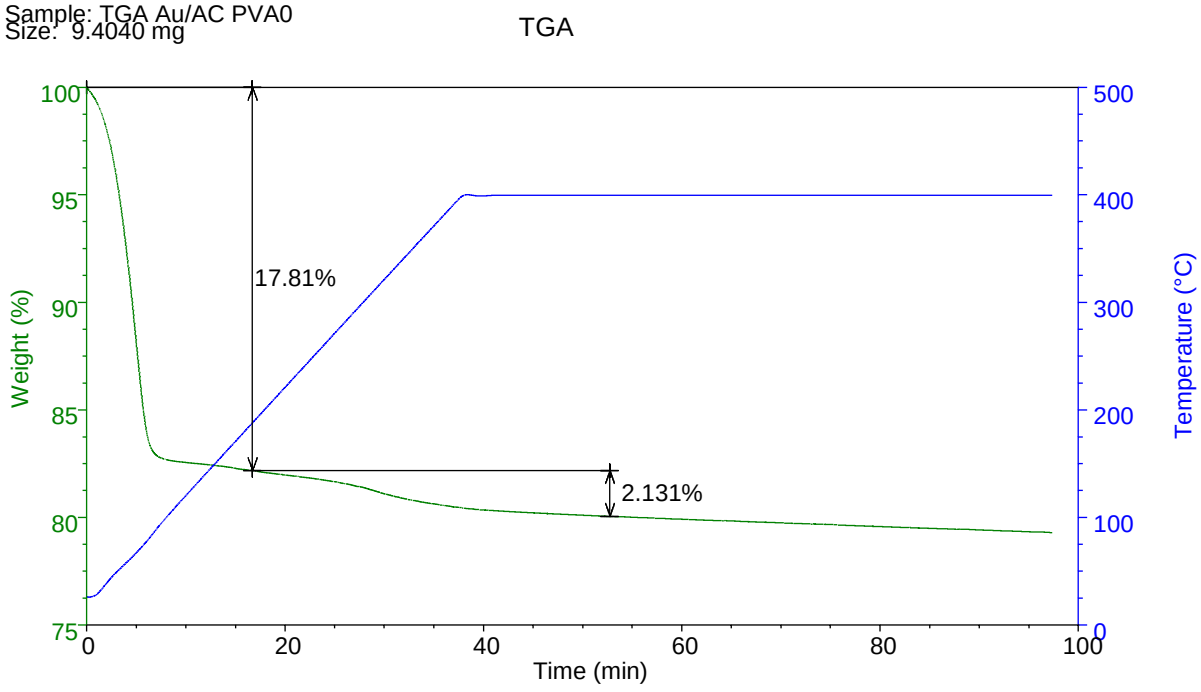

Figure 32. TGA of Au/AC PVA0 at 400°C for 60 min in Air

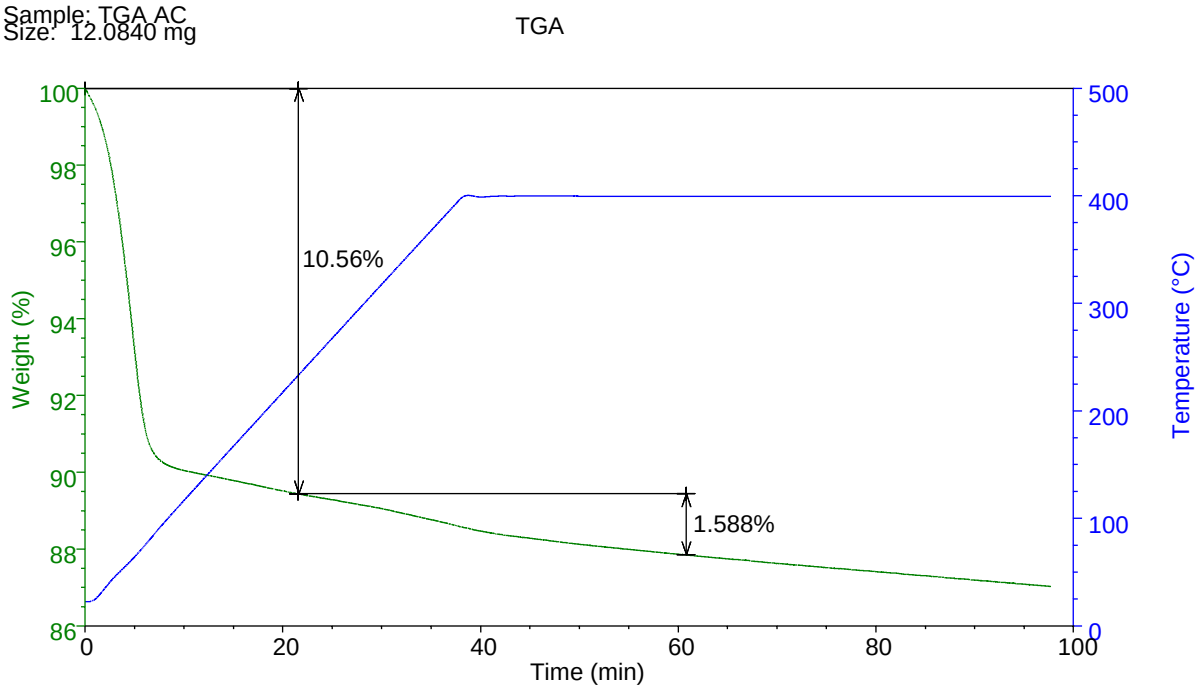

Figure 33. TGA of Activated carbon at 400°C for 60 min in Air

In Au colloidal solution, apparent small nanoparticles are formed (except for Au/AC PVA0) and ideally this size should be preserved during and after their deposition over the activated carbon surface. In this case, PVA on the catalyst preparation has essentially three functions: i) to stabilize the nanoparticles during and after their formation, ii) prevent aggregation of nanoparticles by steric stabilization and, iii) with this protective ligand surrounding the nanoparticles, to help in the dispersion over the support. Au/AC PVA0 shows clearly the effect of the absence of stabilizing agent. In TEM images and XRD calculations, the formation of larger nanoparticles is evident in Au/AC PVA0 compared to the other two samples since Au/AC PVA0 does not contain any stabilizer, the agglomeration was expected mostly to occur. As predicted, small gold nanoparticles were obtained as increasing the PVA concentration in the colloidal preparation where the elevated quantities of ligands helped to preserve the original size during the deposition step (table 3). Assuming total deposition of gold nanoparticles in the support, the catalyst with the smallest

dimensions should display higher catalytic activity (gluconic acid conversion to glucaric acid) compared to the other catalysts. A significant dependence of catalytic activity in the oxidation of glucose relies on the specific Au surface area and hence, Au particle diameter. Such dependence is associated to the adsorption of the substrate over the different plane (crystal) sites. As the metal nanoparticle size decreases, the relative proportions of atoms in edges and corners increases indicating the adsorption of the substrate over these highly exposed sites. It must be noted that the catalytic activity is structure sensitive caused by a cooperative effect of particle size, rounding effect and the multiple twinned particles.[62]

Furthermore, the removal of PVA is key for the activity of the catalyst since the stabilizing agent is no longer required and PVA ligands can block active sites. When comparing the removal treatment, elevated temperatures (250°C Air/H_2) strongly induce the aggregation and sintering of NPs increasing the average crystallite size up to 7.5 nm. Since the highest temperature used in this work is below to common temperature reported in literature (>300°C)[63] we could expect an increase of large particles but TEM images showed as well evenly spaced nanoparticles over the carbon surface. In contrast, at lower temperature (120°C Air/H_2) Au NPs seemed to maintain the original size (~3 nm) obtained in the colloidal solution (table 3). Two factors could play in the final size of the nanoparticles: temperature and the presence of PVA (PVA:Au 0.65:1 in the three heat treated catalysts and PVA:Au 0.5:1 for Au/AC). At high temperature, PVA has been removed (as implied from TGA graph in figure 30) to a large proportion allowing the sintering of some nanoparticles and therefore, creating larger particles. At lower temperature (120°C for heat treatment with Air/H_2 or washing with water at 60°C) some traces of PVA could still be present, stabilizing the nanoparticles and preventing their agglomeration/sintering. For that reason, a mild treatment is proposed for the stabilizing agent removal over the catalyst surface to not affect size and shape of the nanoparticles as it has also been reported previously in the literature.[64] A narrower particle size distribution should be expected for these treatments. The effect of thermal treatment and PVA residues will be evidenced in the catalytic testing.

Ultimately, the colloid solution preparation is worth to be discussed. Method A and method B/C/D have two different preparations of colloidal solution. Method A has a concentrated solution of gold (0.51 M Au) while method B/C/D a more diluted ($1.30 * 10^{-4}$ M Au). The former case helps to increase the distance between Au ions making it prone for an even dispersion in the formation of Au NPs. Considering sample Au/AC PVA0.6 (as the closest PVA:Au weight ratio

from method C) we can compare it with the reference catalyst (PVA:Au weight ratio 0.5:1). XRD showed average crystallite size of 5.5 nm for Au/AC and 3.1 nm for Au/AC PVA0.6. These differences could be derived from different proportions of polymer and reductant as well the concentration of precursor solution and the final treatment for PVA removal but additional analysis in nanoparticle size (and morphology) is required to elucidate the impact of these factors. Considering that both methods present the same quantity of $HAuCl_4*3H_2O$ (0.02 vs 0.0209 g (per gram of catalyst) for method A and method B/C/D, respectively) but the amounts of PVA and $NaBH_4$ are slightly different which affects directly in the velocity of nucleation, particle growth and stabilization of the recently formed nanoparticle. Since the stabilization of the nanoparticles count on the steric stabilization provided by PVA, the polymer concentration, temperature and average chain length play an important role during the NPs synthesis. Strong reductants as $NaBH_4$, can decrease the time of nucleation and increase the reduction rate. This step is very important given that a fast reduction induces a rapid build up of nuclei (supersaturation). Consequently, many nucleation events lead to many small NPs and few events to less and bigger particles (LaMer's Theory).[65] In summary, a combination of stoichiometric amounts of precursor, stabilizing agent, reductant and volume of reaction medium could lead to different particle size distributions and dispersion. However, further studies are required to understand the impact of colloidal preparation on support deposition and change in size during PVA removal step.

4.2. Optimization of parameters conditions

In previous work performed in the lab, a set of conditions were established as the optimum for the oxidation of glucose to glucaric acid: 60°C, 3 h, 400 rpm, 10 bar of O_2, Glu:Au molar ratio of 500:1, Glu:NaOH molar ratio of 1:3.[58] In the following sections, the effect of stirring rate, time of reaction and the effect of Glu:Au molar ratio were investigated. The catalyst Au/AC synthesized by method A was selected for this purpose.

4.2.1. Effect of stirring

Different rates of stirring were tested: 400, 600, 800, 1000 and 1200 rpm. The next table shows the main results.

Stirring rate (rpm)	Glucose conversion %	Gluconic acid yield %	Glucaric acid yield %	Isomers [a] yield %	Others [b] yield %
400	88.8	52.6	0.8	8.1	20.5
600	82.8	63.8	1.5	5.5	13.1
800	83.0	70.3	2.1	2.2	7.4
1000	87.3	53.0	15.1	1.0	18.5
1200	89.9	54.1	15.8	0.0	19.7

Table 5. Effect of stirring rate on glucose oxidation. Reaction conditions: 15 min, 60°C, 10 bar O_2, Glu:Au:NaOH ratio of 1000:1:3000. [a] Isomers corresponding to fructose and mannose combined. [b] The complete table with byproducts formed is supplementary information (table S1).

We can notice that glucose conversion is relatively similar in all stirring rates (>82%). At high stirring rates, 1000 and 1200 rpm, glucaric acid yield are the highest (~15%), while at lower stirring rates, gluconic acid formation predominates (52 -70%). Meanwhile, isomerization of the glucose is visible at lower stirring rates (up to 8.1% yield of isomers). In order to measure intrinsic kinetics, the experimental data were verified in the absence of external mass transfer limitations (chemical kinetics regime). Therefore, the occurrence of mass transfer limitations (external diffusion) was experimentally investigated. The effect of stirring rate and mass of the catalyst was studied. By increasing the stirring rate (stirring rate can influence the presence of mass transfer limitations and to ensure perfect mixing and to avoid segregation of both fluid and solid catalyst) an increase of glucaric acid formation was observed and reached a plateau above 800 rpm indicating the stirrer speed at this range has a minor effect in the conversion of gluconic acid to glucaric acid and hence, the reaction is in kinetic regime. By accelerating the oxidation reaction,

the competition with isomerization of glucose decreases dramatically to less than 1% of fructose and mannose and not formation at all at 1200 rpm. It is well-known that alkaline environment promotes higher yields to glucaric acid with noble metal nanoparticles but also accelerates the isomerization of glucose. This last reaction can be overthrown by increasing the stirring rate.

To corroborate this assumption and to calculate the amount of isomers formed during the preparation of the solution in the reactor until it reaches the desired temperature, two experiments were set at time zero. Since glucose is a very reactive molecule, lower conversions are needed to study the initial rate. The reaction mixture was set up at 1200 rpm or 0 rpm and stopped when it reached 60°C.

Stirring rate (rpm)	Glucose conversion %	Gluconic acid yield %	Glucaric acid yield %	Isomers [a] yield %	Others [b] yield %
0	42.7	0.9	0.0	25.7	9.6
1200	85.6	68.4	8.6	0.0	9.6

Table 6. Effect of stirring rate on glucose oxidation at time zero. Reaction conditions: 0 min (until the reaction reaches 60°C), 10 bar O_2, Glu:Au:NaOH molar ratio of 1000:1:3000. [a] Isomers corresponding to fructose and mannose combined. [b] The complete table with byproducts formed is supplementary information (table S2).

When no stirring is present at all in the reaction mixture, very low amount of gluconic acid is obtained (0.9% yield of GO) and no glucaric acid is formed even in the presence of the catalyst. Meanwhile, a high quantity of isomeric products is formed (25% yield of isomers) indicating the isomerization of glucose predominance. Therefore, vigorous agitation is required to ensure the homogeneity of the mixture and the mass transferring of the substrate to the available active sites inside the pores of the activated carbon where the gold nanoparticles could be deposited.

On the other hand, O_2 is the most used oxidant agent reported in literature for oxidation of glucose and high pressures could increase the reaction rate due to a higher solubility of O_2 on the reaction medium (table 7).

O_2 pressure (bar)	Glucose conversion %	Gluconic acid yield %	Glucaric acid yield %	Isomers [a] yield %	Others [b] yield %
10	87.3	53.0	15.1	1.0	18.5
15	78.5	76.9	1.2	1.3	2.6

Table 7. Effect of O_2 pressure. Reaction conditions: 15 min, 60°C, 1000 rpm, Glu:Au:NaOH molar ratio of 1000:1:3000. [a] Isomers corresponding to fructose and mannose combined. [b] The complete table with byproducts formed is supplementary information (table S3).

It seems that higher pressure does not help to increase the reaction rate of conversion of gluconic acid to glucaric acid (15% yield GA at 10 bar O_2 vs 1.2% at 15 bar O_2) contrary to what has been reported in the literature.[55, 56] Further studies are required to elucidate the effect of O_2 concentration in the reaction. Since better results are obtained at 10 bar of O_2 the subsequent reactions are performed at this pressure.

For the study of the evolution of the reaction through time, 1000 rpm is selected since low formation of isomers and the yield of gluconic acid and glucaric acid are very similar at 1200 and 1000 rpm.

4.2.2. Time on line studies

Following the conditions established in the previous section, the reaction (kinetic studies) was followed at time 15, 30, 60 and 120 minutes.

Time (min)	Glucose conversion %	Gluconic acid yield %	Glucaric acid yield %	Glucaric acid selectivity %	Others [a] yield %
15	87.3	53.0	15.1	17.3	19.5
30	89.5	44.2	19.6	21.9	25.4
60	92.6	37.9	24.2	26.2	27.6
120	92.0	32.5	24.5	26.6	29.8

Table 8. Glucose conversion and Gluconic acid and Glucaric acid formation through time. Reaction conditions: 60°C, 1000 rpm, 10 bar O_2, Glu:Au:NaOH molar ratio of 1000:1:3000. [a] The complete table with byproducts formed is supplementary information (table S4).

It can be observed that gluconic acid is formed very rapidly while the formation of glucaric acid reaches certain yield (24.2%) after 60 minutes of reaction. Since aldehyde groups are easily oxidizable, high concentration of gluconic acid is expected at short reaction times. While in the formation of glucaric acid, the oxidation of alcohol group -CH_2OH requires first dehydrogenation to -CHO followed by oxidation to –COOH, which is a more demanding step. Hydroxyl groups play an important role during alcohol oxidation and little or no activity is observed on Au catalysts without a base.[58] In the presence of a base, OH ions activate and deprotonate the alcohol group on the interface of Au but the energy required for the formation of the aldehyde is higher than its further oxidation.[66] As a result, the formation of glucaric acid is slower than gluconic acid.

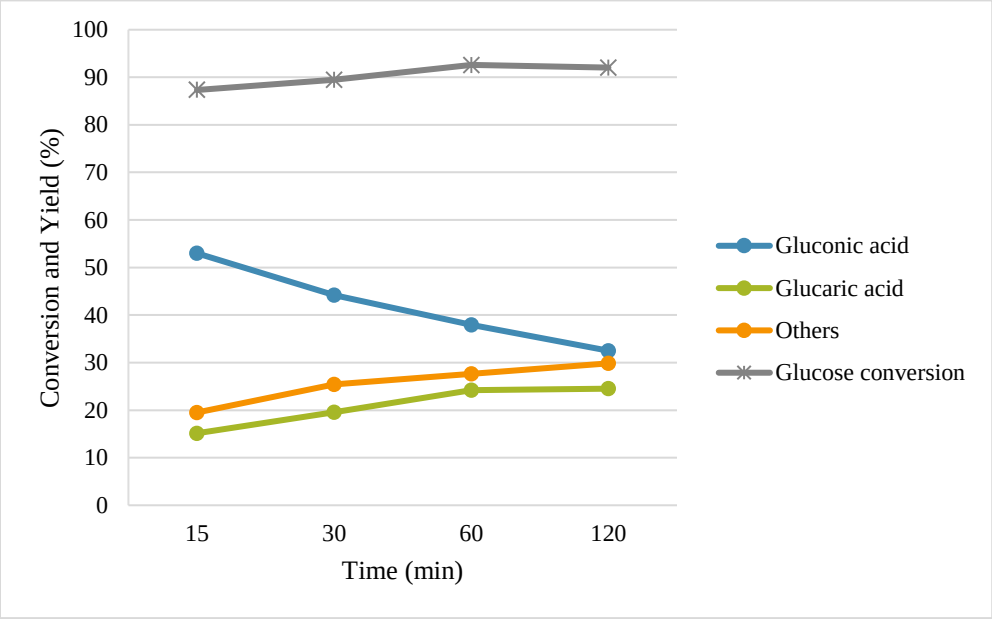

Figure 34. Glucose conversion and formation of GO, GA and other byproducts as a function of time

However, after 60 min of reaction, the oxidation of gluconic acid slows down leading to the formation of byproducts. This can be explained if we consider the blocking of the active sites by glucaric acid and similar byproducts. The reactants and products have a multifunctional nature where they can interact with the catalyst via multiple groups. Glucose and gluconic acid absorb possibly with similar strength to the active site (-CHO and –COOH group respectively) whereas, glucaric acid can interact by both C=O groups (belonging to the carboxylic groups) with the Au surface of the catalyst.

To understand better the reaction pathway, gluconic acid was used as substrate in the same concentration as glucose (0.29 M)

Time (min)	Gluconic acid conversion %	Glucaric acid yield %	Glucaric acid selectivity %	Others [a] yield %	Others selectivity %
15	34.2	9.3	27.2	10.7	31.3
60	51.0	18.1	35.4	20.4	39.9

Table 9. Gluconic acid conversion and Glucaric acid formation through time. Reaction conditions: 60°C, 1000 rpm, 10 bar O_2, GO:Au:NaOH molar ratio of 1000:1:3000. [a] The complete table with byproducts formed is supplementary information (table S5).

The catalyst is more selective to glucose conversion than gluconic acid: at 15 min of reaction 87% of glucose is converted; in contrast, gluconic acid conversion only reaches 34%. Starting from gluconic acid, the selectivity to glucaric acid (35.4% at 60 minutes) is higher compared to the selectivity obtained by glucose oxidation at the same time (26.2%) using the same reference catalyst Au/AC. The selectivity to other byproducts (table S5) is higher starting from GO with 39.9% compared to 29.8% starting from Glu. This could indicate that the formation of other compounds besides glucaric acid rises from parallel oxidation reactions starting from gluconic acid. These results suggest that gluconic acid is a key intermediate for the formation of these light carboxylic acids (tartaric, tartronic, oxalic acids and others).[68] Moreover, the synthesis of byproducts with C=O and COOH groups seems to deactivate the catalyst due to the strong interaction surface of the gold nanoparticles. Although, the presence of the base could serve in the desorption forming the corresponding salts, the deactivation still occurs.

The formation of other compounds has been proposed to derive mainly from gluconic acid decomposition at the interface of the metal/support (C-C cleavage) or due to the thermal degradation. Based on reaction pathways described in the literature[67], we proposed a simplified scheme of product formation and byproducts found in the reaction medium (figure 35).

Time (min)	Glucose conversion %	Gluconic acid yield %	Glucaric acid yield %	Isomers [a] yield %	Others [b] yield %
0	44.0	0.9	0.0	25.1	9.4
1	44.1	1.4	0.0	26.2	11.0
15	93.6	1.5	0.0	54.5	29.9

Table 10. Blank test. Reaction conditions: 60℃, 1200 rpm, 10 bar O_2, Glu:NaOH molar ratio of 1:3. [a] Isomers corresponding to fructose and mannose. [b] The complete table with byproducts formed is supplementary information (table S6).

By performing a series of blank tests at high stirring rate (1200 rpm), glucose conversion is very high after 15 min, but isomers are the main compounds (54% yield fructose + mannose). In table S6, tartaric acid (C_3 dicarboxylic acid) is not formed at all indicating that probably comes from gluconic acid degradation due to C-C cleavage in the catalyst (figure 35). Glucaric acid is a highly stable molecule under alkaline conditions as demonstrated in previous work.[58]

Summarizing, in order to achieve the highest selectivity to glucaric acid, it is necessary to increase glucose conversion to promote the transformation of gluconic acid, but this is inevitably

leading to simultaneous formation of other byproducts. Gluconic acid conversion to glucaric acid is more difficult compared to the oxidation of glucose and C−C cleavage reactions and oxidations can occur after gluconic acid is formed. Methods for desorption of glucaric acid and byproducts should be proposed to overcome this event and continue the total conversion of gluconic to glucaric acid.

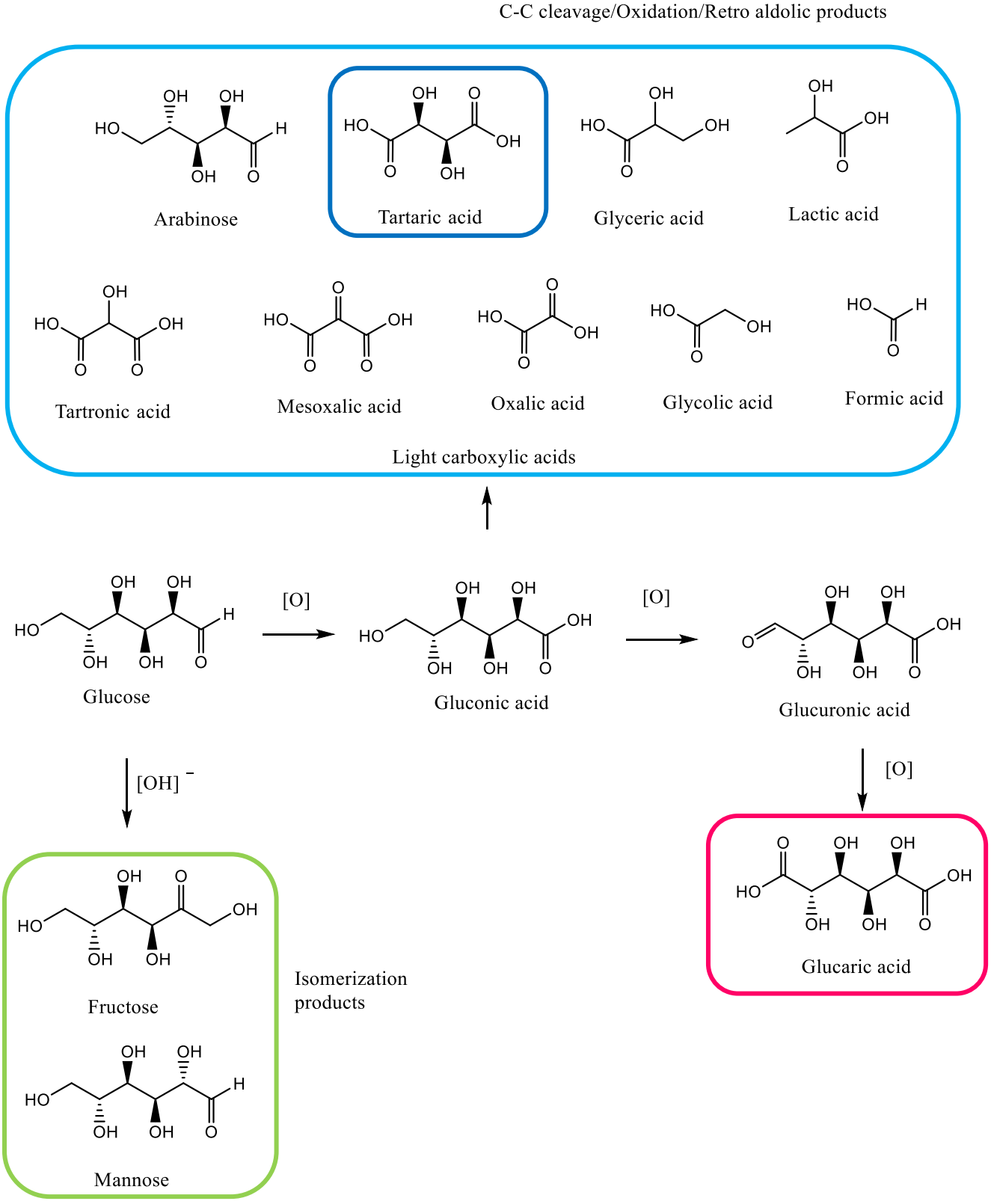

Figure 35. Proposed reaction pathway and reaction products and other compounds

4.2.3. Effect of Glu:Au molar ratio

The effect of Au:Glu molar ratio (1/500 to 1/1500) is studied to understand the influence of mass of catalyst in terms of activity and yield to specific products. The results are presented in table 11.

Au:Glu molar ratio	Glucose conversion %	Gluconic acid yield %	Glucaric acid yield %	Isomers [a] yield %	Others [b] yield %
1:500	92.2	31.0	27.6	0.5	31.5
1:1000	92.6	37.9	24.2	1.0	26.6
1:1500	90.2	39.7	19.1	1.6	26.4

Table 11. Study of Au:Glu ratio. Reaction conditions: 1 h, 60°C, 1000 rpm, 10 bar O_2, Glu:NaOH molar ratio of 1:3. [a] Isomers corresponding to fructose and mannose. [b] The complete table with byproducts formed is supplementary information (table S7).

It can be noted that glucose conversion is very high in the three cases. Isomers yield slightly increases as the catalyst quantity decrease. Inversely, glucaric acid concentration decreases as Au:Glu molar ratio decreases. The yield to other compounds remains similar (~26%) in 1:1000 and 1:1500 molar ratios meanwhile glucose conversion remains the same (~92%) for molar ratios 1:500 and 1:1000. Evidently, higher metal:substrate molar ratios generate higher amount of glucaric acid (27.6% yield GA at Au:Glu molar ratio or 1:500) due to the increase number of active sites available for the chemical transformation.

4.3. Screening of catalysts

After the optimization of reaction conditions, and using the conditions selected in section 4.1 and 4.2, the catalysts synthesized by the procedures described in section 3.2 were tested for the oxidation of glucose to glucaric acid. Results from Au/AC PVA set of catalysts are presented in table 12.

Catalysts Au/AC PVA	Glucose conversion %	Gluconic acid yield %	Glucaric acid yield %	Gluconic acid selectivity %	Glucaric acid selectivity %	Others [a] yield %
Au/AC PVA0	91.5	37.9	22.1	41.4	24.2	27.7
Au/AC PVA 0.3	90.2	36.4	21.9	40.4	24.3	29.3
Au/AC PVA 0.6	91.2	37.0	22.4	40.5	24.6	29.2
Au/AC PVA 1.2	91.1	38.7	19.8	42.5	21.7	27.1
Au/AC PVA 2.4	90.2	43.8	17.5	48.6	19.4	24.6

Table 12. Screening of catalysts Au/AC PVA series. Reaction conditions: 1 h, 60℃, 1000 rpm, 10 bar O_2, Glu:Au:NaOH molar ratio of 1000:1:3000.[a] The complete table with byproducts formed is supplementary information (table S8).

The variation of PVA:Au weight ratio affects significantly the nanoparticle size and in consequence should affect the catalytic activity to a certain degree. At 1 hour of reaction, similar glucose conversions are obtained (~90%) but lower conversions are necessary to study the initial rates. A combined yield around 58-61% of GO + GA is obtained. However, there is a tendency of decreasing glucaric acid yield as PVA concentration increases suggesting Au nanoparticle size has an influence. Thereby, 15 minutes reactions were performed with catalysts Au/AC PVA0, Au/AC PVA1.2 and Au/AC PVA2.4.

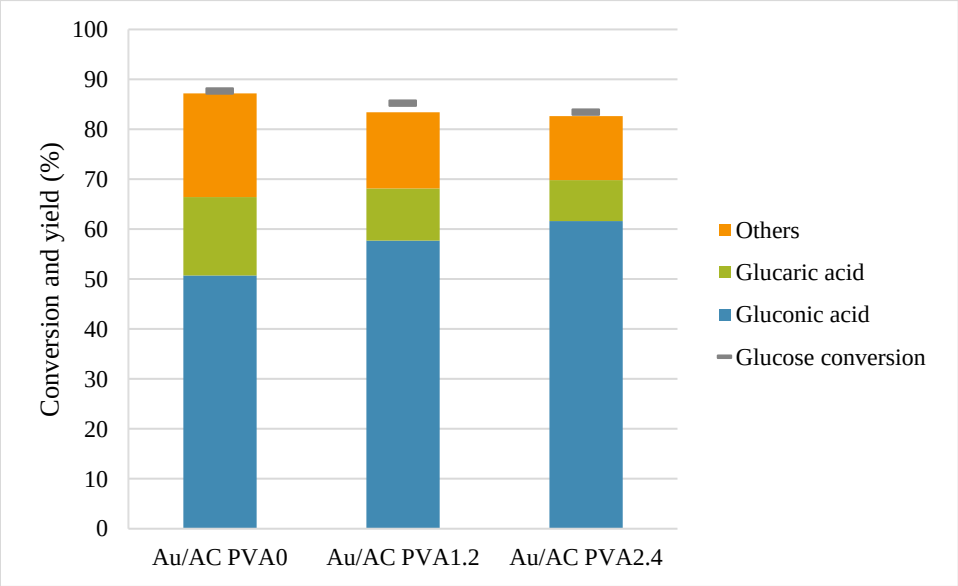

Figure 36. Comparison of Au/AC PVA catalysts. Reaction conditions: 15 min, 60℃, 1000 rpm, 10 bar O_2, Glu:Au:NaOH molar ratio of 1000:1:3000

Glucose conversion decreases as the PVA concentration increases in the synthesized catalysts. The quantity of glucaric acid decreases as the PVA concentration increases in the catalysts while for gluconic acid is the opposite. It seems that the initial rate of the reaction is slower in the catalyst with higher concentration of PVA despite the fact Au/AC PVA2.4 has the smallest nanoparticles (crystallite size of 2.2 nm) of the set of catalysts prepared. PVA could be partially blocking the active sites in the nanoparticles which during the course of the reaction these start to be available due to the solubilization of PVA. PVA is soluble in water and dissolves at 60°C, the same reaction temperature. In this case, the PVA present in the catalyst seems influence on a higher degree the reaction rate and product distribution than the Au nanoparticle. Therefore, the procedure of the removal of PVA should be efficient and not cause a dramatic change in the nanoparticles size or distribution. It is important to highlight the higher yield to glucaric acid formed in the absence of PVA (16% yield GA), emphasizing the role of PVA blocking specific active sites.

The effect of heat treatment has been investigated (120-250°C) as described in section 3.2. The catalysts Au/AC HT120°C, Au/AC HT200°C, Au/AC HT250°C and Au/AC washing were prepared with PVA:Au weight ratio of 0.65:1. Similar size of nanoparticles should be envisaged in the colloidal solution during the preparation of these catalysts and we can assume a similar size to the one estimated by XRD for catalyst Au/AC PVA0.6 (crystallite size of 3.1 nm). The type of heat treatment and temperature is expected to impact the final nanoparticle size, nanoparticle size distribution, PVA removal, and consequently, the catalytic activity.

Catalyst	Glucose conversion %	Gluconic acid yield %	Glucaric acid yield %	Isomers [a] yield %	Others [b] yield %
Au/AC HT120°C	91.5	42.0	18.1	0.9	26.8
Au/AC HT200°C	88.0	45.4	15.2	2.4	21.9
Au/AC HT250°C	90.1	43.7	17.3	1.9	23.5
Au/AC washing	91.3	35.0	22.6	0.9	30.4

Table 13. Screening of catalysts with two different procedures of PVA removal. Reaction conditions: 1 h, 60°C, 1000 rpm, 10 bar O_2, Glu:Au:NaOH molar ratio of 1000:1:3000. [a] The complete table with byproducts formed is supplementary information (table S9).

As we can see in table 13, similar glucose conversions are obtained by the four types of catalysts varying in the formation of gluconic acid and glucaric acid. Au/AC washing catalyst

reached the highest quantity of glucaric acid (22.6% yield) showing the best performance among all. To examine the initial rate, 15 minutes reactions were performed with catalysts Au/AC HT120°C, Au/AC HT200°C, Au/AC HT250°C and Au/AC washing.

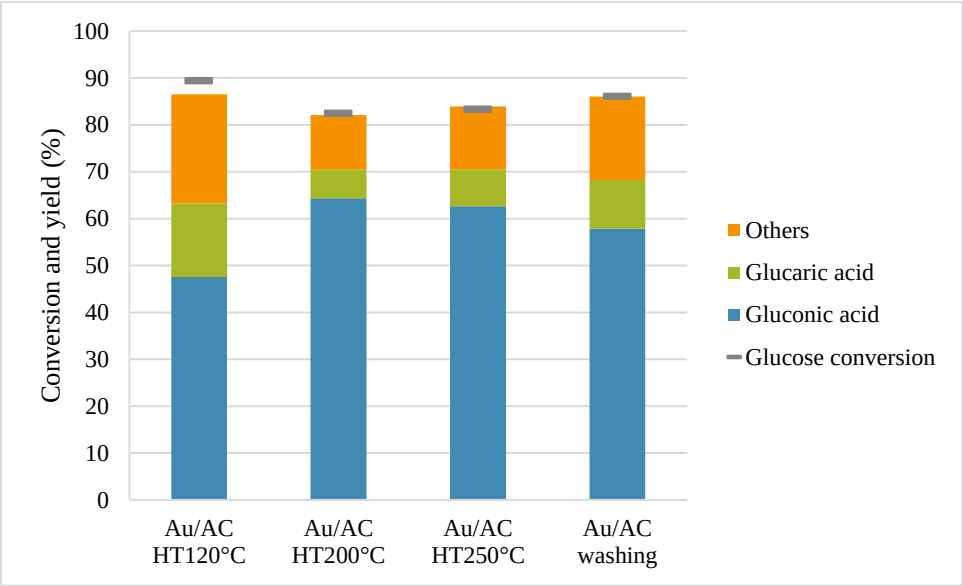

Figure 37. Comparison of catalysts with different PVA removal procedure. Reaction conditions: 15 min, 60℃, 10 bar O_2, 1000 rpm, Glu:Au:NaOH molar ratio of 1000:1:3000

Catalyst	Glucose conversion %	Gluconic acid yield %	Glucaric acid yield %	Isomers [a] yield %	Others [b] yield %
Au/AC HT120°C	89.5	47.5	15.7	0.7	22.5
Au/AC HT200°C	82.5	64.3	6.2	1.8	9.8
Au/AC HT250°C	83.4	62.6	7.9	2.0	11.4
Au/AC washing	86.1	57.9	10.3	1.0	16.8

Table 14. Screening of catalysts with two different procedures of PVA removal. Reaction conditions: 15 min, 60℃, 1000 rpm, 10 bar O_2, Glu:Au:NaOH molar ratio of 1000:1:3000. [a] The complete table with byproducts formed is supplementary information (table S10).

In figure 37 we can easily see that Au/AC HT120°C had the best initial catalytic performance (15.7% yield of GA) followed by the Au/AC washing catalyst (10.3% yield GA). Meanwhile, Au/AC HT200°C catalyst showed the poorest performance of the four catalysts at 1 hour and 15 minutes reaction. This could be due to the increase of nanoparticle size during the treatment and the incomplete removal of PVA ligand over the surface of the catalyst. Au/AC HT250°C has larger

mean nanoparticle size but maybe a higher calcination temperature a higher amount of PVA has been removed, therefore, a higher number of active sites are free for accessibility of substrate/intermediates. Hence, a mild calcination treatment at 120°C Air/H_2 or washing with water at 60°C seem to offer an effective treatment (as previously reported in literature[64]) to clean off the catalyst surface without altering the original mean nanoparticle size (crystallite size of 3.1 nm).

4.4. Effect of the support

The nature of the support was studied since the effect of dispersion, the metal-support interaction and metal-support interface are markedly influenced by the support used. Metal oxides are known to have a stronger interaction with metallic nanoparticles than activated carbon. Zirconium oxide is a chemically stable, nontoxic metal oxide, insoluble in water and resistant to oxidant agents. ZrO_2 has an amphoteric character (containing cationic and anionic ion exchange) which can help in the interaction with the gold nanoparticles while such character is not present in activated carbon. Therefore, Au nanoparticles supported on ZrO_2 were prepared with method A in an effort to improve the selectivity/yield to glucaric acid. The catalyst was evaluated using the conditions reported by Solmi et al. and the conditions established in this work. The results are shown in the table 15.

Au/ZrO_2 (Time)	Glucose conversion %	Gluconic acid yield %	Glucaric acid yield %	Gluconic acid selectivity %	Glucaric acid selectivity %	Isomers [a] yield %	Others [b] yield %
15 min[c]	80.8	67.9	2.4	84.0	3.0	4.2	7.6
1 h[c]	88.6	43.7	16.1	49.4	18.1	2.7	25.0
3 h[d]	95.4	23.9	11.0	25.0	11.5	6.0	43.1

Table 15. Testing of Au/ZrO_2 catalyst in the oxidation reaction of glucose. [a] Isomers corresponding to fructose and mannose. [b] The complete table with byproducts formed is supplementary information (table S11). [c] Reaction conditions: 60℃, 1000 rpm, 10 bar O_2, Glu:Au:NaOH molar ratio of 1000:1:3000. [d] Reaction conditions: 60℃, 400 rpm, 10 bar O_2, Glu:Au:NaOH molar ratio of 500:1:1500.

The glucose conversion is higher than 80% in the three experiments while the highest yield of glucaric acid (16.1%) was obtained at conditions optimized in this work. We can confirm from previous studies (section 4.2) that elevated stirring rates can increase the reaction rate and minimize the formation of isomers and byproducts. Also, less amount of catalyst could be used to

reach higher yields of glucaric acid if we compare 11% yield GA at 3 hours of reaction with Glu:Au molar ratio of 500:1 against 16.1% yield GA obtained at 1 hour of reaction with Glu:Au molar ratio of 1000:1.

Au/AC (Time)	Glucose conversion %	Gluconic acid yield %	Glucaric acid yield %	Gluconic acid selectivity %	Glucaric acid selectivity %	Isomers [a] yield %	Others [b] yield %
15 min[c]	87.3	53.0	15.1	60.7	17.3	1.0	18.5
1 h[c]	92.6	37.9	24.2	41.0	26.2	1.0	26.6

Table 16. Testing of Au/AC catalyst in the oxidation reaction of glucose. [a] Isomers corresponding to fructose and mannose. [b] The complete table with byproducts formed is supplementary information (table S11). [c] Reaction conditions: 60℃, 1000 rpm, 10 bar O_2, Glu:Au:NaOH molar ratio of 1000:1:3000

Comparing the support at the same reaction time and operative conditions (table 16 for Au/AC catalyst) we can see a significant difference in the yield and selectivity to glucaric acid. Using Au/ZrO_2 the selectivity to glucaric acid at 1 h is 18,1% while 26.2% is achieved by Au/AC. To clearly visualize the difference in catalytic performance figure 38 display this effect. At 15 minutes of reaction, Au/AC has reached 15.1% yield GA while Au/ZrO_2 only 2.4%.

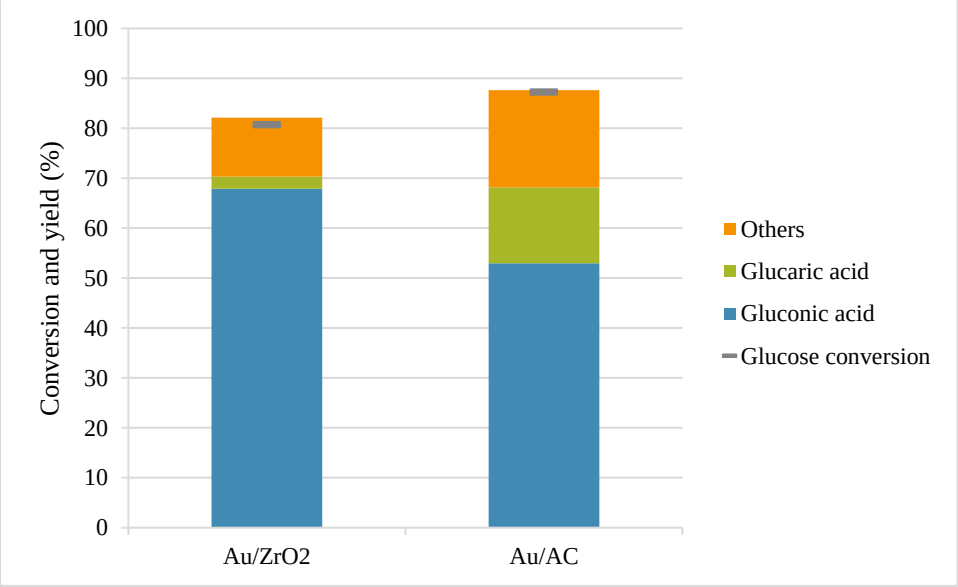

Figure 38. Comparison of Au/AC and Au/ZrO_2 catalyst at 15 min of reaction. Reaction conditions: 60℃, 1000 rpm, 10 bar O_2, Glu:Au:NaOH molar ratio of 1000:1:3000

Several factors can play in this reduced catalytic activity. Although, ZrO_2 is chemically stable and has been proved to enhance the catalytic activity in other reactions (e.g. CO oxidation[68]), synergistic effects could not be observed during these experiments. In a theoretical study, the effect of graphite, ZrO_2 and SnO_2 as supports for Au NPs were examined in the glucose oxidation under alkaline conditions. Au on carbon and ZrO_2 (111) supports will not show higher activity for glucose oxidation reaction because the energy diagram for these surfaces are similar to that of unsupported Au catalysts. When electron transfers from Au catalyst to support materials, the activity of Au catalyst is expected to become high which in this reaction, it is not the case.[69]

Another effect influencing the formation of glucaric acid is the interaction of gold nanoparticles with the support. It has been noticed in Au-Pd bimetallic nanoparticles that the spherical shape is maintained in activated carbon, while in a metal oxide (TiO_2 in this case) the nanoparticles tend to form an extended flat interface with the underlying crystalline TiO_2 phase. This effect is known as **wetting** and it implies that the ligands have been locally displaced from the particle-support interface region leading to an enhanced adhesion of the nanoparticle to the support. This leads to a change in the morphology of the nanoparticle possibly affecting the catalytic activity. Further studies as TEM imaging and XRD are required to elucidate the presence of this effect in Au/ZrO_2.[70]

On the other hand, activated carbon has a larger surface area (compared to ZrO_2) where high dispersion of nanoparticles can be obtained. At better dispersion of nanoparticles, more available active sites and therefore, better catalytic activity.[71] Since the adsorption of glucose in the active site competes with the isomerization of glucose, more isomers are obtained using Au/ZrO_2 and a lower formation of glucaric acid.

5. CONCLUSIONS

Gold based catalysts were synthesized according to several preparation procedures and tested in the direct oxidation of glucose to glucaric acid. We have studied (i) the effect of stirring, time on line of the reaction and the amount of catalyst to reach the kinetic regime and therefore optimizing reaction conditions, (ii) the effect of PVA and the heat treatment of the catalysts to study the influence in terms of determining and influencing the nanoparticle size of Au, and therefore the catalytic activity and selectivity/yield and (iii) the effect of support (metal oxide versus carbon) to investigate the influence of support in terms of metal-support interaction and hence, the impact in terms of activity and selectivity/yield.

The effect of PVA:Au weight ratio was assessed in the control of nanoparticles size, nanoparticle size distribution, given that higher PVA concentrations led to smaller nanoparticles (down to crystallite size of 2.2 nm with PVA:Au weight ratio of 2.4:1). Two different treatments where applied for the removal of PVA: washing with water at 60°C or heat treatment with Air/H_2. Washing treatment and heat treatment at 120°C may have resulted in the mildest treatments for the enhanced removal of PVA while at 200 and 250°C with Air/H_2 the average crystallite size increased (4.1 and 7.5 nm respectively). By the evaluation of stirring rate, Glu:Au molar ratio and time on line study, the operational conditions were optimized obtaining 24% of yield of GA, 37% to GO and 27% to byproducts in 1 h, 1000 rpm, 10 bar of O_2, Glu:Au:NaOH molar ratio of 1000:1:3000. Under such conditions, all catalysts show relatively high glucose conversion (≥82%) even at shorter times. The oxidation reaction was then performed for 15 min where Au/AC PVA0 reached the highest yield of GA (16%) and Au/AC PVA2.4 gave the lowest (8%). It is evident that the presence of PVA influences to a higher degree the reaction rate than the Au NPs size. Au/AC HT200°C and Au/AC HT250°C catalysts in the oxidation reaction resulted in a lower formation of GA (6.2 and 7.9% yield GA, respectively) compared to catalysts Au/AC HT120°C and Au/AC washing (15.7 and 10.3% yield GA, respectively). Finally, two different supports have been used in the immobilization of Au NPs: zirconium oxide and activated carbon. Au/AC catalyst demonstrated a higher conversion of gluconic acid to glucaric acid at short reaction times (15.1% yield GA) compared to gold supported on ZrO_2 (2.4% yield GA).

6. FUTURE WORK

The results presented in this thesis served as a starting point for a more extensive and exhaustive analysis of the gold-based catalysts prepared here. TEM and XRD analysis should be performed in all the samples to clearly evaluate the nanoparticle size, shape and crystalline phases. Raman FT could be used to study the presence of the ligands in the water used for its extraction and evaluate the effectiveness of polymer removal process.

Other studies should be focused on the reusability of the catalyst. Therefore, understating of the deactivation of the catalyst is key for this purpose and some methods should be evaluated to remove the organic matter that could be possible blocking the active sites without affecting the original state of Au and nanoparticle size. Additionally, a modest increase in temperature after 1 h of reaction could help in the desorption of glucaric acid and byproducts from Au surface. Another approach could be the use of a more diluted solution of glucose (1 or 2% wt).

Another aspect to be considered is the stability of the catalyst over time. In general, particles at the nanoscale are unstable and tend to agglomerate because at short interparticle distances they are attracted to each other by van der Waals, electrostatic or magnetic forces. If small nanoparticles are present in the recently synthesized catalyst without protective ligands, a change on the NPs size could be expected after certain time. This effect should be studied thoroughly to determine a shelf life to the catalysts.

At last, bimetallic nanoparticles have been used to study the oxidation of glucose to glucaric acid. This approach could help in the reduction of base concentration or to minimize the deactivation of the catalyst by introducing Pt or Pd in the nanoparticle's preparation. Also, to improve the selectivity with a promoter like bismuth.

7. SUPLEMENTARY INFORMATION

7.1. TEM images

- Au/AC

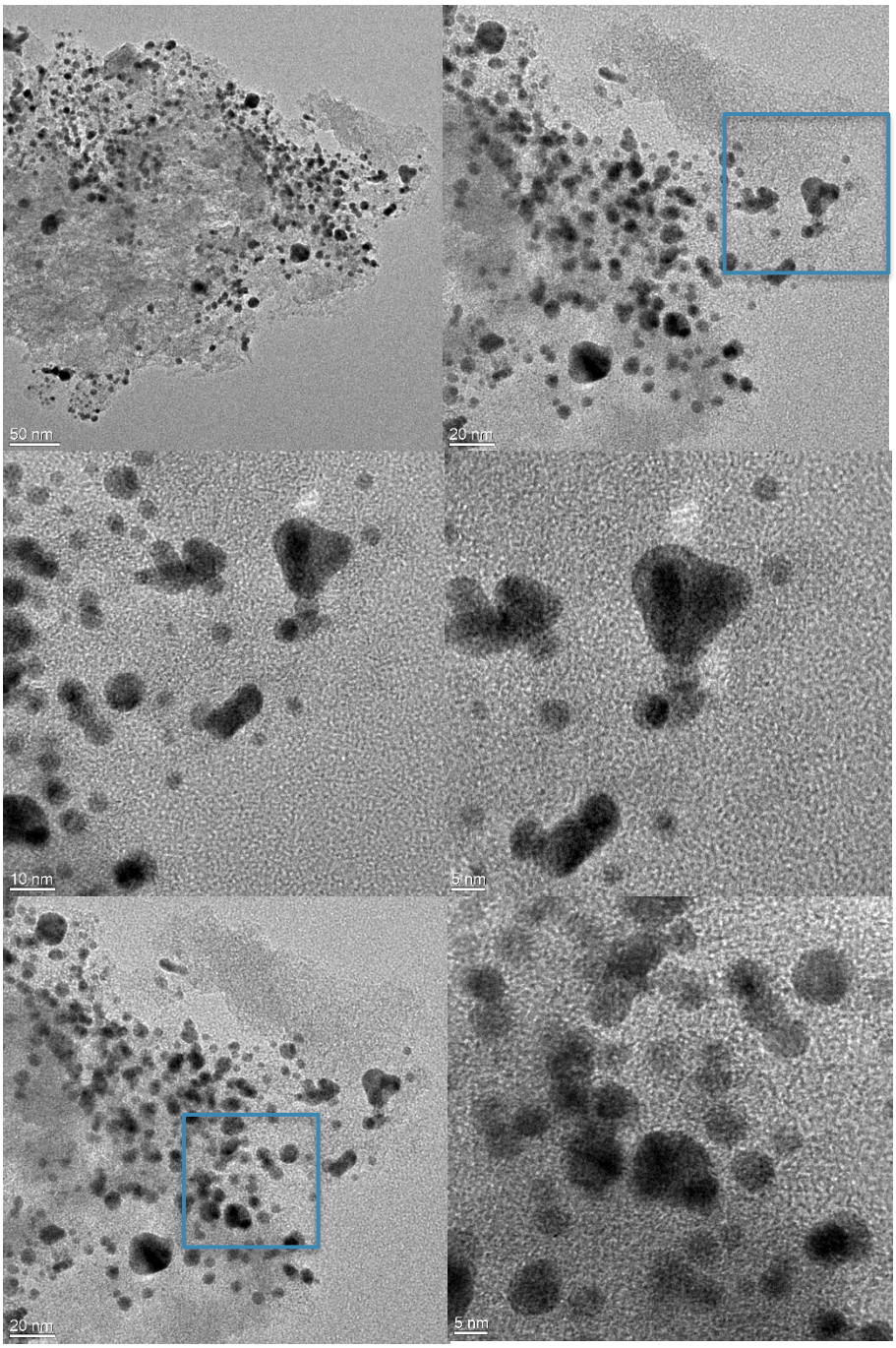

Images both at low and high magnifications that highlight the presence on the support of Au particles of different shape and size (2-19 nm).

Figure S1. Images and amplifications of catalyst Au/AC. TEM images

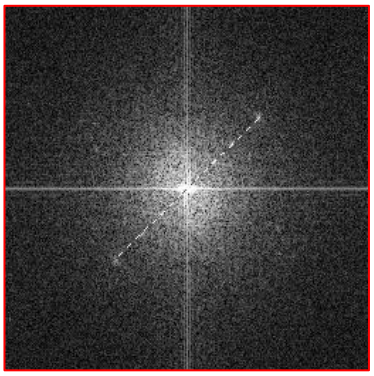

FFT D[Å]
2.34 → Au 1 1 1

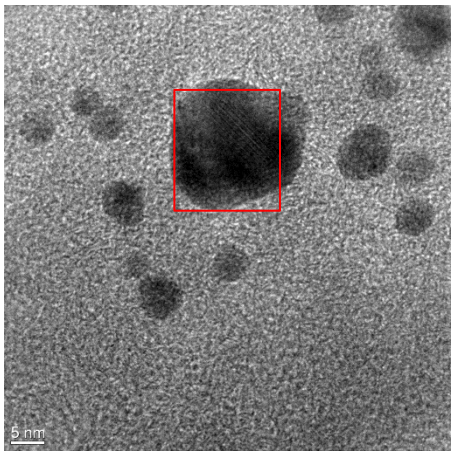

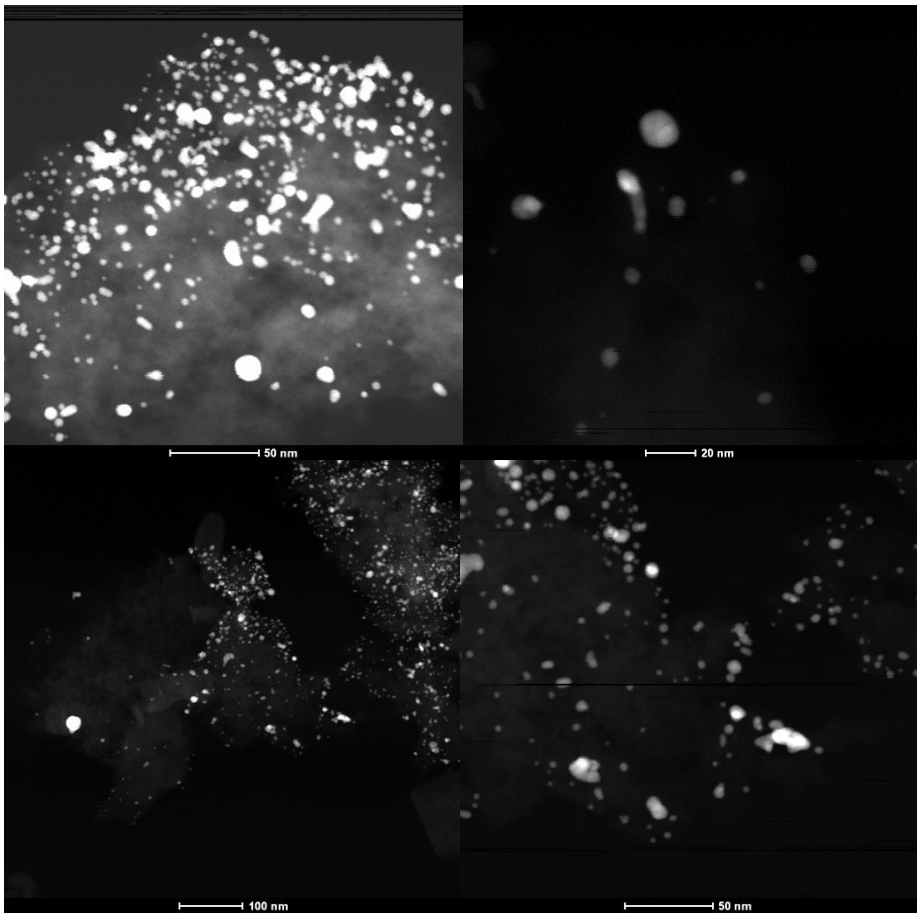

Figure S2. Lattice fringe (top) and contrast images (bottom) of Au/AC

- Au/AC PVA0

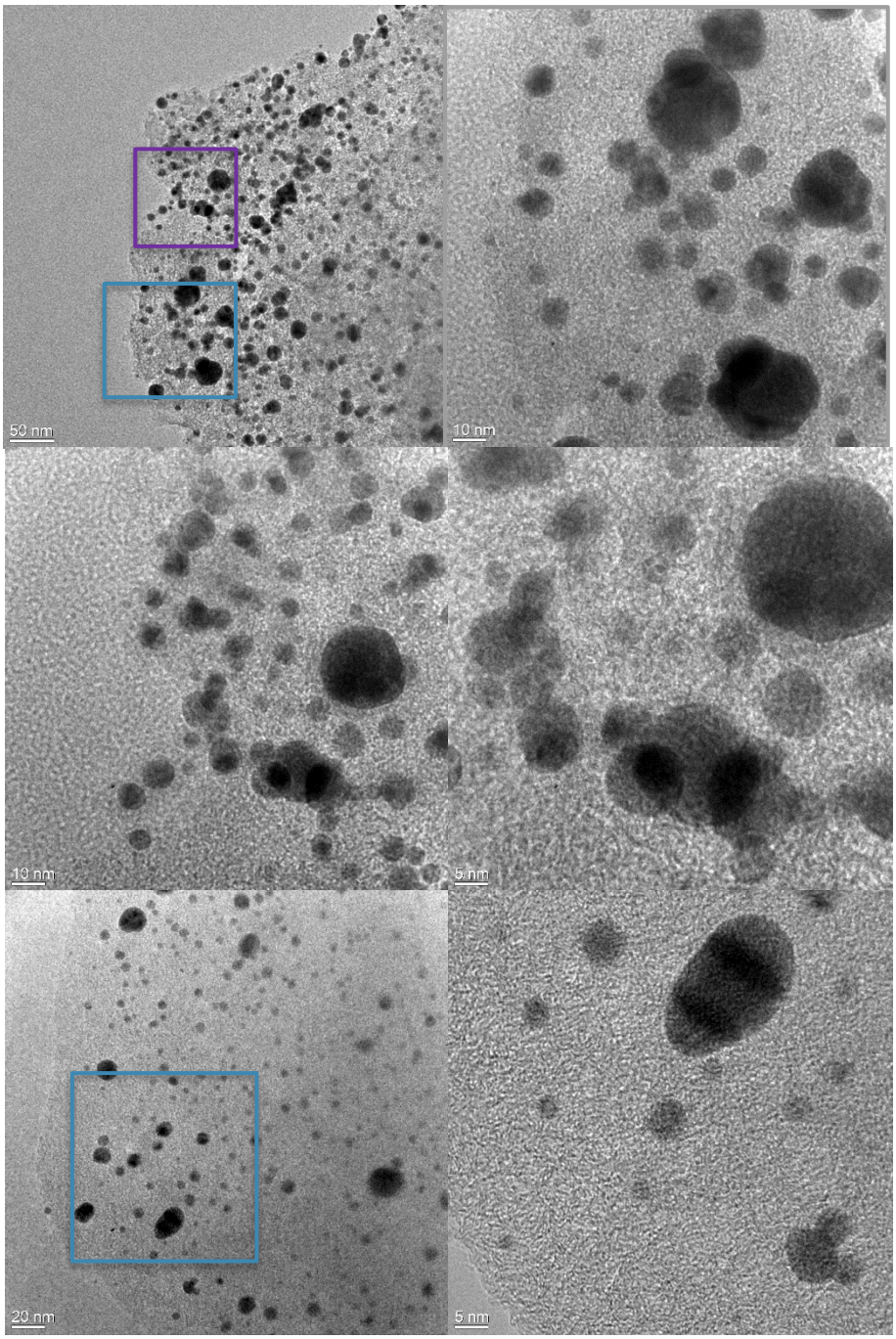

Images both at low and high magnifications that highlight the presence on the support of Au particles of different shape and size (2-30 nm).

Figure S3. TEM images and amplifications of catalyst Au/AC PVA0.

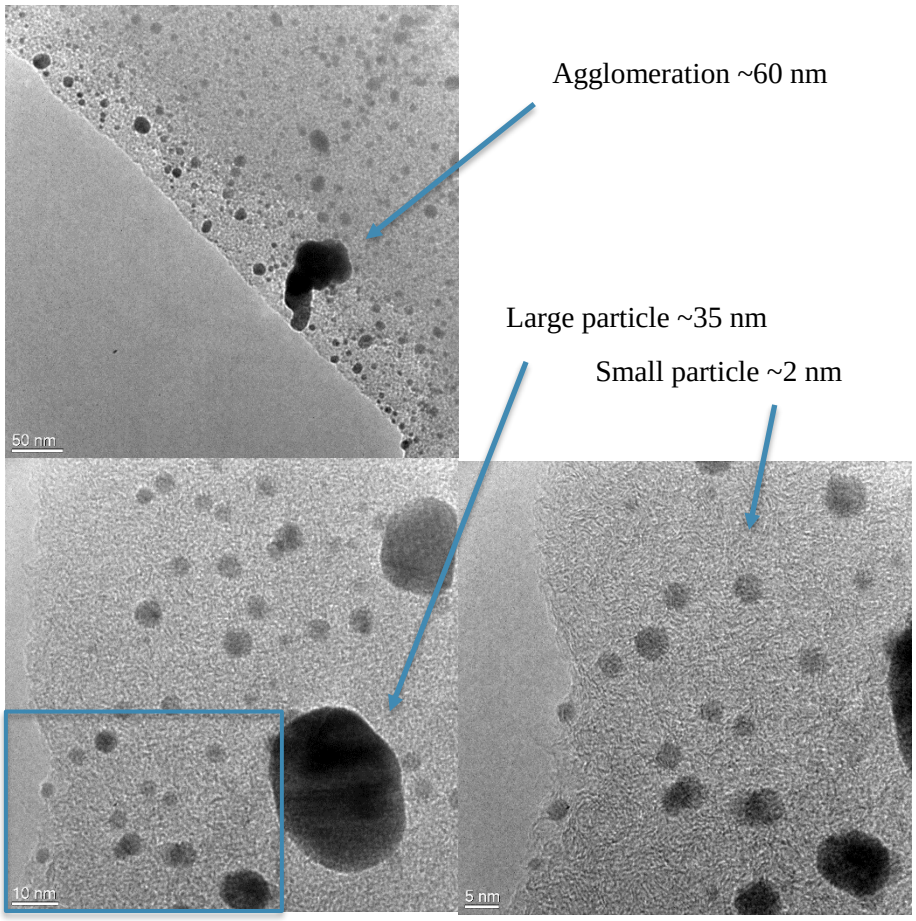

Figure S4. TEM images of agglomeration and large particles in catalyst Au/AC PVA0.

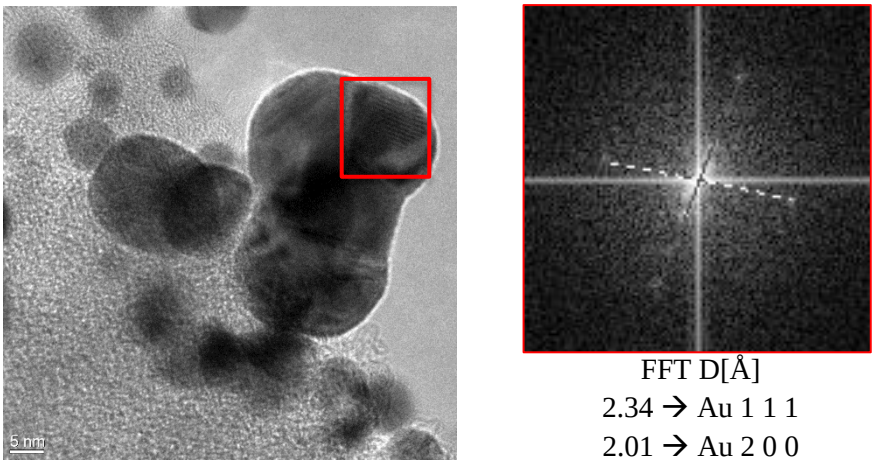

Figure S5. Lattice fringe of Au/AC PVA0

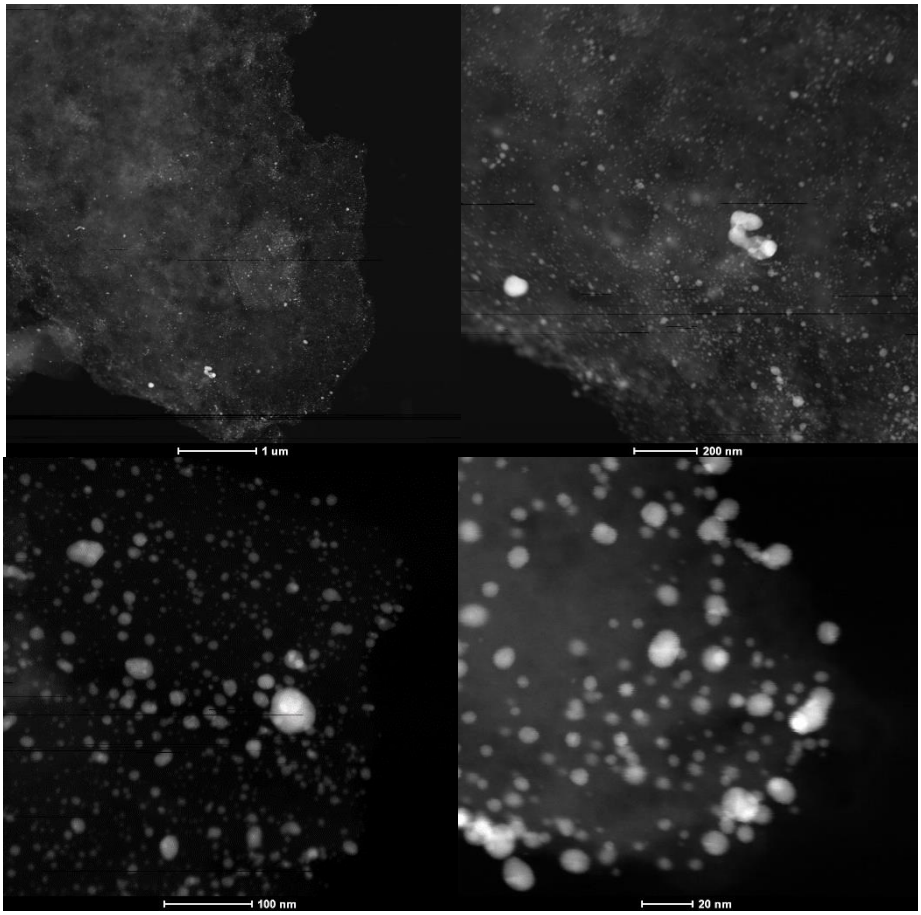

Figure S6. Contrast images of Au/AC PVA0

- Au/AC HT250°C

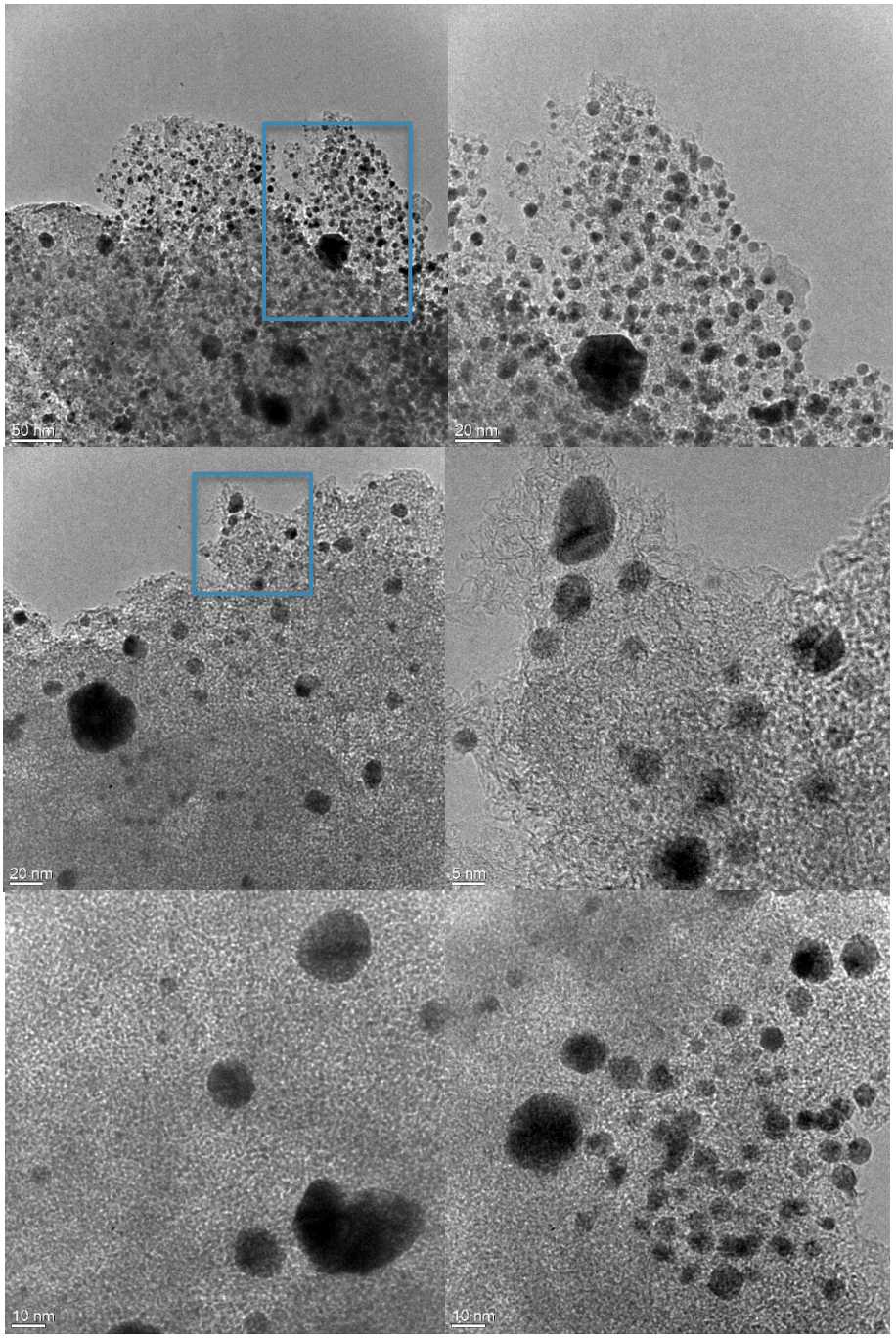

Images both at low and high magnifications that highlight the presence on the support of Au particles of different shape and size (2-27 nm).

Figure S7. TEM images and amplifications of catalyst Au/AC HT250°C

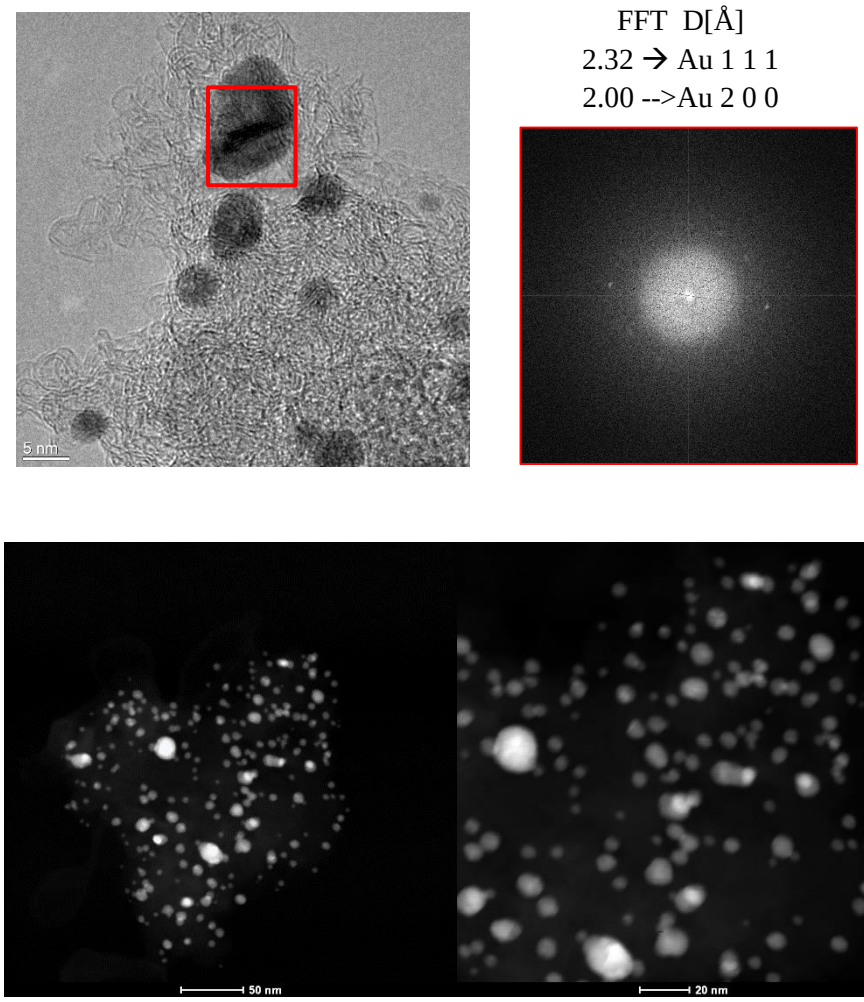

Figure S8. Lattice fringe (top) and contrast images (bottom) of Au/AC HT250°C

7.2. Distribution of byproducts

Stirring rate (rpm)	Oxalic acid	Arabinose + Glyceric acid	Glycolic acid	Tartronic acid	Tartaric acid	Lactic acid	Formic acid	Mesoxalic acid	5KDG
400	0.10	7.1	3.6	1.3	0.3	4.0	3.7	0.1	0.2
600	0.12	4.3	2.8	1.3	0.1	0.8	2.7	0.2	0.8
800	0.11	1.3	1.7	1.2	0.3	0.2	1.7	0.2	0.8
1000	0.8	1.3	3.5	4.0	3.5	0.1	4.6	0.7	0.0
1200	0.9	1.3	3.8	4.8	3.4	0.1	4.7	0.7	0.0

Table S1. Yield (%) of byproducts formed in the study of the effect of stirring rate on glucose oxidation. Reaction conditions: 15 min, 60℃, 10 bar O_2, Glu:Au:NaOH molar ratio of 1000:1:3000.

Stirring rate (rpm)	Oxalic acid	Arabinose + Glyceric acid	Glycolic acid	Tartronic acid	Tartaric acid	Lactic acid	Formic acid	Mesoxalic acid
0	0.12	1.74	1.11	0.01	0.00	0.09	6.36	0.21
1200	0.41	0.63	1.84	2.13	1.90	0.05	2.33	0.35

Table S2. Yield (%) of byproducts formed in the study of the effect of stirring rate on glucose oxidation at time zero. Reaction conditions: 0 min (from the preparation time until the reaction reaches 60℃), 60℃ 10 bar O_2, Glu:Au:NaOH molar ratio of 1000:1:3000.

O_2 pressure (bar)	Oxalic acid	Arabinose + Glyceric acid	Glycolic acid	Tartronic acid	Tartaric acid	Lactic acid	Formic acid	Mesoxalic acid
10	0.8	1.3	3.5	4.0	3.5	0.1	4.6	0.7
15	0.0	0.6	0.6	0.5	0.2	0.1	0.5	0.1

Table S3. Yield (%) of byproducts formed in the study of O_2 pressure on glucose oxidation. Reaction conditions: 15 min, 60℃, 1000 rpm, Glu:Au:NaOH molar ratio of 1000:1:3000.

Time (min)	Isomers[a]	Oxalic acid	Arabinose + Glyceric acid	Glycolic acid	Tartronic acid	Tartaric acid	Lactic acid	Formic acid	Mesoxalic acid
15	1.04	0.80	1.31	3.50	3.98	3.50	0.11	4.57	0.70
30	1.16	1.04	2.28	3.46	5.52	4.26	0.36	4.61	0.83
60	1.04	1.34	2.77	4.01	6.79	4.95	0.09	5.54	1.10
120	1.42	1.48	3.22	4.59	7.16	4.46	0.32	6.19	0.99

Table S4. Yield (%) of byproducts formed in the study through time of glucose oxidation. Reaction conditions: 60℃, 1000 rpm,10 bar O_2, Glu:Au:NaOH molar ratio of 1000:1:3000. [a] Isomers corresponding to fructose and mannose combined

Time (min)	Oxalic acid	Arabinose + Glyceric acid	Glycolic acid	Tartronic acid	Tartaric acid	Lactic acid	Formic acid	Mesoxalic acid
15	0.4	1.2	1.8	2.8	1.8	0.0	2.3	0.4
60	0.9	2.1	3.5	5.9	2.5	0.1	4.4	0.8

Table S5. Yield (%) of byproducts formed by starting GO as substrate. Reaction conditions: 60℃, 1000 rpm, 10 bar O_2, GO:Au:NaOH molar ratio of 1000:1:3000.

Time (min)	Oxalic acid	Arabinose + Glyceric acid	Glycolic acid	Tartronic acid	Tartaric acid	Lactic acid	Formic acid	Mesoxalic acid
0	0.1	1.7	1.1	0.0	0.0	0.1	6.2	0.2
1	0.1	2.0	1.5	0.3	0.0	0.0	7.1	0.0
15	0.3	5.0	5.0	0.7	0.0	0.4	18.0	0.6

Table S6. Yield (%) of byproducts formed in blank test. Reaction conditions: 60℃, 1200 rpm, 10 bar O_2, Glu:NaOH molar ratio of 1:3.

Au:Glu molar ratio	Oxalic acid	Arabinose + Glyceric acid	Glycolic acid	Tartronic acid	Tartaric acid	Lactic acid	Formic acid	Mesoxalic acid
1:500	2.1	2.6	4.4	8.6	6.5	0.3	6.0	1.0
1:1000	1.3	2.8	4.0	6.8	4.9	0.1	5.5	1.1
1:1500	1.0	2.7	4.3	5.9	5.3	0.2	6.0	0.9

Table S7. Yield (%) of byproducts Study of Au:Glu molar ratio. Reaction conditions: 1 h, 60℃, 1000 rpm, 10 bar O_2, Glu:NaOH molar ratio of 1:3.

Catalysts Au/AC PVA	Oxalic acid	Arabinose + Glyceric acid	Glycolic acid	Tartronic acid	Tartaric acid	Lactic acid	Formic acid	Mesoxalic acid
Au/AC PVA0	1.3	2.4	4.2	7.2	4.8	0.2	5.9	1.0
Au/AC PVA 0.3	1.3	2.9	4.1	7.4	5.1	0.5	6.1	0.9
Au/AC PVA 0.6	1.2	2.8	4.6	7.1	4.8	0.3	6.4	0.9
Au/AC PVA 1.2	1.0	2.5	4.7	6.7	4.2	0.2	6.1	0.8
Au/AC PVA 2.4	0.9	2.6	3.7	5.4	3.7	0.2	5.2	0.7

Table S8. Yield (%) of byproducts formed in the catalytic screening of Au/AC PVA set. Reaction conditions: 1 h, 60℃, 1000 rpm, 10 bar O_2, Glu:Au:NaOH molar ratio of 1000:1:3000.

Catalyst	Oxalic acid	Arabinose + Glyceric acid	Glycolic acid	Tartronic acid	Tartaric acid	Lactic acid	Formic acid	Mesoxalic acid
Au/AC HT120°C	1.0	2.4	5.4	6.3	4.3	0.2	6.5	0.7
Au/AC HT200°C	0.6	2.3	4.2	5.0	3.2	0.3	5.7	0.6
Au/AC HT250°C	0.7	2.2	4.5	5.6	3.5	0.2	6.1	0.7
Au/AC washing	1.5	3.3	4.3	7.2	6.4	0.6	6.2	0.9

Table S9. Yield (%) of byproducts formed in the screening of catalysts with two different procedures of PVA removal. Reaction conditions: 1 h, 60℃,1000 rpm, 10 bar O_2, Glu:Au:NaOH molar ratio of 1000:1:3000.

Catalyst	Oxalic acid	Arabinose + Glyceric acid	Glycolic acid	Tartronic acid	Tartaric acid	Lactic acid	Formic acid	Mesoxalic acid
Au/AC HT120°C	0.9	1.9	3.1	4.4	6.5	0.1	4.9	0.6
Au/AC HT200°C	0.2	1.1	1.5	1.9	2.1	0.1	2.5	0.3
Au/AC HT250°C	0.3	1.2	2.1	2.3	2.1	0.1	3.0	0.3
Au/AC washing	0.5	2.0	2.1	3.3	3.0	2.2	3.2	0.4

Table S10. Yield (%) of byproducts formed in the screening of catalysts with two different procedures of PVA removal. Reaction conditions: 15 min, 60℃, 1000 rpm, 10 bar O_2, Glu:Au:NaOH molar ratio of 1000:1:3000.

Catalyst	Time	Oxalic acid	Arabinose + Glyceric acid	Glycolic acid	Tartronic acid	Tartaric acid	Lactic acid	Formic acid	Mesoxalic acid
Au/ZrO_2	15 min[a]	0.1	1.8	1.4	0.9	0.8	0.4	2.0	0.2
	1 h[a]	0.7	3.2	4.2	5.0	4.8	0.3	6.1	0.7
	3 h[b]	0.7	11.9	7.8	5.4	1.5	6.7	8.0	1.0
Au/AC	15 min[a]	0.8	1.3	3.5	4.0	3.5	0.1	4.6	0.7
	1 h[a]	1.3	2.8	4.0	6.8	4.9	0.1	5.5	1.1

Table S11. Yield (%) of byproducts formed in the comparison of support. [a] Reaction conditions: 60℃, 1000 rpm, 10 bar O_2, Glu:Au:NaOH molar ratio of 1000:1:3000. [b] Reaction conditions: 60℃, 400 rpm, 10 bar O_2, Glu:Au:NaOH molar ratio of 500:1:1500.

8. ABBREVIATIONS

AC: Activated Carbon

GA: Glucaric acid

Glu: Glucose

GO: Gluconic acid

HAADF: High-angle annular dark-field imaging

HPLC: High Performance Liquid Chromatography

NPs: Nanoparticles

PVA: Poly vinyl alcohol

STEM: Scanning Transmission Electron Microscopy

TEM: Transmission Electron Microscopy

TGA: Thermal Gravimetric Analysis

XRD: X-ray diffraction

9. REFERENCES

[1] Qian, Z., & Park, S. J. (2014). Silver seeds and aromatic surfactants facilitate the growth of anisotropic metal nanoparticles: gold triangular nanoprisms and ultrathin nanowires. *Chemistry of Materials*, *26*(21), 6172-6177.

[2] Han, J., Zhang, J., Yang, M., Cui, D., & Jesus, M. (2015). Glucose-functionalized Au nanoprisms for optoacoustic imaging and near-infrared photothermal therapy. *Nanoscale*, *8*(1), 492-499.

[3] Peng, X., Wan, G., Wu, L., Zeng, M., Lin, S., & Wang, G. (2018). Peroxidase-like activity of Au@ TiO2 yolk-shell nanostructure and its application for colorimetric detection of H2O2 and glucose. *Sensors and Actuators B: Chemical*, *257*, 166-177

[4] Fujita, T., Horikawa, M., Takei, T., Murayama, T., & Haruta, M. (2016). Correlation between catalytic activity of supported gold catalysts for carbon monoxide oxidation and metal–oxygen binding energy of the support metal oxides. *Chinese Journal of Catalysis*, *37*(10), 1651-1655.

[5] Liu, B., & Liu, J. (2017). Surface modification of nanozymes. *Nano Research*, *10*(4), 1125-1148.

[6] Zheng, X., Liu, Q., Jing, C., Li, Y., Li, D., Luo, W., ... & Fan, C. (2011). Catalytic gold nanoparticles for nanoplasmonic detection of DNA hybridization. *Angewandte Chemie International Edition*, *50*(50), 11994-11998.

[7] Kelly, K. L., Coronado, E., Zhao, L. L., & Schatz, G. C. (2003). The optical properties of metal nanoparticles: the influence of size, shape, and dielectric environment.

[8] Amendola, V., Pilot, R., Frasconi, M., Marago, O. M., & Iati, M. A. (2017). Surface plasmon resonance in gold nanoparticles: a review. *Journal of Physics: Condensed Matter*, *29*(20), 203002.

[9] Stratakis, M., & Garcia, H. (2012). Catalysis by supported gold nanoparticles: beyond aerobic oxidative processes. *Chemical Reviews*, *112*(8), 4469-4506.

[10] Della Pina, C., Falletta, E., Prati, L., & Rossi, M. (2008). Selective oxidation using gold. *Chemical Society Reviews*, *37*(9), 2077-2095.

[11] Haruta, M. (1997). Size-and support-dependency in the catalysis of gold. *Catalysis today*, *36*(1), 153-166.

[12] Takei, T., Okuda, I., Bando, K. K., Akita, T., & Haruta, M. (2010). Gold clusters supported on La (OH) 3 for CO oxidation at 193 K. *Chemical Physics Letters*, *493*(4-6), 207-211.

[13] Gluhoi, A. C., Bakker, J. W., & Nieuwenhuys, B. E. (2010). Gold, still a surprising catalyst: Selective hydrogenation of acetylene to ethylene over Au nanoparticles. *Catalysis Today*, *154*(1-2), 13-20.

[14] Segura, Y., López, N., & Pérez-Ramírez, J. (2007). Origin of the superior hydrogenation selectivity of gold nanoparticles in alkyne+ alkene mixtures: Triple-versus double-bond activation. *Journal of Catalysis*, *247*(2), 383-386.

[15] Corma, A., & Serna, P. (2006). Chemoselective hydrogenation of nitro compounds with supported gold catalysts. *Science*, *313*(5785), 332-334.

[16] Corma, A., Concepción, P., & Serna, P. (2007). A different reaction pathway for the reduction of aromatic nitro compounds on gold catalysts. *Angewandte Chemie International Edition*, *46*(38), 7266-7269.

[17] Esumi, K., Miyamoto, K., & Yoshimura, T. (2002). Comparison of PAMAM–Au and PPI–Au nanocomposites and their catalytic activity for reduction of 4-nitrophenol. *Journal of colloid and interface science*, *254*(2), 402-405.

[18] Praharaj, S., Nath, S., Ghosh, S. K., Kundu, S., & Pal, T. (2004). Immobilization and recovery of Au nanoparticles from anion exchange resin: resin-bound nanoparticle matrix as a catalyst for the reduction of 4-nitrophenol. *Langmuir*, *20*(23), 9889-9892.

[19] Tang, R., Liao, X. P., & Shi, B. (2008). Heterogeneous gold nanoparticles stabilized by collagen and their application in catalytic reduction of 4-nitrophenol. *Chemistry letters*, *37*(8), 834-835.

[20] Wei, H., & Lu, Y. (2012). Catalysis of gold nanoparticles within lysozyme single crystals. *Chemistry–An Asian Journal*, *7*(4), 680-683.

[21] Markus, J., Mathiyalagan, R., Kim, Y. J., Abbai, R., Singh, P., Ahn, S., ... & Yang, D. C. (2016). Intracellular synthesis of gold nanoparticles with antioxidant activity by probiotic Lactobacillus kimchicus DCY51T isolated from Korean kimchi. *Enzyme and microbial technology*, *95*, 85-93.

[22] Mishra, A., Kumari, M., Pandey, S., Chaudhry, V., Gupta, K. C., & Nautiyal, C. S. (2014). Biocatalytic and antimicrobial activities of gold nanoparticles synthesized by Trichoderma sp. *Bioresource technology*, *166*, 235-242.

[23] Li, G., & Jin, R. (2013). Catalysis by gold nanoparticles: carbon-carbon coupling reactions. *Nanotechnology Reviews*, *2*(5), 529-545.

[24] Shah, M., Badwaik, V., Kherde, Y., Waghwani, H. K., Modi, T., Aguilar, Z. P., ... & Lawrenz, M. B. (2014). Gold nanoparticles: various methods of synthesis and antibacterial applications. Front. Biosci, 19(1320), 10-2741.

[25] Gandarias, I., Miedziak, P. J., Nowicka, E., Douthwaite, M., Morgan, D. J., Hutchings, G. J., & Taylor, S. H. (2015). Selective Oxidation of n-Butanol Using Gold-Palladium Supported Nanoparticles Under Base-Free Conditions. ChemSusChem, 8(3), 473-480.

[26] Boronat, M., Concepción, P., & Corma, A. (2009). Unravelling the nature of gold surface sites by combining IR spectroscopy and DFT calculations. Implications in catalysis. *The Journal of Physical Chemistry C*, *113*(38), 16772-16784.

[27] Kim, K. J., & Ahn, H. G. (2009). Complete oxidation of toluene over bimetallic Pt–Au catalysts supported on ZnO/Al2O3. *Applied Catalysis B: Environmental*, *91*(1-2), 308-318.

[28] Ivanova, S., Petit, C., & Pitchon, V. (2004). A new preparation method for the formation of gold nanoparticles on an oxide support. *Applied Catalysis A: General*, *267*(1-2), 191-201.

[29] Ivanova, S., Pitchon, V., & Petit, C. (2006). Application of the direct exchange method in the preparation of gold catalysts supported on different oxide materials. *Journal of Molecular Catalysis A: Chemical*, *256*(1-2), 278-283.

[30] Delannoy, L., El Hassan, N., Musi, A., Le To, N. N., Krafft, J. M., & Louis, C. (2006). Preparation of supported gold nanoparticles by a modified incipient wetness impregnation method. *The Journal of Physical Chemistry B*, *110*(45), 22471-22478.

[31] Khan, Z., Singh, T., Hussain, J. I., & Hashmi, A. A. (2013). Au (III)–CTAB reduction by ascorbic acid: Preparation and characterization of gold nanoparticles. *Colloids and Surfaces B: Biointerfaces*, *104*, 11-17.

[32] Álvarez Cerimedo, M. S., Baronio, L. G., Hoppe, C. E., & Ayude, M. A. (2019). The Effect of Poly (vinylpyrrolidone)(PVP) on the Au Catalyzed Reduction of p–nitrophenol: The Fundamental Role of NaBH4. *ChemistrySelect*, *4*(2), 608-616.

[33] Thanh, N. T., Maclean, N., & Mahiddine, S. (2014). Mechanisms of nucleation and growth of nanoparticles in solution. *Chemical reviews*, *114*(15), 7610-7630.

[34] Polte, J., Erler, R., Thunemann, A. F., Sokolov, S., Ahner, T. T., Rademann, K., ... & Kraehnert, R. (2010). Nucleation and growth of gold nanoparticles studied via in situ small angle X-ray scattering at millisecond time resolution. *ACS nano*, *4*(2), 1076-1082.

[35] Signoretto, M., Menegazzo, F., Di Michele, A., & Fioriniello, E. (2016). Effects of Support and Synthetic Procedure for Sol-Immobilized Au Nanoparticles. *Catalysts*, *6*(6), 87.

[36] Megías-Sayago, C., Santos, J. L., Ammari, F., Chenouf, M., Ivanova, S., Centeno, M. A., & Odriozola, J. A. (2018). Influence of gold particle size in Au/C catalysts for base-free oxidation of glucose. *Catalysis Today*, *306*, 183-190.

[37] Tareq, S., Yap, Y. H. T., Saleh, T. A., Abdullah, A. H., Rashid, U., & Saiman, M. I. (2018). Synthesis of bimetallic gold-pallidum loaded on carbon as efficient catalysts for the oxidation of benzyl alcohol into benzaldehyde. *Journal of Molecular Liquids*, *271*, 885-891.

[38] Wang, W., Hu, H., Xu, J., Wang, Q., Qi, G., Wang, C., ... & Deng, F. (2018). Tuning Pd–Au Bimetallic Catalysts for Heterogeneous Parahydrogen-Induced Polarization. *The Journal of Physical Chemistry C*, *122*(2), 1248-1257.

[39] Kobayashi, H., & Fukuoka, A. (2013). Synthesis and utilisation of sugar compounds derived from lignocellulosic biomass. *Green Chemistry*, *15*(7), 1740-1763.

[40] Ramachandran, S., Fontanille, P., Pandey, A., & Larroche, C. (2006). Gluconic acid: Properties, applications and microbial production. *Food Technology & Biotechnology*, *44*(2).

[41] Choudhury, P. S., Savio, E., Solanki, K. K., Alonso, O., Gupta, A., Gambini, J. P., ... & Dondi, M. (2012). 99mTc glucarate as a potential radiopharmaceutical agent for assessment of tumor viability: from bench to the bed side. *World journal of nuclear medicine*, *11*(2), 47.

[42] Mehltretter, C. L., Alexander, B. H., & Rist, C. E. (1953). Sequestration by sugar acids. *Industrial & Engineering Chemistry*, *45*(12), 2782-2784.

[43] Werpy, T., and G. Petersen. (2004). *Top. value added chemicals from biomass, volume 1—results of screening for potential candidates from sugars and synthesis gas.* U.S. Department of Energy, Washington, DC.

[44] Jang, Y. S., Kim, B., Shin, J. H., Choi, Y. J., Choi, S., Song, C. W., ... & Lee, S. Y. (2012). Bio-based production of C2–C6 platform chemicals. *Biotechnology and bioengineering*, *109*(10), 2437-2459.

[45] Beerthuis, R., Rothenberg, G., & Shiju, N. R. (2015). Catalytic routes towards acrylic acid, adipic acid and ε-caprolactam starting from biorenewables. *Green Chemistry*, *17*(3), 1341-1361.

[46] Bose, R., Hullar, T., Lewis, B., & Smith, F. (1961). Isolation of 1, 4-and 6, 3-Lactones of D-Glucaric Acid. *The Journal of Organic Chemistry*, *26*(4), 1300-1301.

[47] Sohst, O., & Tollens, B. (1888). Über krystallisirte Zuckersäure (Zuckerlactonsäure). *Justus Liebigs Annalen der Chemie*, *245*(1-2), 1-27.

[48] Moon, T. S., Yoon, S. H., Lanza, A. M., Roy-Mayhew, J. D., & Prather, K. L. J. (2009). Production of glucaric acid from a synthetic pathway in recombinant Escherichia coli. *Appl. Environ. Microbiol.*, *75*(3), 589-595.

[49] Merbouh, N., Thaburet, J. F., Ibert, M., Marsais, F., & Bobbitt, J. M. (2001). Facile nitroxide-mediated oxidations of D-glucose to D-glucaric acid. *Carbohydrate research*, *336*(1), 75-78.

[50] Bin, D., Wang, H., Li, J., Wang, H., Yin, Z., Kang, J., ... & Li, Z. (2014). Controllable oxidation of glucose to gluconic acid and glucaric acid using an electrocatalytic reactor. *Electrochimica Acta*, *130*, 170-178.

[51] Zhang, Z., & Huber, G. W. (2018). Catalytic oxidation of carbohydrates into organic acids and furan chemicals. Chemical Society Reviews, 47(4), 1351-1390.

[52] Biella, S., Prati, L., & Rossi, M. (2002). Selective oxidation of D-glucose on gold catalyst. Journal of Catalysis, 206(2), 242-247.

[53] Önal, Y., Schimpf, S., & Claus, P. (2004). Structure sensitivity and kinetics of D-glucose oxidation to D-gluconic acid over carbon-supported gold catalysts. *Journal of Catalysis*, *223*(1), 122-133.

[54] Miedziak, P. J., Alshammari, H., Kondrat, S. A., Clarke, T. J., Davies, T. E., Morad, M., ... & Hutchings, G. J. (2014). Base-free glucose oxidation using air with supported gold catalysts. *Green Chemistry*, *16*(6), 3132-3141.

[55] Murphy, V.J., Shoemaker, J., Zhu, G., Archer, R., Salem, F. & Dias, E. L. (2011) US Pat, 2011/0306790A1

[56] Lee, J., Saha, B., & Vlachos, D. G. (2016). Pt catalysts for efficient aerobic oxidation of glucose to glucaric acid in water. *Green Chemistry*, *18*(13), 3815-3822.

[57] Derrien, E., Mounguengui-Diallo, M., Perret, N., Marion, P., Pinel, C., & Besson, M. (2017). Aerobic oxidation of glucose to glucaric acid under alkaline-free conditions: Au-based bimetallic catalysts and the effect of residues in a hemicellulose hydrolysate. *Industrial & Engineering Chemistry Research*, *56*(45), 13175-13189.

[58] Solmi, S., Morreale, C., Ospitali, F., Agnoli, S., & Cavani, F. (2017). Oxidation of d-Glucose to Glucaric Acid Using Au/C Catalysts. *ChemCatChem*, *9*(14), 2797-2806

[59] Comotti, M., Della Pina, C., Falletta, E., & Rossi, M. (2006). Aerobic oxidation of glucose with gold catalyst: hydrogen peroxide as intermediate and reagent. *Advanced Synthesis & Catalysis*, *348*(3), 313-316.

[60] Saliger, R., Decker, N., & Prüße, U. (2011). D-Glucose oxidation with H2O2 on an Au/Al2O3 catalyst. *Applied Catalysis B: Environmental*, *102*(3-4), 584-589.

[61] Qi, P., Chen, S., Chen, J., Zheng, J., Zheng, X., & Yuan, Y. (2015). Catalysis and reactivation of ordered mesoporous carbon-supported gold nanoparticles for the base-free oxidation of glucose to gluconic acid. ACS Catalysis, 5(4), 2659-2670.

[62] Mohr, C., Hofmeister, H., & Claus, P. (2003). The influence of real structure of gold catalysts in the partial hydrogenation of acrolein. *Journal of Catalysis*, *213*(1), 86-94.

[63] Mott, D., Luo, J., Njoki, P. N., Lin, Y., Wang, L., & Zhong, C. J. (2007). Synergistic activity of gold-platinum alloy nanoparticle catalysts. *Catalysis Today*, *122*(3-4), 378-385.

[64] Lopez-Sanchez, J. A., Dimitratos, N., Hammond, C., Brett, G. L., Kesavan, L., White, S., ... & Knight, D. (2011). Facile removal of stabilizer-ligands from supported gold nanoparticles. *Nature chemistry*, *3*(7), 551.

[65] Polte, J. (2015). Fundamental growth principles of colloidal metal nanoparticles–a new perspective. *CrystEngComm*, *17*(36), 6809-6830.

[66] Zope, B. N., Hibbitts, D. D., Neurock, M., & Davis, R. J. (2010). Reactivity of the gold/water interface during selective oxidation catalysis. *Science*, *330*(6000), 74-78.

[67] Jin, X., Zhao, M., Vora, M., Shen, J., Zeng, C., Yan, W., ... & Chaudhari, R. V. (2016). Synergistic effects of bimetallic PtPd/TiO2 nanocatalysts in oxidation of glucose to glucaric acid: Structure dependent activity and selectivity. *Industrial & Engineering Chemistry Research*, *55*(11), 2932-2945.

[68] Galeano, C., Güttel, R., Paul, M., Arnal, P., Lu, A. H., & Schüth, F. (2011). Yolk-Shell Gold Nanoparticles as Model Materials for Support-Effect Studies in Heterogeneous Catalysis: Au,@ C and Au,@ ZrO2 for CO Oxidation as an Example. *Chemistry–A European Journal*, *17*(30), 8434-8439.

[69] Ishimoto, T., Hamatake, Y., Kazuno, H., Kishida, T., & Koyama, M. (2015). Theoretical study of support effect of Au catalyst for glucose oxidation of alkaline fuel cell anode. *Applied Surface Science*, *324*, 76-81.

[70] Tiruvalam, R. C., Pritchard, J. C., Dimitratos, N., Lopez-Sanchez, J. A., Edwards, J. K., Carley, A. F., ... & Kiely, C. J. (2011). Aberration corrected analytical electron microscopy studies of sol-immobilized Au+ Pd, Au {Pd} and Pd {Au} catalysts used for benzyl alcohol oxidation and hydrogen peroxide production. *Faraday Discussions*, *152*, 63-86.

[71] Sanchez, F., Motta, D., Bocelli, L., Albonetti, S., Roldan, A., Hammond, C., ... & Dimitratos, N. (2018). Investigation of the catalytic performance of Pd/CNFs for hydrogen evolution from additive-free formic acid decomposition. *C*, *4*(2), 26.